Measurement of density correlations in pseudorapidity via charged particle multiplicity fluctuations in Au+Au collisions at $\sqrt{s_{NN}} = 200$ GeV

S.S. Adler,[5] S. Afanasiev,[17] C. Aidala,[5] N.N. Ajitanand,[43] Y. Akiba,[20,38] J. Alexander,[43] R. Amirikas,[12] L. Aphecetche,[45] S.H. Aronson,[5] R. Averbeck,[44] T.C. Awes,[35] R. Azmoun,[44] V. Babintsev,[15] A. Baldisseri,[10] K.N. Barish,[6] P.D. Barnes,[27] B. Bassalleck,[33] S. Bathe,[30] S. Batsouli,[9] V. Baublis,[37] A. Bazilevsky,[39,15] S. Belikov,[16,15] Y. Berdnikov,[40] S. Bhagavatula,[16] J.G. Boissevain,[27] H. Borel,[10] S. Borenstein,[25] M.L. Brooks,[27] D.S. Brown,[34] N. Bruner,[33] D. Bucher,[30] H. Buesching,[30] V. Bumazhnov,[15] G. Bunce,[5,39] J.M. Burward-Hoy,[26,44] S. Butsyk,[44] X. Camard,[45] J.-S. Chai,[18] P. Chand,[4] W.C. Chang,[2] S. Chernichenko,[15] C.Y. Chi,[9] J. Chiba,[20] M. Chiu,[9] I.J. Choi,[52] J. Choi,[19] R.K. Choudhury,[4] T. Chujo,[5] V. Cianciolo,[35] Y. Cobigo,[10] B.A. Cole,[9] P. Constantin,[16] D. d'Enterria,[45] G. David,[5] H. Delagrange,[45] A. Denisov,[15] A. Deshpande,[39] E.J. Desmond,[5] A. Devismes,[44] O. Dietzsch,[41] O. Drapier,[25] A. Drees,[44] K.A. Drees,[5] A. Durum,[15] D. Dutta,[4] Y.V. Efremenko,[35] K. El Chenawi,[49] A. Enokizono,[14] H. En'yo,[38,39] S. Esumi,[48] L. Ewell,[5] D.E. Fields,[33,39] F. Fleuret,[25] S.L. Fokin,[23] B.D. Fox,[39] Z. Fraenkel,[51] J.E. Frantz,[9] A. Franz,[5] A.D. Frawley,[12] S.-Y. Fung,[6] S. Garpman,[29,*] T.K. Ghosh,[49] A. Glenn,[46] G. Gogiberidze,[46] M. Gonin,[25] J. Gosset,[10] Y. Goto,[39] R. Granier de Cassagnac,[25] N. Grau,[16] S.V. Greene,[49] M. Grosse Perdekamp,[39] W. Guryn,[5] H.-Å. Gustafsson,[29] T. Hachiya,[14] J.S. Haggerty,[5] H. Hamagaki,[8] A.G. Hansen,[27] E.P. Hartouni,[26] M. Harvey,[5] R. Hayano,[8] N. Hayashi,[38] X. He,[13] M. Heffner,[26] T.K. Hemmick,[44] J.M. Heuser,[44] M. Hibino,[50] J.C. Hill,[16] W. Holzmann,[43] K. Homma,[14] B. Hong,[22] A. Hoover,[34] T. Ichihara,[38,39] V.V. Ikonnikov,[23] K. Imai,[24,38] D. Isenhower,[1] M. Ishihara,[38] M. Issah,[43] A. Isupov,[17] B.V. Jacak,[44,†] W.Y. Jang,[22] Y. Jeong,[19] J. Jia,[44] O. Jinnouchi,[38] B.M. Johnson,[5] S.C. Johnson,[26] K.S. Joo,[31] D. Jouan,[36] S. Kametani,[8,50] N. Kamihara,[47,38] J.H. Kang,[52] S.S. Kapoor,[4] K. Katou,[50] S. Kelly,[9] B. Khachaturov,[51] A. Khanzadeev,[37] J. Kikuchi,[50] D.H. Kim,[31] D.J. Kim,[52] D.W. Kim,[19] E. Kim,[42] G.-B. Kim,[25] H.J. Kim,[52] E. Kistenev,[5] A. Kiyomichi,[48] K. Kiyoyama,[32] C. Klein-Boesing,[30] H. Kobayashi,[38,39] L. Kochenda,[37] V. Kochetkov,[15] D. Koehler,[33] T. Kohama,[14] M. Kopytine,[44] D. Kotchetkov,[6] A. Kozlov,[51] P.J. Kroon,[5] C.H. Kuberg,[1,27,*] K. Kurita,[39] Y. Kuroki,[48] M.J. Kweon,[22] Y. Kwon,[52] G.S. Kyle,[34] R. Lacey,[43] V. Ladygin,[17] J.G. Lajoie,[16] A. Lebedev,[16,23] S. Leckey,[44] D.M. Lee,[27] S. Lee,[19] M.J. Leitch,[27] X.H. Li,[6] H. Lim,[42] A. Litvinenko,[17] M.X. Liu,[27] Y. Liu,[36] C.F. Maguire,[49] Y.I. Makdisi,[5] A. Malakhov,[17] V.I. Manko,[23] Y. Mao,[7,38] G. Martinez,[45] M.D. Marx,[44] H. Masui,[48] F. Matathias,[44] T. Matsumoto,[8,50] P.L. McGaughey,[27] E. Melnikov,[15] F. Messer,[44] Y. Miake,[48] J. Milan,[43] T.E. Miller,[49] A. Milov,[44,51] S. Mioduszewski,[5] R.E. Mischke,[27] G.C. Mishra,[13] J.T. Mitchell,[5] A.K. Mohanty,[4] D.P. Morrison,[5] J.M. Moss,[27] F. Mühlbacher,[44] D. Mukhopadhyay,[51] M. Muniruzzaman,[6] J. Murata,[38,39] S. Nagamiya,[20] J.L. Nagle,[9] T. Nakamura,[14] B.K. Nandi,[6] M. Nara,[48] J. Newby,[46] P. Nilsson,[29] A.S. Nyanin,[23] J. Nystrand,[29] E. O'Brien,[5] C.A. Ogilvie,[16] H. Ohnishi,[5,38] I.D. Ojha,[49,3] K. Okada,[38] M. Ono,[48] V. Onuchin,[15] A. Oskarsson,[29] I. Otterlund,[29] K. Oyama,[8] K. Ozawa,[8] D. Pal,[51] A.P.T. Palounek,[27] V. Pantuev,[44] V. Papavassiliou,[34] J. Park,[42] A. Parmar,[33] S.F. Pate,[34] T. Peitzmann,[30] J.-C. Peng,[27] V. Peresedov,[17] C. Pinkenburg,[5] R.P. Pisani,[5] F. Plasil,[35] M.L. Purschke,[5] A.K. Purwar,[44] J. Rak,[16] I. Ravinovich,[51] K.F. Read,[35,46] M. Reuter,[44] K. Reygers,[30] V. Riabov,[37,40] Y. Riabov,[37] G. Roche,[28] A. Romana,[25,*] M. Rosati,[16] P. Rosnet,[28] S.S. Ryu,[52] M.E. Sadler,[1] N. Saito,[38,39] T. Sakaguchi,[8,50] M. Sakai,[32] S. Sakai,[48] V. Samsonov,[37] L. Sanfratello,[33] R. Santo,[30] H.D. Sato,[24,38] S. Sato,[5,48] S. Sawada,[20] Y. Schutz,[45] V. Semenov,[15] R. Seto,[6] M.R. Shaw,[1,27] T.K. Shea,[5] T.-A. Shibata,[47,38] K. Shigaki,[14,20] T. Shiina,[27] C.L. Silva,[41] D. Silvermyr,[27,29] K.S. Sim,[22] C.P. Singh,[3] V. Singh,[3] M. Sivertz,[5] A. Soldatov,[15] R.A. Soltz,[26] W.E. Sondheim,[27] S.P. Sorensen,[46] I.V. Sourikova,[5] F. Staley,[10] P.W. Stankus,[35] E. Stenlund,[29] M. Stepanov,[34] A. Ster,[21] S.P. Stoll,[5] T. Sugitate,[14] J.P. Sullivan,[27] E.M. Takagui,[41] A. Taketani,[38,39] M. Tamai,[50] K.H. Tanaka,[20] Y. Tanaka,[32] K. Tanida,[38] M.J. Tannenbaum,[5] P. Tarján,[11] J.D. Tepe,[1,27] T.L. Thomas,[33] A. Toia,[44] J. Tojo,[24,38] H. Torii,[24,38] R.S. Towell,[1] I. Tserruya,[51] H. Tsuruoka,[48] S.K. Tuli,[3] H. Tydesjö,[29] N. Tyurin,[15] J. Velkovska,[5,44] M. Velkovsky,[44] V. Veszprémi,[11] L. Villatte,[46] A.A. Vinogradov,[23] M.A. Volkov,[23] E. Vznuzdaev,[37] X.R. Wang,[13] Y. Watanabe,[38,39] S.N. White,[5] F.K. Wohn,[16] C.L. Woody,[5] W. Xie,[6] Y. Yang,[7] A. Yanovich,[15] S. Yokkaichi,[38,39] G.R. Young,[35] I.E. Yushmanov,[23] W.A. Zajc,[9] C. Zhang,[9] S. Zhou,[7] S.J. Zhou,[51] L. Zolin,[17] R. duRietz,[29] and H.W. vanHecke[27]

(PHENIX Collaboration)

[1] *Abilene Christian University, Abilene, TX 79699, USA*
[2] *Institute of Physics, Academia Sinica, Taipei 11529, Taiwan*
[3] *Department of Physics, Banaras Hindu University, Varanasi 221005, India*
[4] *Bhabha Atomic Research Centre, Bombay 400 085, India*
[5] *Brookhaven National Laboratory, Upton, NY 11973-5000, USA*
[6] *University of California - Riverside, Riverside, CA 92521, USA*

[7]China Institute of Atomic Energy (CIAE), Beijing, People's Republic of China
[8]Center for Nuclear Study, Graduate School of Science, University of Tokyo, 7-3-1 Hongo, Bunkyo, Tokyo 113-0033, Japan
[9]Columbia University, New York, NY 10027 and Nevis Laboratories, Irvington, NY 10533, USA
[10]Dapnia, CEA Saclay, F-91191, Gif-sur-Yvette, France
[11]Debrecen University, H-4010 Debrecen, Egyetem tér 1, Hungary
[12]Florida State University, Tallahassee, FL 32306, USA
[13]Georgia State University, Atlanta, GA 30303, USA
[14]Hiroshima University, Kagamiyama, Higashi-Hiroshima 739-8526, Japan
[15]Institute for High Energy Physics (IHEP), Protvino, Russia
[16]Iowa State University, Ames, IA 50011, USA
[17]Joint Institute for Nuclear Research, 141980 Dubna, Moscow Region, Russia
[18]KAERI, Cyclotron Application Laboratory, Seoul, South Korea
[19]Kangnung National University, Kangnung 210-702, South Korea
[20]KEK, High Energy Accelerator Research Organization, Tsukuba-shi, Ibaraki-ken 305-0801, Japan
[21]KFKI Research Institute for Particle and Nuclear Physics (RMKI), H-1525 Budapest 114, POBox 49, Hungary
[22]Korea University, Seoul, 136-701, Korea
[23]Russian Research Center "Kurchatov Institute", Moscow, Russia
[24]Kyoto University, Kyoto 606-8502, Japan
[25]Laboratoire Leprince-Ringuet, Ecole Polytechnique, CNRS-IN2P3, Route de Saclay, F-91128, Palaiseau, France
[26]Lawrence Livermore National Laboratory, Livermore, CA 94550, USA
[27]Los Alamos National Laboratory, Los Alamos, NM 87545, USA
[28]LPC, Université Blaise Pascal, CNRS-IN2P3, Clermont-Fd, 63177 Aubiere Cedex, France
[29]Department of Physics, Lund University, Box 118, SE-221 00 Lund, Sweden
[30]Institut für Kernphysik, University of Muenster, D-48149 Muenster, Germany
[31]Myongji University, Yongin, Kyonggido 449-728, Korea
[32]Nagasaki Institute of Applied Science, Nagasaki-shi, Nagasaki 851-0193, Japan
[33]University of New Mexico, Albuquerque, NM 87131, USA
[34]New Mexico State University, Las Cruces, NM 88003, USA
[35]Oak Ridge National Laboratory, Oak Ridge, TN 37831, USA
[36]IPN-Orsay, Universite Paris Sud, CNRS-IN2P3, BP1, F-91406, Orsay, France
[37]PNPI, Petersburg Nuclear Physics Institute, Gatchina, Russia
[38]RIKEN (The Institute of Physical and Chemical Research), Wako, Saitama 351-0198, JAPAN
[39]RIKEN BNL Research Center, Brookhaven National Laboratory, Upton, NY 11973-5000, USA
[40]St. Petersburg State Technical University, St. Petersburg, Russia
[41]Universidade de São Paulo, Instituto de Física, Caixa Postal 66318, São Paulo CEP05315-970, Brazil
[42]System Electronics Laboratory, Seoul National University, Seoul, South Korea
[43]Chemistry Department, Stony Brook University, SUNY, Stony Brook, NY 11794-3400, USA
[44]Department of Physics and Astronomy, Stony Brook University, SUNY, Stony Brook, NY 11794, USA
[45]SUBATECH (Ecole des Mines de Nantes, CNRS-IN2P3, Université de Nantes) BP 20722 - 44307, Nantes, France
[46]University of Tennessee, Knoxville, TN 37996, USA
[47]Department of Physics, Tokyo Institute of Technology, Tokyo, 152-8551, Japan
[48]Institute of Physics, University of Tsukuba, Tsukuba, Ibaraki 305, Japan
[49]Vanderbilt University, Nashville, TN 37235, USA
[50]Waseda University, Advanced Research Institute for Science and Engineering, 17 Kikui-cho, Shinjuku-ku, Tokyo 162-0044, Japan
[51]Weizmann Institute, Rehovot 76100, Israel
[52]Yonsei University, IPAP, Seoul 120-749, Korea

(Dated: February 1, 2008)

Longitudinal density correlations of produced matter in Au+Au collisions at $\sqrt{s_{NN}} = 200$ GeV have been measured from the inclusive charged particle distributions as a function of pseudorapidity window sizes. The extracted $\alpha\xi$ parameter, related to the susceptibility of the density fluctuations in the long wavelength limit, exhibits a non-monotonic behavior as a function of the number of participant nucleons, N_{part}. A local maximum is seen at $N_{part} \sim 90$, with corresponding energy density based on the Bjorken picture of $\epsilon_{Bj}\tau \sim 2.4$ GeV/(fm$^2\cdot c$) with a transverse area size of 60 fm^2. This behavior may suggest a critical phase boundary based on the Ginzburg-Landau framework.

PACS numbers: 25.75.Dw

*Deceased

†PHENIX Spokesperson: jacak@skipper.physics.sunysb.edu

I. INTRODUCTION

Theoretical studies of Quantum Chromodynamics (QCD) in non-perturbative regimes indicate that QCD matter has a rich phase structure [1]. The phase diagram can be parameterized by temperature T and baryo-chemical potential μ_B. Based on the phase diagram, we can obtain perspectives on how the vacuum structure of the early universe evolved in extremely high temperature states after the Big Bang as well as what happens in extremely high baryon density states such as in the core of neutron stars. Therefore, a comprehensive and quantitative understanding of the QCD phase diagram is one of the most important subjects in modern nuclear physics. At a minimum we expect the phase diagram to exhibit at least two distinct regions: the deconfined phase where the basic degrees of freedom of QCD, quarks and gluons, emerge; and the hadron phase where quarks and gluons are confined. There is a first order phase boundary at $\mu_B > 0$ and $T = 0$ [2, 3, 4, 5, 6, 7, 8, 9]. At $\mu_B = 0$ and $T > 0$ a smooth crossover transition is expected due to finite masses of quarks [10]. Logically we can then expect that a critical end-point (CEP) exists at the end of the first order phase transition line [11]. The location of the CEP would be a landmark in understanding the whole structure of the phase diagram. Although numerical calculations using lattice gauge theory, as well as model calculations, predict the existence of the CEP, none of them have reached a quantitative agreement on the location at present precision [1]. Therefore experimental investigations are indispensable to pin down the location, and to establish properties of the phase point based on fundamental observables.

Strongly interacting, high-density matter has been created in nucleus-nucleus collisions at Relativistic Heavy Ion Collider (RHIC) at Brookhaven National Laboratory (BNL) [12]. Strong suppression of hadrons at high transverse momentum (p_T) observed in central Au+Au collisions at $\sqrt{s_{NN}} = 200$GeV at RHIC indicate creation of high density matter [13, 14]. Strong elliptic flow indicates that the matter thermalizes rapidly and behaves like a fluid with very low viscosity [15]. Furthermore, the valence quark number scaling of elliptic flow suggests that quark-like degrees of freedom are pertinent in the evolution of the flow [16]. Those observations naturally lead us to the expectation that the initial thermalized state of matter is at $T > T_c$ in central Au+Au collisions, and possibly at $T < T_c$ in the most peripheral collisions. Therefore a system with initial $T = T_c$ may exist somewhere between peripheral and central collisions.

Since there could be different T_c's depending on order parameters in the crossover transition [17], it is worth measuring different kinds of order parameters. It is known that density correlations in matter are robust observables for critical temperatures in general [18]. The order parameter we will focus on here is spatial density fluctuations. Following the Ginzburg-Landau (GL) framework [19] we expect a correlation between fluctuations in density at different points which lead to a two-point correlation function of the form of $\alpha e^{-r/\xi}$, where r is the one dimensional distance, α is the strength of the correlation, and $\xi \propto |T - T_c|^{-1/2}$ is the spatial correlation length. This functional form can be derived from the GL free energy density by expanding it with a scalar order parameter which is small enough (see Appendix A). A large increase of ξ near T_c can be a good indicator for a phase transition. In addition to ξ itself, the product $\alpha\xi$ can also be a good indicator of a phase transition. As shown in Sec. II, $\alpha\xi$ behaves as $|1 - T_c/T|^{-1}$. In the GL framework, this quantity is related to the medium's susceptibility in the long wavelength limit. (See Appendix A for the derivation). The matter produced in the collision expands longitudinally from its earliest time, which leads to cooling after the initial thermalization. If the system's evolution takes it near a critical point as it cools, then the large correlated density fluctuations will appear as T approaches T_c from above. If the expansion after that point is rapid enough then these fluctuations can potentially survive into the final state [20].

Experimentally, spatial density fluctuations in longitudinal space z in the early stage of an $A + A$ collision at RHIC can be measured as the density fluctuation in rapidity, or pseudorapidity, space in the final state. The differential length dz between neighboring medium elements at a common proper time $\tau = \sqrt{t^2 - z^2}$ is expressed as $dz = \tau \cosh(y) dy$, where y is rapidity. If we limit the study to only a narrow region around midrapidity, then $dz \sim \tau dy$ is valid with the approximation of $\cosh(y) \sim 1$. Therefore we can observe density fluctuation in z coordinate as being mapped onto density fluctuations in rapidity space. In the region around midrapidity used in this analysis we can approximate rapidity by pseudorapidity (η) for inclusive charged particles, since the mean $\langle p_T \rangle$ ($\langle p_T \rangle$=0.57 GeV/c $\gg m_\pi$) observed in $\sqrt{s_{NN}} = 200$GeV collisions at RHIC is so high.

In this paper we measure charged particle density correlations in pseudorapidity space to search for the critical phase boundary in Au+Au collisions at $\sqrt{s_{NN}} =$ 200GeV. The density correlation is extracted from inclusive charged particle multiplicity distributions measured as a function of pseudorapidity window size $\delta\eta$. Negative Binomial Distributions (NBD) are fit to the measured multiplicity distributions, and the NBD parameters μ (mean) and k^{-1} (deviation from a Poissonian width) are determined. The product of the correlation strength α and the correlation length ξ is extracted from a known relation between the product of $\alpha\xi$ and the NBD k parameter as a function of $\delta\eta$. We expect a monotonic correspondence between initial temperature and measured energy density based on Bjorken picture [21] which in turn has a monotonic relation with the number of participant nucleons N_{part} in a collision [22]. Thus the critical behavior of $\alpha\xi$ near T_c can be observed as a non-monotonic increase as a function of N_{part}.

It is worth noting that most of experimentally accessible points on the phase diagram are neither phase boundaries nor the end-point. Therefore, before searching for a special phase point such as CEP based on particular theoretical assumptions, we would rather observe and define phase boundaries by general methods. The application of the GL framework for density correlations far from T_c provides this approach. It is known that the GL framework is not applicable directly at $T = T_c$ because the fluctuations become too large to be described consistently. The correlation length ξ can not be defined at T_c, where many length scales from small to large emerge. This is the origin of the power law behavior, or fractal nature of fluctuations at the critical phase boundary. However, in the regions relatively far from T_c, the fluctuations are naturally expected to be small. Therefore the GL approach is suitable in the nuclear collision environment as long as the system approaches a phase boundary from a thermalized state with T well above T_c. As a future prospect, once we define a phase boundary even in the crossover region, we can further investigate the characteristic nature of the phase point, such as critical exponents based on the chiral condensate [23, 24, 25] along the phase boundary, to judge whether the point corresponds to CEP or not.

The organization of this paper is as follows. Sec. II provides the exact definition of the experimental observables mentioned briefly above. Sec. III describes the PHENIX detector used to make the measurements. Sec. IV describes the event samples used for this analysis and the method for corrections applied to the measured multiplicity fluctuations. The systematic errors on the measured fluctuations are also explained in this section. In Sec. V, fit results of the NBD parameters in each collision centrality and pseudorapidity window size are presented, and the behaviors of the $\alpha\xi$ product as a function of N_{part} are presented. In Sec. VI, in addition to the discussion on the observed N_{part} dependence of $\alpha\xi$, other possible sources of correlation between inclusive charged particles are discussed. The relation between the measured energy density and N_{part} is discussed to relate N_{part} to the initial temperature. Conclusions are given in Sec. VII. In Appendix A, the density correlation length and susceptibility are exactly defined based on the GL framework. Finally, in Appendix B all measured NBD parameters in all collision centralities are tabulated.

II. EXPERIMENTAL OBSERVABLES

In this analysis the density fluctuation will be discussed via charged particle multiplicity distributions as a function of the pseudorapidity window size for each collision centrality or N_{part} range.

It is known that the charged particle multiplicity distributions are empirically well described by the Negative Binomial Distribution (NBD) in $A + A$, $p + p$ and e^+e^- collisions [26]. The distribution is expressed as

$$P_{k,\mu}(n) = \frac{\Gamma(n+k)}{\Gamma(n-1)\Gamma(k)} \left(\frac{\mu/k}{1+\mu/k}\right) \frac{1}{1+\mu/k}, \quad (1)$$

Here μ is the mean of the distribution and k^{-1} corresponds to the difference between its width and that of a Poisson with that mean. Thus the NBD coincides with the Poisson distribution in the case of $k = \infty$, and with the Bose-Einstein distribution in the case of $k = 1$. In this sense, the NBD k directly reflects the degree of correlation between the particles produced into the experimental window.

We can relate the k parameter for the multiplicity distribution within an η window to the correlation between phase-space densities in different η windows. Specifically k can be mathematically related with the second order normalized factorial moment F_2

$$k^{-1} = F_2 - 1 \quad (2)$$

where F_2 corresponds the integrated two-particle correlation function, which can be expressed as [27]

$$\begin{aligned} F_2(\delta\eta) &= \frac{\langle n(n-1)\rangle}{\langle n\rangle^2} = \frac{\iint^{\delta\eta} \rho_2(\eta_1,\eta_2) d\eta_1 d\eta_2}{\{\int^{\delta\eta} \rho_1(\eta) d\eta\}^2} \\ &= \frac{1}{(\delta\eta)^2} \iint^{\delta\eta} \frac{C_2(\eta_1,\eta_2)}{\bar{\rho_1}^2} d\eta_1 d\eta_2 + 1, \end{aligned} \quad (3)$$

where n is the number of produced particles and $\delta\eta$ is the pseudorapidity window size inside which the multiplicities are measured. In Eq. (3) we introduced one- and two-particle inclusive multiplicity densities ρ_1 and ρ_2 based on the inclusive differential cross section relative to the total inelastic cross section σ_{inel} as follows [26]

$$\begin{aligned} \frac{1}{\sigma_{inel}} d\sigma &= \rho_1(\eta) d\eta, \\ \frac{1}{\sigma_{inel}} d^2\sigma &= \rho_2(\eta_1,\eta_2) d\eta_1 d\eta_2. \end{aligned} \quad (4)$$

Here $\bar{\rho_1}$ is the average density per unit length within $\delta\eta$ which is defined as

$$\bar{\rho_1} = \frac{1}{\delta\eta} \int^{\delta\eta} \rho_1(\eta) d\eta. \quad (5)$$

With these densities, the two particle density correlation function is defined as

$$C_2(\eta_1,\eta_2) = \rho_2(\eta_1,\eta_2) - \rho_1(\eta_1)\rho_1(\eta_2). \quad (6)$$

Instead of measuring C_2 or F_2 directly, in this analysis we extract the NBD k parameter as a measure of particle correlations over η. This is partly for historical reasons [28], but also because, as shown in Sec. IV, we can correct the measurement of k for the detector imperfections in a very robust way by using a statistical property of NBD, while the same correction made at the level of

F_2 would require additional information on the parent distribution.

The normalized two particle correlation function C_2 in the experiment can be parametrized as follows, based on the one-dimensional functional form obtained in the GL framework (see Eq. (A8)):

$$\frac{C_2(\eta_1,\eta_2)}{\bar{\rho_1}^2} = \alpha e^{-|\eta_1-\eta_2|/\xi} + \beta, \quad (7)$$

where $\bar{\rho_1}$ is proportional to the mean multiplicity in each collision centrality bin, or range of N_{part}, and the scale factor α is the strength of the correlations at the zero separation. The constant term β arises from any kind of experimental and physical correlations which are independent of the pseudorapidity separation, such as the residual effect of finite centrality binning.

Further, one has to take into account the fact that the damping behavior in Eq. (A8) is caused only by the spatial inhomogeneity of the system at a fixed temperature. In realistic collisions and event samples there is no single relevant temperature. For instance, finite centrality binning adds together a range of fluctuations originating from collisions with different N_{part}. However, in principle these centrality-correlated fluctuations are independent of the thermally-induced spatial fluctuations. In addition, although the self correlation at the zero distance between two sub-volumes in Eq. (A6) was excluded, the self correlation cannot be excluded in the integrated two particle correlation function contained in Eq. (3). We have tried various kind of functional forms for C_2 which contained power terms and also plural correlation lengths. However, we found empirically that just adding the constant term in Eq. (7) produced the best fit results to all data points.

Finally, the relation between the NBD k parameter and the pseudorapidity window size $\delta\eta$ can be obtained by the substitution of Eq. (7) into Eq. (3) [28, 29]

$$k^{-1}(\delta\eta) = F_2 - 1 = \frac{2\alpha\xi^2(\delta\eta/\xi - 1 + e^{-\delta\eta/\xi})}{\delta\eta^2} + \beta. \quad (8)$$

In the limit of $\xi \ll \delta\eta$, which we believe holds in this analysis, Eq. (8) can be approximated as

$$k(\delta\eta) = \frac{1}{2\alpha\xi/\delta\eta + \beta} \quad (\xi \ll \delta\eta), \quad (9)$$

where experimentally we can not resolve α and ξ separately, but the product $\alpha\xi$ can be directly determined. The product is related to the susceptibility in the long wavelength limit, $\chi_{\omega=0} \propto |T - T_c|^{-1}$ for a given temperature T based on Eq. (A11). Combined with the parametrization in Eq. (7), the $\alpha\xi$ product should then follow

$$\alpha\xi \propto \bar{\rho_1}^{-2} \frac{1}{|1 - T_c/T|}. \quad (10)$$

Since we expect that $\bar{\rho_1}$ is a monotonic function of T, in the limit of T far from T_c, $\alpha\xi$ should vary monotonically as a function of T. However, if T approaches T_c, the $\alpha\xi$ product will show a singular behavior. Therefore, any non-monotonic increase of $\alpha\xi$ could be an indication of $T \sim T_c$ near a critical point. If the experimental bias term β is excluded in Eq. (9), the slope in k versus $\delta\eta$ thus contains crucial information on the phase transition.

It is worth mentioning that in this method, correlations on scales even smaller than the minimum $\delta\eta$ window can be meaningfully discussed based on the differences of the NBD k as a function of $\delta\eta$ window sizes, since the correlations are always integrated from the limit of the detector resolution to $\delta\eta$ window size.

III. PHENIX DETECTOR

PHENIX is one of four experiments operating at RHIC [30]. The PHENIX detector has two central spectrometer arms, denoted East and West. Each central arm covers the pseudorapidity range $|\eta| < 0.35$ and subtends an azimuthal angle range $\Delta\phi$ of $\pi/2$ around the beam axis (z direction). PHENIX includes global detectors which provide information for event triggers as well as measurement of collision points along the beam axis and collision centralities. A detailed description of the PHENIX detector can be found in [30]. The detector subsystems relevant for this analysis will be briefly explained below.

Charged particles are measured by a drift chamber (DC) and two multi-wire chambers with pad readout (PC1 and PC3) located at 2.2, 2.5 and 5 m from the beam axis in the East arm, respectively. The collision vertex points were measured using the time difference between two Beam-Beam Counters (BBC) located at z = +144 cm (north side) and z = -144 cm (south side) from the nominal interaction point (IP) along the beam line, which cover pseudorapidity ranges of $3.0 < \eta < 3.9$ (north) and $-3.9 < \eta < -3.0$ (south), respectively. Each BBC has 64 Čerenkov counter elements with the typical time resolution of 50 ps. Combined with BBC's, two Zero Degree Calorimeters (ZDC) were further used. The ZDC's are designed to measure energies of spectator neutrons within a cone of 2 mrad around the beam axis. The two ZDC's are located at z = ± 18.25 m from IP, respectively. The Au+Au minimum bias trigger and collision centralities were provided by combining information from both BBC's and ZDC's.

IV. DATA ANALYSIS

A. Run and Event selection

We have used data taken in Au+Au collisions at $\sqrt{s_{NN}}$ = 200 GeV with the magnetic field off condition during RHIC Run-2 in 2002, in order to optimize acceptance for the low p_T charged particles. The basic trigger required coincident hits in the two BBC's (equal

or more than two hit Čerenkov elements in each side) and the two ZDC's (equal or more than one neutron in each side). The efficiency of this minimum-bias trigger is estimated as $92.2^{+2.5}_{-3.0}$% to the total Au+Au inelastic cross section by the Monte Carlo (MC) simulation based on the Glauber model [13]. Events with collision points within ± 5 cm from the nominal IP as measured by the BBC were analyzed. In total, 258k events taken by the minimum-bias trigger were used in this analysis. We have rigorously checked the detector stability by looking at multiplicity correlations between the relevant sub-detector systems, as well as by monitoring positions of inefficient areas over the span of the analyzed dataset. We allowed 2% fluctuation on the average multiplcity of measured number of charged tracks in entire analyzed run ranges.

B. Track selection

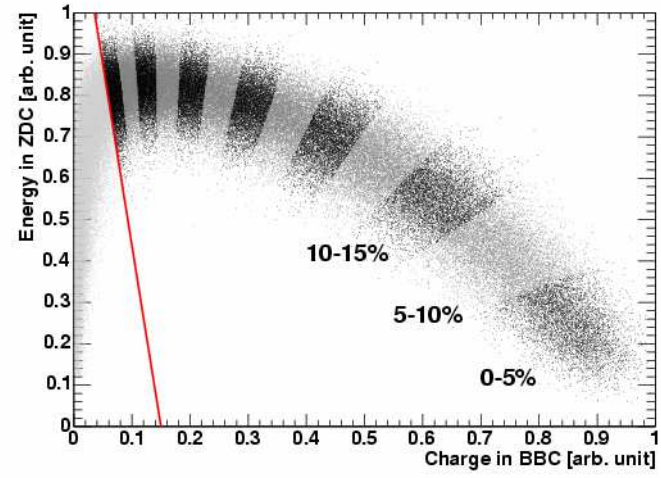

FIG. 1: (Color online) Definition of collision centrality, BBC charges versus ZDC energy. Event samples in 5% bin width are plotted from 0 - 5% (central) to 60 - 65% (peripheral). The solid line indicates the limit of the most peripheral sample used for this analysis.

In this analysis, charged tracks detected in the East arm ($|\eta| < 0.35$, $\Delta\phi < \pi/2$) were used. As charged track selection criteria, we required that each straight-line track reconstructed by a DC hit pattern associated with a PC1 hit be aligned with a PC3 hit and the collision vertex point measured by BBC. We required associations between DC tracks and PC3 hits to be within 10 cm in the distance of closest approach (DCA), which was determined to minimize the random associations. The DC has six types of wire modules; two of them are used for the track reconstruction for the azimuthal angle and others are used for the pattern recognition. Selected tracks were reconstructed by using all wire modules of DC.

In addition to the single track selection, we required a minimum two-track separation in order to minimize effects from fake tracks and associated secondary particles. When we find tracks within the minimum separation window of $\delta\eta < 0.001$ and $\delta\phi < 0.012$ rad, we count them as one track independent of the number of reconstructed tracks in the window. These cut values were determined by looking at $\delta\eta$ and $\delta\phi$ distributions on the $\eta-\phi$ plane of any two track pairs in the real data sample. The DC track resolution of 2 mm in the z direction at a reference radius of 220 cm from the beam axis corresponds to 1.0×10^{-3} in η. PC1 and PC3, which are used for the track association, have the same solid angle each other, and these pixel sizes are 8.4 mm and 14.7 mm, respectively. These pixel sizes are greater than the requirement of two-track separation cuts, however, these resolutions are 1.7 mm and 3.6 mm for PC1 and PC3 respectively in z direction, and these values also corresponds to 1.0×10^{-3} in η. The resolution in ϕ is 1 mrad, but the maximum drift length in DC corresponds to 0.012 rad. Therefore the two-track separation window size in η and ϕ is consistent with what is expected.

In the case of normal magnetic field condition at the PHENIX detector, which is used to identify the charged particles, the threshold transverse momenta p_T correspond to 0.2 GeV/c, 0.4 GeV/c and 0.6 GeV/c for charged pions $\pi^{\pm}$, charged kaons $K^{\pm}$ and protons p(antiprotons $\bar{p}$), respectively [31]. Since this analysis used the data taken without magnetic field, the threshold transverse momenta p_T can be lowered to 0.1 GeV/c, 0.25 GeV/c and 0.35 GeV/c for $\pi^{\pm}$, $K^{\pm}$ and $p(\bar{p})$, respectively. They were estimated by the GEANT-based Monte Carlo (MC) [32] simulation by requiring the equivalent single track selection criteria. The average transverse momentum p_T for the detected inclusive charged particles used in this analysis corresponds to 0.57 GeV/c, which was also estimated by using the measured p_T spectra [31] with the MC simulation. Therefore, the difference of the rapidity and pseudorapidity is at most 3% at the edge of the PHENIX acceptance.

C. Centrality definition and the number of participant nucleons N_{part}

The collision centrality was determined by looking the correlation between a deposited charge sum in both north and south BBC's and an energy sum in both ZDC's on an event-by-event basis. As shown in Fig. 1, the centrality percentile is defined as the fraction of the number of events in a selected centrality bin on the correlation plot to the total number of minimum bias events, corrected for the min-bias trigger efficiency. Each axis is normalized to its maximum dynamic range. As the standard centrality definition, we adopt 5% centrality bin width from 0 - 5%(central) to 60 - 65%(peripheral) as indicated in the figure. The lower limit of 65% is indicated by the solid line in the figure. In the following analysis, as control samples, we also adopt 10% bin width by merging two 5% bin width samples from 0 - 10% to 50 - 60% and

from 5 - 15% to 55 - 65%. The latter is referred to as a 5% shifted 10% bin width. It is worth noting that the change of the centrality bin width shifts the mean values in the charged particle multiplicity distributions, which becomes a strict systematic check on parameter extractions with different event ensembles, even with the same total event sample.

Mapping the centralities to the number of participant nucleons, N_{part}, is based on the Glauber model, which is described in detail in [22]. The quoted mean N_{part} and its error can be obtained from [31]. In only the 5% shifted 10% bin width case, the mean N_{part} and its error were evaluated by averaging two 5% centrality bins and estimated from its error propagations, respectively.

D. Measurement of multiplicity distributions of charged particles

Multiplicity distributions of charged particles were measured while changing the pseudorapidity window size $\delta\eta$ from 0.066 to 0.7 with a step size of $0.7/2^5 = 0.022$. For a given pseudorapidity window size, the window position in the pseudorapidity axis was shifted by a step of $0.7/2^8 = 0.0027$ as long as the window is fully contained within the PHENIX acceptance of $|\eta| < 0.35$. For each window position NBD fits were performed to the multiplicity distributions. Biases originating from inefficient detector areas were corrected with the procedure explained in Sec. IV E. Since even corrected NBD k parameters are not necessarily equal in the case of extremely inefficient window positions, we have truncated window positions where the reconstruction efficiency is below 50%. This truncation is mainly to exclude biases from the largest hole in the middle of the charged particle detector as shown in Fig. 2 (a) and (c). After the truncation, we obtained weighted mean of corrected NBD parameters ($\langle\mu_c\rangle$, $\langle k_c\rangle$) for a given window size, which are defined as

$$\begin{aligned}\langle\mu_c\rangle &\equiv \sum_{i=1}^{n} \delta{\mu_{c_i}}^{-2}\mu_{ci} / \sum_{i=1}^{n} \delta{\mu_{c_i}}^{-2}, \\ \langle k_c\rangle &\equiv \sum_{i=1}^{n} \delta{k_{c_i}}^{-2}k_{ci} / \sum_{i=1}^{n} \delta{k_{c_i}}^{-2}, \end{aligned} \tag{11}$$

where n is the number of valid window positions after the truncation and δ indicates errors on fitting parameters by the Minuit program [33] in each window position i. We have performed this procedure in each centrality bin with 5% and 10% centrality bin width, respectively.

The lower limit of 0.066 was determined so that small window sizes, where corrected NBD k was seen to depend heavily on window position, are all excluded. The lower limit is common for all centrality bins.

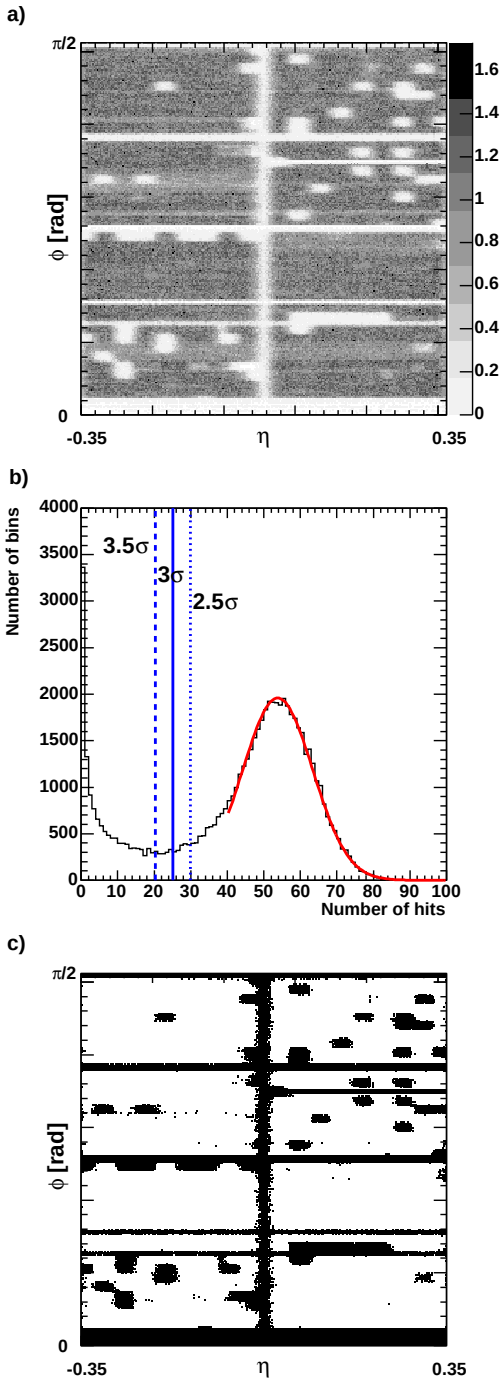

FIG. 2: (Color online) 2-dimensional dead map definitions. a) Track projection points onto the $\eta - \phi$ plane in the data after all track selections. The scale is normalized to the mean number of hits in the peak position in b). b) The number of bins among subdivided $2^8 \times 2^8$ bins as a function of the accumulated number of hits over the total event sample. c) Definition of the central dead map by excluding the detector region below 3 σ, where black parts are identified as dead areas.

E. Correction of NBD k and μ

Any dead or inefficient areas in the detector have been identified and the bias on the NBD parameters has been corrected based on a suitable statistical property of NBD. Maps of dead areas were produced from the track projection points onto the $\eta - \phi$ plane in the data after the track selections, as shown in Fig. 2 a), where the detector acceptance is divided into $2^8 \times 2^8$ bins in the $\eta - \phi$ plane. The accumulated number of hits over the total event sample in each bin is shown by a gray scale reflecting the statistical weights. The scale is normalized to the mean number of hits in the peak position shown in Fig. 2 b). Figure 2 b) shows the number of bins among subdivided $2^8 \times 2^8$ bins as a function of the accumulated number of hits over the total event sample in each $1/2^8 \times 1/2^8$ acceptance. If there were no dead or inefficient area, a binomial distribution is expected with a probability of $1/2^8 \times 1/2^8$ to the total acceptance. For the binomial part, we took a $\pm$ 3 σ region. On the other hand, if there are any dead or inefficient areas they tend to contaminate the lower tail of the binomial distribution. We defined a central dead map by excluding detector region below 3 σ as shown in Fig. 2 c) where black indicates regions that are identified as dead areas. The fraction of good area corresponds to 78% of the total acceptance. This map was used to completely suppress particles which hit the dead areas in the real data.

As long as the baseline distribution is approximated as an NBD, which is certainly true as observed in E802 [28] and in the present analysis, one can estimate the relation between true k values of the NBD and biased k values due to dead or inefficient areas based on the convolution theorem of NBD. For two independent NBD's with (μ_1, k_1) and (μ_2, k_2), it is known that the convolution of the two NBD's is an NBD with (μ_c, k_c), which satisfies relations as

$$\begin{aligned} k_c &= k_1 + k_2, \\ \mu_c &= \mu_1/k_1(k_1 + k_2), \end{aligned} \tag{12}$$

where $\mu_1/k_1 = \mu_2/k_2$ holds [34, 35]. Therefore the correction can be applied by multiplying a ratio of the total number of $\eta - \phi$ bins in a given η window size to the number of bins excluding dead area, as the geometrical acceptance corrections can be applied.

Strictly speaking we can not completely reproduce the original k by this correction, since NBD's in different positions are not completely independent. However, except for the large hole which is already excluded by the truncation, small holes are scattered rather uniformly in azimuthal direction for any position of the $\delta\eta$ windows. As the simplest overall correction to each window position, we applied the convolution theorem [34, 35] by assuming collection of independent NBD sources. As long as the correction is applied in the same manner for all the azimuthal holes, it does not greatly affect the differential measurement to the pseudorapidity space. If the correction is accurate enough, we can expect a constancy of the corrected k values which should be independent of the fraction of dead areas. Based on the degree of constancy of corrected k as a function of the fraction of dead areas in each window position for a given $\delta\eta$ window size, the incompleteness of the correction in each window size has been checked. As briefly mentioned in the last paragraph of Sec. IV D, the window sizes to be analyzed were determined so that systematic error bands on $\langle k_c \rangle$ explained in Sec. IV F, can contain the most of the corrected k values independently of the fraction of dead areas in each window position.

F. Statistical and systematic errors

As a convolution of statistical errors, we adopted errors on weighted mean values ($\delta\langle\mu_c\rangle$, $\delta\langle k_c\rangle$) on corrected NBD parameters after the window truncation mentioned in Sec. IV D, which are defined as

$$\begin{aligned} \delta\langle\mu_c\rangle^2 &\equiv \frac{\delta\bar{\mu_{ci}}^2}{n_{ind}}, \\ \delta\langle k_c\rangle^2 &\equiv \frac{\delta\bar{k_{ci}}^2}{n_{ind}}, \end{aligned} \tag{13}$$

where $\delta\bar{\mu_{ci}}$ and $\delta\bar{k_{ci}}$ are respectively defined as $\sum_{i=1}^{n} \delta\mu_c/n$ and $\sum_{i=1}^{n} \delta k_c/n$ with the number of valid window positions n after the truncation and $n_{ind} \equiv 0.75/\delta\eta$ is the number of statistically independent window positions for a given $\delta\eta$ window size. This statistical error on $\delta\langle k_c\rangle$ is referred to as $\delta\langle k_c\rangle$ (stat).

The dominant sources of systematic errors for the correlation length measurement are the correction procedure with dead maps and the two-track separation cuts, since both introduce unphysical correlations. We have allowed 2% fluctuation on the average multiplicity of measured number of charged tracks. This fluctuation is also a result of dead channels in the tracking detectors discussed in Sec. IV B. In order to estimate this, we defined two more patterns of dead maps with the definition of 3 $\sigma \pm 0.5$ σ as indicated in Fig. 2 c). The deviation of $\langle k_c\rangle$ from the central dead map definition is referred to as $\delta\langle k_c\rangle$ (dead), which corresponds to 3.4% typically.

The two-track separation cut serves mainly to reject fake track effects; these are dominantly observed in the ϕ direction rather than η, since the PC1 hit requirement fixes z positions along the beam axis. Therefore, the effect of the $\delta\phi$ cut was estimated as $\pm$ 0.002 rad around the central cut value of 0.012 rad with a fixed cut value on $\delta\eta$ of 0.001. The deviation of $\langle k_c\rangle$ from the central value due to the fake track rejection cut is referred to as $\delta\langle k_c\rangle$ (fake). This systematic error increases at higher centrality bins, and is estimated as 5.8% and 0.3% at 0 - 5% and 60 - 65% centrality bins, respectively.

The $\langle k_c\rangle$ (stat) is related to agreement between multiplicity distributions and NBD. The $\langle k_c\rangle$ (dead) and $\langle k_c\rangle$ (fake) depends on the position of the window and

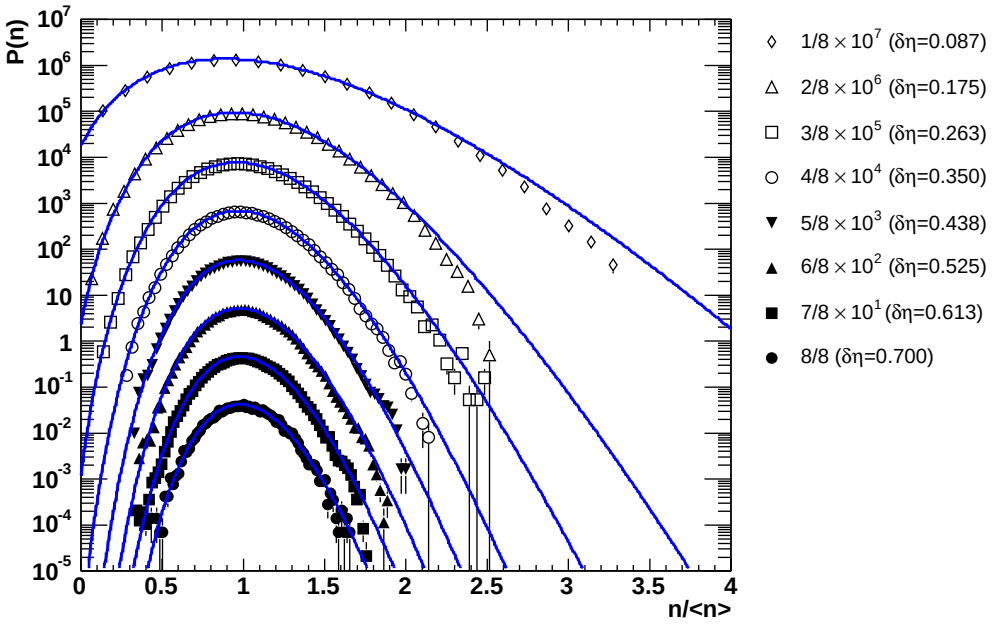

FIG. 3: (Color online) Uncorrected charged particle multiplicity distributions in each pseudorapidity window size, as indicated in the legend, at 0 - 10% collision centrality. The distributions are shown as a function of the number of tracks n normalized to the mean multiplicity $\langle n\rangle$ in each window. The error bars show the statistical errors. The solid curves are fit results of NBD.

the average multiplicity in a selected centrality bin, respectively. By treating these contributions as independent systematic error sources, the total systematic error $\delta\langle k_c\rangle$ (total) on $\langle k_c\rangle$ in each $\delta\eta$ in each centrality, was obtained by the quadratic sum over $\delta\langle k_c\rangle$ (stat), $\delta\langle k_c\rangle$ (dead) and $\delta\langle k_c\rangle$ (fake).

V. RESULTS

In this section the results of the NBD fits are first tabulated. Then the measured NBD k as a function of the pseudorapidity window sizes in various centrality bins are shown. Lastly, the N_{part} dependences of extracted $\alpha\xi$ product in Eq. (9) are presented.

A. NBD fit

NBD fit results in all window sizes in all centrality bins are summarized in Appendix Table III through Table XXVII where $\langle\mu_c\rangle$ and $\langle\mu\rangle$ are weighted means of corrected and uncorrected μ over all window positions respectively, $\langle k_c\rangle$ and $\langle k\rangle$ are weighted means of corrected and uncorrected k over all window positions, respectively. The $\langle\mu_c\rangle$'s are corrected only for the effect of the detector dead areas as described in Sec. IV E. The mean multiplicities were confirmed to be consistent with the result of the independent analysis by the different method using only PC1 and PC3 [22], after known additional correction factors were taken into account. Statistical errors on weighted means $\delta\langle k_c\rangle$ (stat) are obtained as explained in Sec. IV F. $\langle\chi^2/NDF\rangle$ is the average of reduced χ^2 of NBD fits over all window positions. $\langle NDF\rangle$ is the average of the degree of freedom of NBD fits over all window positions, and the systematic errors $\delta\langle k_c\rangle$ (dead), $\delta\langle k_c\rangle$ (fake) and $\delta\langle k_c\rangle$ (total) are already explained in Sec. IV F.

The mean and r.m.s. of the reduced χ^2 values in the NBD fit over all window positions and all $\delta\eta$ sizes and all centralities were obtained as 0.75 and 0.33 respectively. The mean value corresponds to typically 80% confidence level. Therefore, it is good enough to assume NBD as a baseline multiplicity distribution to obtain the integrated correlation function via the k parameter.

As a demonstration to show how well the NBD fits work, Figure 3 shows the charged particle multiplicity distributions in each pseudorapidity window size in 1/8 fractions of the full rapidity coverage of $|\eta| < 0.35$ with 0 - 10% events in the collision centrality, where the uncorrected multiplicity distributions within the total error bands on $\langle k_c\rangle$ in Appendix Table III are all merged. The distributions are shown as a function of the number of tracks n normalized to the mean multiplicity $\langle n\rangle$ in each window. The error bars show the statistical errors on the merged distributions. The solid curves are fit results with NBD only for the demonstration purpose. The fit results in Appendix Table III through Table XXVII are not obtained from these convoluted distributions whose accuracies are degraded by the convolutions with different μ values due to different detector biases depending on the window positions.

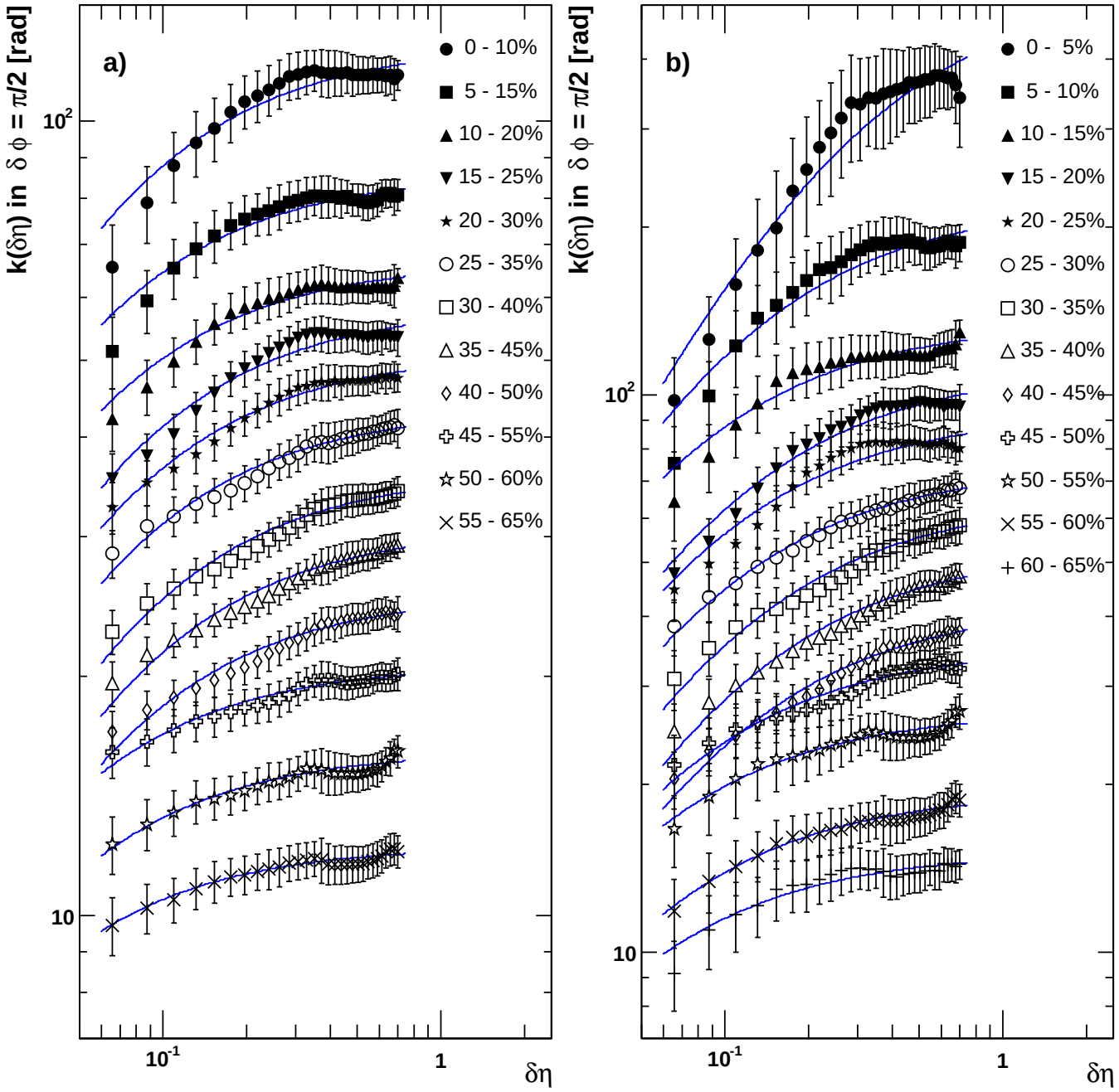

FIG. 4: (Color online) Weighted mean of corrected NBD k, $\langle k_c \rangle$ as a function of pseudorapidity window size with a) 10% and b) 5% centrality bin widths. Centrality classes are indicated in the figure legend. The error bars show $\delta\langle k_c \rangle$ (total), as explained in Sec. IV F. The solid lines indicate the fit curves of Eq. (9).

B. k versus $\delta\eta$

Figures 4 a) and b) show $\langle k_c \rangle$ as a function of pseudorapidity window size with 10% and 5% centrality bin width, respectively. Centrality classes are indicated inside the figures. The error bars show $\delta\langle k_c \rangle$ (total) defined in Sec. IV F. The solid lines in Fig. 4 indicate the fit results based on Eq. (9). The fits were performed in the $\delta\eta$ region from 0.066 to 0.7 as explained in Sec. IV D.

If we could reliably measure the NBD k parameter for arbitrarily small $\delta\eta \sim 0$ windows, then α and ξ could be treated as independent free parameters for each centrality. In the real experimental situation, there is an anti-correlation between α and ξ due to the lack of reliable data points close to $\delta\eta \sim 0$, if we attempt to fit with Eq.(8). However, at least an upper limit on the ab-

solute scale of ξ was obtained as $\xi < 0.035$ by the free parameter fits based on Eq. (8). It is qualitatively consistent with expectation from numerical calculations [36] that the correlation lengths become smaller in the RHIC energy than for $p+p$ collisions [26] and low energy $A+A$ collisions [28].

Since the upper limit of ξ is small enough compared to the fitting region of $\delta\eta$ ($\xi \ll \delta\eta$), Eq. (9) can be applied for the fits to the NBD k as a function of $\delta\eta$. In this case, the $\alpha\xi$ product, which is related to the susceptibility in the long wavelength limit as defined in Eq.(A11), can be obtained by the fits without any physical assumptions. The typical χ^2/NDF in the fit based on Eq. (9) is 0.132, which corresponds to 99% confidence level. Therefore, the small correlation length is confirmed as below the minimum $\delta\eta$ window sizes of 0.066.

As explained in Sec. II for Eq. (9), in the limit of $\beta = 0$, the slopes in k versus $\delta\eta$ have crucial information on the phase transition. In Fig. 4 we can identify different behaviors in slopes around 40-50% centrality region even without fit curves.

C. $\alpha\xi$ product versus N_{part}

Figures 5 a) and b) show the obtained fit parameters β and $\alpha\xi$ with Eq. (9) as a function of N_{part}, where results for both the 5% and 10% centrality bin width cases are plotted as filled and open circles, respectively. The smooth solid and dotted curves are provided to guide the eye. The horizontal error bars correspond to ambiguities on the mean value of N_{part} as explained in Sec. IV C. The vertical error bars are obtained from errors on the fitting parameter by the Minuit program [33].

Table I summarizes the fit results where centralities, corresponding N_{part}, $\alpha\xi$, β and χ^2/NDF obtained by the fit with Eq. (9) are shown for 10% and 5% centrality bin cases respectively.

It should be emphasized that the parametrization in Eq. (7) is practically necessary. The β parameter can absorb any effects independent of pseudorapidity space correlations. For a wider centrality bin, the width of the multiplicity distribution becomes broader, since events with a wider range of centralities are included in the bin. This causes the systematic difference of β in the 5% and 10% centrality data sets as shown in Fig. 5 a). The systematic shift of β parameters to smaller values in the smaller centrality bin width, suggests that β dominantly contains fluctuations on N_{part}. The ambiguity of N_{part}measured by PHENIX is not large compared, for example, to NA49 where a non-monotonic behavior of the scaled variance of multiplicities was seen as a function of the number of projectile participant nucleons [37]. In NA49, only spectators from the projectile nucleus are measurable, causing an increase of scaled variance of multiplicity distributions in peripheral collisions due to dominantly large N_{part}fluctuations in the target nucleus [38]. This is due to the partial sampling with

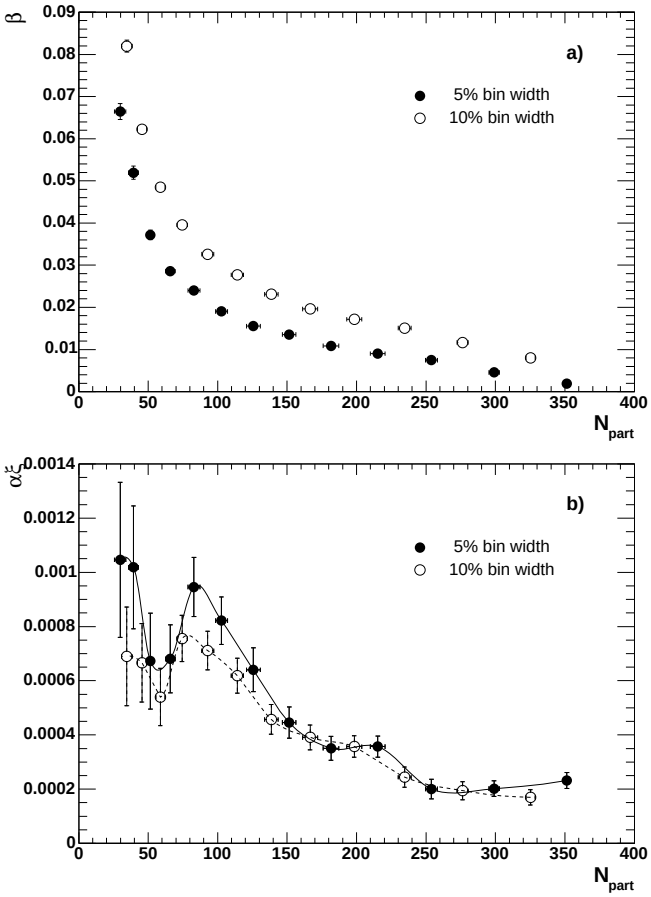

FIG. 5: Fit results based on Eq. (9). a) is β and b) is products of $\alpha\xi$ as a function of N_{part}. The horizontal error bars correspond to ambiguities in the mean value of N_{part} as explained in Sec. IV C. The vertical error bars are obtained from errors on the fitting parameter.

respect to the total number of nucleons in two colliding nuclei. Since both projectile and target nuclei on both sides can be measured by BBC and ZDC at PHENIX, such ambiguities of $N_{part}$are suppressed, even in peripheral collisions. Some N_{part}fluctuations remain, but the β parameter can absorb this kind of fluctuation offset. Consequently, N_{part}fluctuations are not harmful for the measurement of the $\alpha\xi$ products, since they are based on the differential values of fluctuations for a given centrality bin. In addition, β is expected to absorb effects from azimuthal correlations. Since the PHENIX detector does not cover the full azimuthal range, fluctuations of low p_T particles caused by reaction plane rotations and elliptic flow should contribute to the two particle correlation function even in the pseudorapidity direction as an offset in principle. Owing to the β parameter, the non-monotonic behavior of the measured $\alpha\xi$ in the pseudorapidity direction cannot be biased by elliptic flow nor by initial geometrical biases, since the azimuthal correlations are constant over the narrow pseudorapidity window of $|\eta| < 0.35$ [39].

TABLE I: The $\alpha\xi$ and β in Eq. (9) obtained by the fits to $\langle k_c \rangle$ versus $\delta\eta$. Upper and lower column corresponds to 10% and 5% centrality bin width cases, respectively.

Centrality (%)	$\langle N_{part} \rangle$	$\alpha\xi$ ($\propto \chi_{\omega=0}$)	β	χ^2/NDF ($NDF = 27$)
$0-10$	325.2 ± 3.3	$0.17 \times 10^{-3} \pm 0.03 \times 10^{-3}$	$0.80 \times 10^{-2} \pm 0.02 \times 10^{-2}$	0.24
$5-15$	276.4 ± 4.0	$0.19 \times 10^{-3} \pm 0.03 \times 10^{-3}$	$1.17 \times 10^{-2} \pm 0.02 \times 10^{-2}$	0.16
$10-20$	234.6 ± 4.7	$0.24 \times 10^{-3} \pm 0.04 \times 10^{-3}$	$1.51 \times 10^{-2} \pm 0.03 \times 10^{-2}$	0.14
$15-25$	198.4 ± 5.4	$0.36 \times 10^{-3} \pm 0.04 \times 10^{-3}$	$1.72 \times 10^{-2} \pm 0.03 \times 10^{-2}$	0.26
$20-30$	166.6 ± 5.4	$0.39 \times 10^{-3} \pm 0.05 \times 10^{-3}$	$1.96 \times 10^{-2} \pm 0.03 \times 10^{-2}$	0.09
$25-35$	138.6 ± 4.9	$0.46 \times 10^{-3} \pm 0.06 \times 10^{-3}$	$2.31 \times 10^{-2} \pm 0.04 \times 10^{-2}$	0.09
$30-40$	114.2 ± 4.4	$0.62 \times 10^{-3} \pm 0.06 \times 10^{-3}$	$2.77 \times 10^{-2} \pm 0.05 \times 10^{-2}$	0.13
$35-45$	92.8 ± 4.3	$0.71 \times 10^{-3} \pm 0.07 \times 10^{-3}$	$3.26 \times 10^{-2} \pm 0.05 \times 10^{-2}$	0.14
$40-50$	74.4 ± 3.8	$0.76 \times 10^{-3} \pm 0.09 \times 10^{-3}$	$3.96 \times 10^{-2} \pm 0.07 \times 10^{-2}$	0.14
$45-55$	58.8 ± 3.3	$0.54 \times 10^{-3} \pm 0.11 \times 10^{-3}$	$4.85 \times 10^{-2} \pm 0.08 \times 10^{-2}$	0.05
$50-60$	45.5 ± 3.3	$0.67 \times 10^{-3} \pm 0.14 \times 10^{-3}$	$6.22 \times 10^{-2} \pm 0.11 \times 10^{-2}$	0.11
$55-65$	34.6 ± 3.8	$0.69 \times 10^{-3} \pm 0.18 \times 10^{-3}$	$8.19 \times 10^{-2} \pm 0.14 \times 10^{-2}$	0.05
$0-5$	351.4 ± 2.9	$0.23 \times 10^{-3} \pm 0.03 \times 10^{-3}$	$0.19 \times 10^{-2} \pm 0.02 \times 10^{-2}$	0.18
$5-10$	299.0 ± 3.8	$0.20 \times 10^{-3} \pm 0.03 \times 10^{-3}$	$0.46 \times 10^{-2} \pm 0.02 \times 10^{-2}$	0.27
$10-15$	253.9 ± 4.3	$0.20 \times 10^{-3} \pm 0.04 \times 10^{-3}$	$0.75 \times 10^{-2} \pm 0.02 \times 10^{-2}$	0.17
$15-20$	215.3 ± 5.3	$0.36 \times 10^{-3} \pm 0.04 \times 10^{-3}$	$0.90 \times 10^{-2} \pm 0.03 \times 10^{-2}$	0.18
$20-25$	181.6 ± 5.6	$0.35 \times 10^{-3} \pm 0.04 \times 10^{-3}$	$1.08 \times 10^{-2} \pm 0.03 \times 10^{-2}$	0.32
$25-30$	151.5 ± 4.9	$0.45 \times 10^{-3} \pm 0.06 \times 10^{-3}$	$1.35 \times 10^{-2} \pm 0.04 \times 10^{-2}$	0.02
$30-35$	125.7 ± 4.9	$0.64 \times 10^{-3} \pm 0.08 \times 10^{-3}$	$1.55 \times 10^{-2} \pm 0.05 \times 10^{-2}$	0.09
$35-40$	102.7 ± 4.3	$0.82 \times 10^{-3} \pm 0.09 \times 10^{-3}$	$1.90 \times 10^{-2} \pm 0.05 \times 10^{-2}$	0.08
$40-45$	82.9 ± 4.3	$0.95 \times 10^{-3} \pm 0.11 \times 10^{-3}$	$2.40 \times 10^{-2} \pm 0.07 \times 10^{-2}$	0.06
$45-50$	65.9 ± 3.4	$0.68 \times 10^{-3} \pm 0.13 \times 10^{-3}$	$2.86 \times 10^{-2} \pm 0.08 \times 10^{-2}$	0.08
$50-55$	51.6 ± 3.2	$0.67 \times 10^{-3} \pm 0.18 \times 10^{-3}$	$3.72 \times 10^{-2} \pm 0.11 \times 10^{-2}$	0.11
$55-60$	39.4 ± 3.5	$1.02 \times 10^{-3} \pm 0.23 \times 10^{-3}$	$5.19 \times 10^{-2} \pm 0.16 \times 10^{-2}$	0.06
$60-65$	29.8 ± 4.1	$1.05 \times 10^{-3} \pm 0.29 \times 10^{-3}$	$6.64 \times 10^{-2} \pm 0.19 \times 10^{-2}$	0.08

VI. DISCUSSION

A. Other correlation sources

We discuss three other sources of correlation which are not related to density correlations we are interested in, but could affect the measurement of the inclusive charged particle multiplicity fluctuations. The first is charged track pairs from particle decays in flight. The second is background charged track pairs originating from secondary particle interactions in detector materials (i.e. showers, conversion pairs). For these two sources we have estimated the effects of contaminations to the inclusive charged particle multiplicity fluctuations by GEANT-based MC [32] simulations. The third source is the known short-range correlation due to Bose-Einstein correlation of identical particles.

The detectable charged particle compositions in the no magnetic field condition with the selection criteria of charged tracks in Sec. IV B are estimated as 94% for charged pions, 4% for charged kaons and 2% for proton and antiproton in 0 - 70% centrality. These are obtained by MC simulations based on identified charged particle spectra measured by the PHENIX [31] up to 4 GeV/c of transverse momentum, p_T. The statistically dominant weak decay particles which can contribute to the inclusive charged particle multiplicity are $K^0_S \to \pi^+\pi^-$ and $\Lambda(\overline{\Lambda}) \to p(\overline{p})\pi^-(\pi^+)$. The relative invariant yields of those particles to charged pions are 15% and 5% for K^0_S and $\Lambda(\overline{\Lambda})$ [40], respectively. They were calculated by the measured production cross section in Au+Au collisions at $\sqrt{s_{NN}} = 200$ GeV. The production cross section of K^0_S is assumed to be same as charged kaons [31]. The detection efficiency of the charged track pairs from weak decay particles in the one arm acceptance of PHENIX detector ($|\eta| < 0.35$, $\Delta\phi < \pi/2$) is obtained by the MC simulation. We estimated it by using the p_T spectra of charged kaons for K^0_S as the most dominant meson, and by using the p_T spectra of charged pions with transverse mass scaling for $\Lambda(\overline{\Lambda})$ as the most dominant baryon, which contribute to the inclusive charged particle multiplicity fluctuation. As the result, the ratios of charged track pairs originating from those weak decay particles to the number of produced charged pions per event are 0.7% and 0.9% for K^0_S and $\Lambda + \overline{\Lambda}$, respectively. The effects of those correlations on k were estimated as follows. Suppose two independent NBD's in different windows have the same NBD parameters of μ and k for a given window size of $\delta\eta/2$. If there is no correlation between the two windows, NBD in the $\delta\eta$ window size becomes a convoluted distribution between the two NBD's. This is certainly true, since we know the correlation length is well below the minimum size of $\delta\eta$ windows as already discussed. Based on the NBD convolution theorem, the convoluted NBD parameters, μ_{conv} and k_{conv} are expressed as $\mu_{conv} = 2\mu$ and $k_{conv} = 2k$ respectively in the case of no correlation. For the case where the correlated pairs are embedded, we define the fraction of the number of correlated pairs with respected to μ as f. Then the mean value before the correlated pairs are embedded is expressed as $\mu(1-f)$ in the $\delta\eta/2$ window. The effect of the embedded corre-

lation on k_{conv} can be estimated by adding the number of correlated pairs to both windows simultaneously with the fraction of f. With $\mu(1-f)$ and k, we can generate NBD with a random number generator in each window of $\delta\eta/2$ and convolute the two NBD's. From the NBD fit to the convoluted distribution, we can obtain k_{conv} including the effect of the correlated pairs. We define the ratio of the deviation of k_{conv} to the independent case, $\Delta k \equiv (k_{conv}-2k)/2k$ for K^0_S and $\Lambda+\overline{\Lambda}$, respectively. For all observed $(\langle\mu_c\rangle, \langle k_c\rangle)$ values in all $\delta\eta$ windows in all centralities, we have estimated Δk. The pair fraction, f depends on $\delta\eta$ window size, since weak decay particles have their own correlation length due to the kinematical constraint. The fraction f's were obtained based on the two particle correlation of decayed pairs as a function of $\delta\eta$ window size which were evaluated from the GEANT-based MC simulation with the actual track selection criteria. It should be noted that the integrated fractions correspond to the above mentioned fractions, 0.7% and 0.9% for K^0_S and $\Lambda+\overline{\Lambda}$, respectively. As the result, the average values of Δk over all data points were estimated as + 0.27% ± 0.35% (standard deviation) and + 0.40% ± 0.35% (standard deviation) for K^0_S and $\Lambda+\overline{\Lambda}$ decays, respectively. On the other hand, the average value of relative errors, $\delta\langle k_c\rangle(total)/\langle k_c\rangle$ in measured k is ± 7.34% ± 3.29% (standard deviation). We confirmed that the estimated Δk values are all included within the range of the relative errors on measured k. Therefore, we can conclude that the effect of the statistically dominant weak decay pairs with a few percent level on the $\alpha\xi$ product can not exceed the full error sizes of the $\alpha\xi$ products in Table I.

The amount of material before the tracking system is 1.3% of a radiation length. It produces electron-positron pairs with 1.0% photon conversion probability. Almost 100% of photons up to 4 GeV/c of p_T are produced by decays from neutral pions. The detection efficiency of electron-positron pairs which survive after the requirement of the charged track associations and two track separations in Sec. IV B is estimated as 0.22%. It was estimated by the MC simulations with flat p_T distribution of photons. Since the opening angle of the conversion pairs are very small, these conversion electrons are strongly suppressed by the two track separation cuts. Consequently, electron-positron pairs of 2.2×10^{-3}% with respect to the produced charged pions per event, contribute to the multiplicity fluctuations. The efficiency of charged track pairs, which is produced by the materials from single charged hadrons as knock-on electrons (positrons), is estimated as less than 5.8×10^{-5}%. Since the total pair fractions are much smaller than that in weak decays by several orders of magnitude, we can conclude that the effect of those secondary particles on the $\alpha\xi$ products are negligible.

If the observed correlation were to originate only from the Bose-Einstein effect, then we would expect α to be directly related to the chaoticity parameter, λ in HBT analysis which is measured in relative momentum space, q. A similar measurement in pseudorapidity space based on Eq. (7) in low energy A+A collisions [41], indicates the direct relation between λ and α. The observed two particle correlation strength α in pseudorapidity space is weaker than λ measured in q space and essentially becomes zero for the particle pairs selected in the higher q region where HBT effect also becomes zero. This indicates that the observed pseudorapidity correlations in the lower energy $A+A$ collisions are essentially explained purely by the HBT effect. In Au+Au collisions at $\sqrt{s_{NN}}=200$ GeV, measured λ shows constant behavior as a function of N_{part} within 12% and a monotonic N_{part} dependence of HBT radii has been observed [42, 43]. This implies that the non-monotonic behavior of the $\alpha\xi$ product can not be explained solely as a result of the known HBT effect, because $\alpha\propto\lambda$ is expected to be constant for any N_{part} and ξ which would be related to the HBT source radii is expected to be monotonic, if the known HBT effect is the only source of the correlation.

B. Evaluation of the non-monotonic behavior of $\alpha\xi$

The $\alpha\xi$ product obtained by Eq. (9) is related to susceptibility in the long wavelength limit, $\chi_{\omega=0}$ as described in Sec. II. According to Eq. (10), if the system temperature T is far from the critical temperature T_c then $\alpha\xi$ is expected to decrease monotonically with increasing T which is a monotonic function of N_{part} as will be discussed in Sec. VI C. Therefore, one can assume a monotonically decreasing function as a hypothesis of the baseline in T far from T_c. As baseline functional forms for $\alpha\xi$ versus T we consider the following two cases. The first is a power law function which is naturally expected from Eq. (10), and the second is a linear function as the simplest assumption. The power law baseline and the linear baseline are parametrized as

$$\alpha\xi(N_{part}) = p_1(N_{part})^{p_2} \tag{14}$$

and

$$\alpha\xi(N_{part}) = p_1 + p_2 N_{part} \tag{15}$$

with fit parameter p_1 and p_2, respectively. As a test hypothesis, we assume a local maximum on the monotonic baselines in $\alpha\xi$ versus N_{part}. Although the functional form around the local maximum is not known a priori without introducing a physical model, we can at least discuss the significance of the local maximum above the monotonic baseline by introducing a Gaussian distribution. The composite functions are defined as

$$\alpha\xi(N_{part}) = p_1(N_{part})^{p_2} + ae^{-\frac{(N_{part}-m)^2}{2w^2}} \tag{16}$$

and

$$\alpha\xi(N_{part}) = p_1 + p_2 N_{part} + ae^{-\frac{(N_{part}-m)^2}{2w^2}}, \tag{17}$$

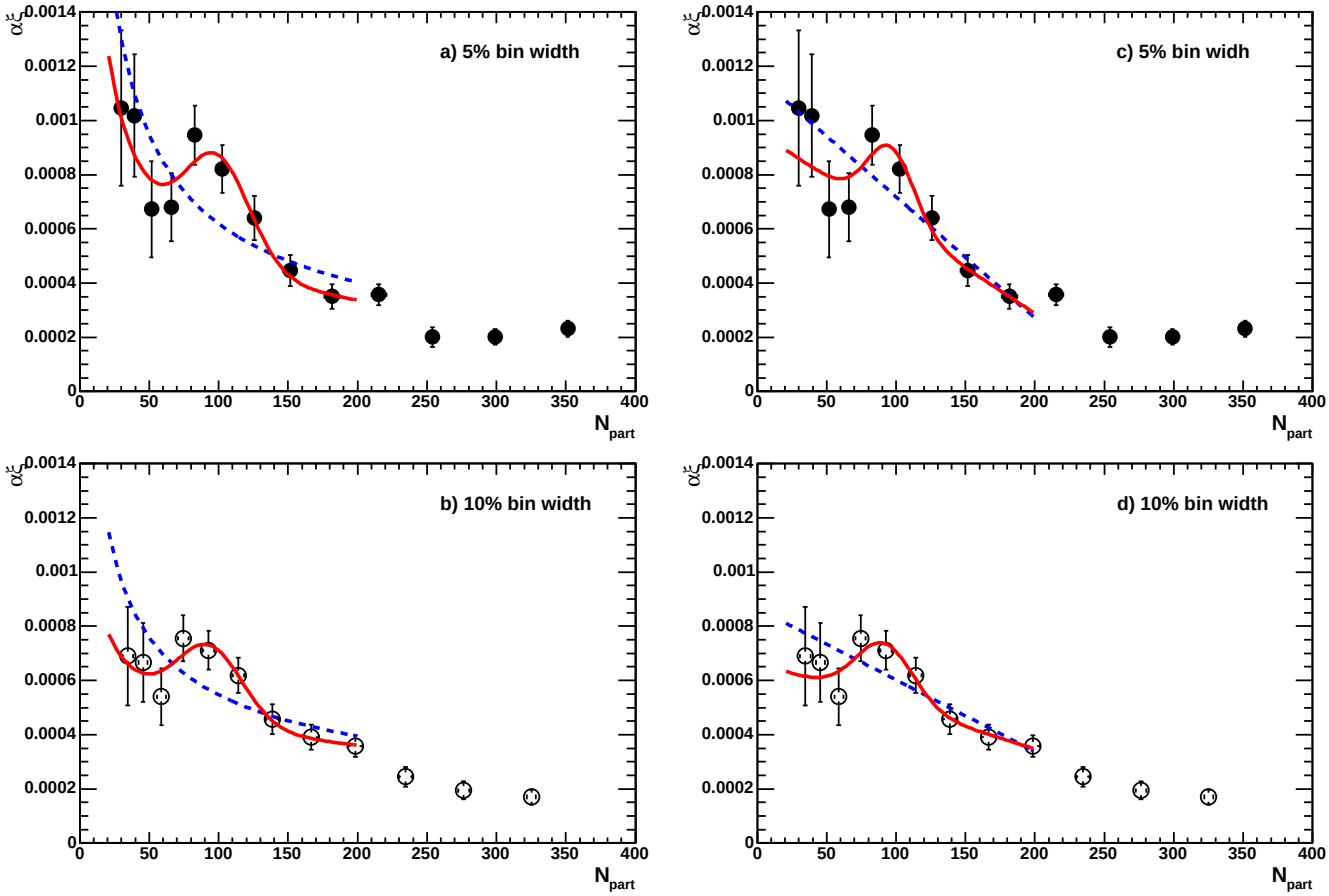

FIG. 6: (Color online) $\alpha\xi$ versus N_{part} in Table I with fit curves. The dashed and solid curves show the fit results with the baseline functions Eq. 14 and 15 and with the composite functions Eq. 16 and 17 respectively. a) and b) correspond to 5% and 10% bin width cases with the power law baselines. c) and d) correspond to 5% and 10% bin width cases with the linear baselines.

TABLE II: The fit parameters in Eq. (14), Eq. (15), Eq. (16) and Eq. (17).

Functional form	Centrality bin width (%)	$\chi^2/NDF(NDF)$	$a \pm \delta a$	Significance $(a/\delta a)$
Power law in Eq. (14)	5	2.76(7)		
Power law + Gaussian in Eq. (16)	5	0.60(4)	$0.37 \times 10^3 \pm 0.09 \times 10^3$	3.98
Linear in Eq. (15)	5	1.23(7)		
Linear + Gaussian in Eq. (17)	5	0.79(4)	$0.27 \times 10^3 \pm 0.21 \times 10^3$	1.24
Power law in Eq. (14)	10	2.10(7)		
Power law + Gaussian in Eq. (16)	10	0.38(4)	$0.27 \times 10^3 \pm 0.08 \times 10^3$	3.21
Linear in Eq. (15)	10	1.09(7)		
Linear + Gaussian in Eq. (17)	10	0.43(4)	$0.22 \times 10^3 \pm 0.13 \times 10^3$	1.69

where a, m and w correspond to amplitude, mean and width of the Gaussian component, respectively. Fits with the four functional forms were performed to $\alpha\xi$ versus N_{part} in $20 < N_{part} < 200$. Figure 6 shows $\alpha\xi$ versus N_{part} from Table I with those fit curves. The dashed and solid curves show the fit results with the baseline functions and with the composite functions. Figures 6 a) and b) correspond to 5% and 10% bin width cases with the power law baselines. Figures 6 c) and d) correspond to 5% and 10% bin width cases with the linear baselines. Table II summarizes all the fit results from the Minuit program [33], including functional forms, centrality bin widths, χ^2/NDF (NDF), the Gaussian amplitude a with its error δa, and the significance of the amplitude defined as $a/\delta a$. Although the significance of the local maximum with the linear baseline is smaller than that with the power law baseline, this is mainly due to the larger uncertainty on a in Eq. (17) than in Eq. (16). This reflects the fact that the combination of a Gaussian distribution with the linear baseline is not as good a fit as that with the power law baseline for the given data points. The difference on the significance between 5%

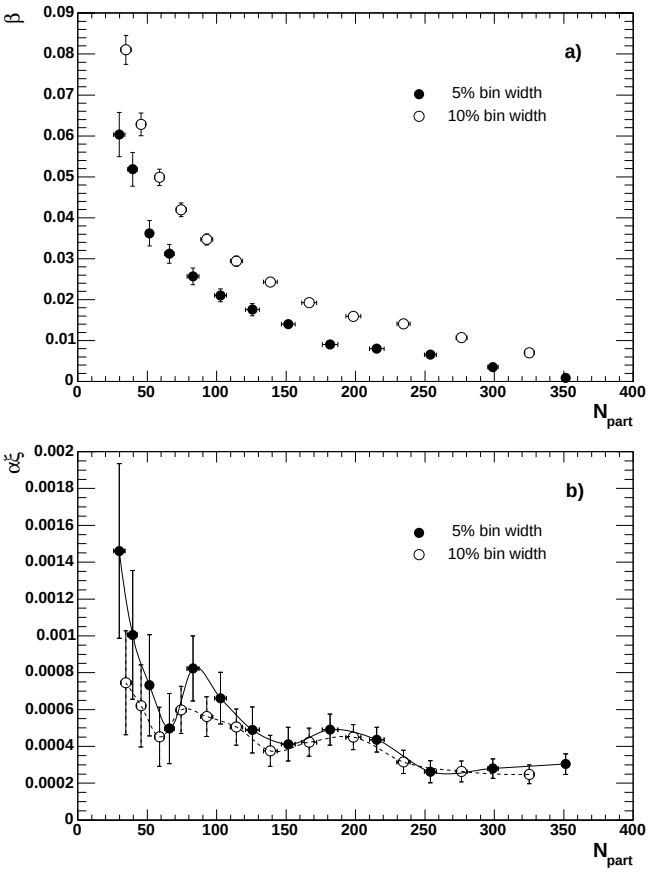

FIG. 7: Fit results based on Eq. (9) by limiting the range of $\delta\eta$ from 0.066 to 0.306. a) is β and b) is products of $\alpha\xi$ as a function of N_{part}. The horizontal error bars correspond to ambiguities in the mean value of N_{part} as explained in Sec. IV C. The vertical error bars are obtained from errors on the fitting parameter.

and 10% centrality bin width cases is not attributed to the correlations with β parameter, since β was introduced as a parameter independent of $\delta\eta$. This can, rather, be understood as the smearing effect of a peak-like shape due to the difference of centrality bin widths around the mean N_{part}. In all cases in Table II, the χ^2/NDF indicate that composite functions are favored over monotonic functions. This result supports the non-monotonicity of $\alpha\xi$ as a function of N_{part}.

Although there is a possibility that more than one correlation length scale is dynamically present, the functional form with one correlation length can reasonably describe the region of $0.066 < \delta\eta < 0.7$ with the average χ^2/NDF of 0.43 over all centralities. We have performed a further check on the N_{part} dependence of the $\alpha\xi$ products by limiting the region of fit to $0.066 < \delta\eta < 0.306$ as shown in Fig. 7. The characteristic behavior of $\alpha\xi$ still present at around $N_{part} \sim 90$.

C. Initial temperature and N_{part}

The Bjorken energy density [21] derived from the measured $dE_T/d\eta$ in the mid-rapidity region is defined as

$$\epsilon_{Bj} = \frac{1}{c\tau A_T}\frac{dE_T}{dy}, \tag{18}$$

where τ is the formation time and A_T is the nuclei transverse overlap area size. It is well known that the energy density monotonically increases with increasing N_{part} in Au+Au collisions at $\sqrt{s_{NN}}$ =200 GeV [22].

This indicates that the change of N_{part} even at the fixed collision energy can yield a fine scan over the initial temperature. Therefore, the non-monotonic behavior in the $\alpha\xi$ products could be an indication of the critical initial temperature as defined in Eq.(A11). The Bjorken energy density, $\epsilon_{Bj}\tau$, at the local maximum of $\alpha\xi$ seen at $N_{part} \sim 90$ corresponds to ~ 2.4 GeV/(fm$^2 \cdot c$) with $A_T = 60$ fm^2.

VII. CONCLUSIONS

The multiplicity distributions measured in Au+Au collisions at $\sqrt{s_{NN}} = 200$ GeV are found to be well-described by negative binomial distributions.

The two-particle density correlations have been measured via the functional form for pseudorapidity density fluctuations derived in the Ginzburg-Landau framework, up to the second order term in the free energy, with a scalar order parameter defined as pseudorapidity-dependent multiplicity fluctuations around the mean value. The functional form can reasonably fit k versus $\delta\eta$ in all centralities in $|\eta| < 0.35$ region with one correlation length assumption and the constant term β which is independent of $\delta\eta$. We found β is necessary to absorb residual effects of finite centrality binning.

We found that the absolute scale of the correlation length, ξ depends on the magnitude of the correlation strength at zero distance, α within the range of pseudorapidity window sizes available in this analysis. However, according to the free parameter fit results, the upper limit on $\xi < 0.035$ was obtained, and it was confirmed by the accuracy of the fits with approximated integrated correlation function in the limit of the small correlation length ($\xi \ll \delta\eta$).

The $\alpha\xi$ product in the correlation function, which is monotonically related to susceptibility in the long wavelength limit $\chi_{\omega=0}$, was seen to exhibit a non-monotonic behavior as a function of the number of participant nucleons N_{part}. A possible indication of a local maximum is seen at $N_{part} \sim 90$ and the corresponding energy density based on the Bjorken picture is $\epsilon_{Bj}\tau \sim 2.4$ GeV/(fm$^2 \cdot c$) with the transverse area size of 60 fm^2.

Trivial particle correlations originating from charged track reconstructions in tracking detectors have been suppressed in this analysis a priori. The ratio of charged

particles from statistically dominant weak decays and secondary particles produced in the detector materials, which contribute as correlated pairs, are respectively estimated below $\sim 1\%$ and $\sim 10^{-3}\%$ with respect to the total number of charged pions in the PHENIX acceptance per event. We have estimated those effects on measured k values and the deviation due to the effect is well inside the total error size of observed $\delta\langle k_c\rangle$. Therefore, we conclude that their contributions are almost negligible to the observed behavior of the $\alpha\xi$ products.

The behavior may be explained by the onset of a mixture of different types of particle production mechanisms which are not necessarily related to temperature or density correlations. However, interpreted within the Ginzburg-Landau framework the local maximum of the $\alpha\xi$ product could be an indication of a critical phase boundary.

Acknowledgments

((Temporally)) We thank the staff of the Collider-Accelerator and Physics Departments at Brookhaven National Laboratory and the staff of the other PHENIX participating institutions for their vital contributions. We acknowledge support from the Department of Energy, Office of Science, Nuclear Physics Division, the National Science Foundation, Abilene Christian University Research Council, Research Foundation of SUNY, and Dean of the College of Arts and Sciences, Vanderbilt University (U.S.A), Ministry of Education, Culture, Sports, Science, and Technology and the Japan Society for the Promotion of Science (Japan), Conselho Nacional de Desenvolvimento Científico e Tecnológico and Fundação de Amparo à Pesquisa do Estado de São Paulo (Brazil), Natural Science Foundation of China (People's Republic of China), Centre National de la Recherche Scientifique, Commissariat à l'Énergie Atomique, Institut National de Physique Nucléaire et de Physique des Particules, and Institut National de Physique Nucléaire et de Physique des Particules, (France), Bundesministerium fuer Bildung und Forschung, Deutscher Akademischer Austausch Dienst, and Alexander von Humboldt Stiftung (Germany), Hungarian National Science Fund, OTKA (Hungary), Department of Atomic Energy and Department of Science and Technology (India), Israel Science Foundation (Israel), Korea Research Foundation and Center for High Energy Physics (Korea), Russian Ministry of Industry, Science and Tekhnologies, Russian Academy of Science, Russian Ministry of Atomic Energy (Russia), VR and the Wallenberg Foundation (Sweden), the U.S. Civilian Research and Development Foundation for the Independent States of the Former Soviet Union, the US-Hungarian NSF-OTKA-MTA, the US-Israel Binational Science Foundation, and the 5th European Union TMR Marie-Curie Programme.

APPENDIX A: DEFINITION OF CORRELATION LENGTH AND SUSCEPTIBILITY IN GINZBURG-LANDAU FRAMEWORK

The Ginzburg-Landau (GL) [19] framework with the Ornstein-Zernike picture [18] for a scalar order parameter is briefly reviewed. The relations with correlation length and susceptibility are explicitly derived in this appendix.

The first attempt to apply free energy discussions to nucleus-nucleus collisions can be found in [44]; application to the QCD phase transition is in [25]. GL describes the relation between a free energy density f and an order parameter ϕ as a function of the system temperature T. By adding a spatially inhomogeneous term $A(T)(\nabla\phi)^2$ and an external field h, the general form is described as follows

$$f(T,\phi,h) = f_0(T) + \frac{1}{2}A(T)(\nabla\phi)^2 + \frac{1}{2}a(T)\phi^2 + \frac{1}{4}b\phi^4 + \cdots - h\phi, \tag{A1}$$

where f_0 is the equilibrium value of the free energy, terms with odd powers are neglected due to the symmetry of the order parameter, and the sign of b is used to classify the transition orders: $b < 0$ for the first order, $b > 0$ for the second order and $b = 0$ at the critical point. Since the order parameter should vanish above a critical temperature T_c, it is natural for the coefficient $a(T)$ to be expressed as $a(T) = a_0|T - T_c|$, while b is usually assumed to be constant in the vicinity of T_c. In the following, we neglect higher order terms beyond the second order term. This approximation corresponds to a picture where a system approaches the phase boundary from afar, since ϕ is close to zero in the regions far from T_c. In this sense, the approximation is insensitive to the details of the phase transition order, *i.e.* higher order terms, but only sensitive to the behavior near T_c.

We apply this GL framework to density correlations in the longitudinal space coordinate z in heavy-ion collisions. The system of the produced matter dynamically evolves, so we introduce the proper time frame for each sub element. The longitudinal space element becomes $dz = \tau\ \cosh(y)dy$, at a fixed proper time τ, where y is rapidity, as introduced in [23]. Since we measure the density fluctuations in the mid-rapidity regions $|\eta| < 0.35$ as described in Sec. III, we use dy in place of dz by the approximation of $\cosh(y) = 1$ to simplify the form of the correlation function derived from GL free energy.

The order parameter of this analysis corresponds to multiplicity density fluctuations of inclusive charged particles around the mean density. Fluctuations are measured as a function of a one-dimensional pseudorapidity point η, defined as

$$\phi(\eta) = \rho(\eta) - \langle\rho(\eta)\rangle, \tag{A2}$$

where the pair of brackets indicates an operator to take the average. In the above mentioned rapidity region, rapidity can be represented by pseudorapidity to a good

approximation, as explained in the last paragraph of Sec. IV B.

With the Fourier expansion of the density fluctuation at pseudorapidity point η, $\phi(\eta) = \sum_\omega \phi_\omega e^{i\omega\eta}$, where ω is wave number, one can express the deviation of the free energy density due to spatial fluctuations from the equilibrium value f_0

$$\begin{aligned}\Delta F/Y &= \frac{1}{Y}\int (f - f_0)d\eta \\ &= \frac{1}{2}\sum_\omega |\phi_\omega|^2(a(T) + A(T)\omega^2), \end{aligned} \quad \text{(A3)}$$

where Y is the total pseudorapidity range corresponding to a one-dimensional volume. Terms up to the second order are included in the approximation in the vicinity of the critical point in Eq. (A1). Given the free energy deviation, one can obtain the statistical weight W for fluctuation $\phi(\eta)$ to occur in a given temperature T

$$W(\phi(\eta)) = Ne^{-\Delta F/T}. \quad \text{(A4)}$$

Therefore the statistical average of the square of the density fluctuation with the wave number ω is described as

$$\begin{aligned}\langle|\phi_\omega|^2\rangle &= \int_{-\infty}^{+\infty} |\phi_\omega|^2 W\left(\sum_\omega \phi_\omega e^{i\omega\eta}\right) d\phi_\omega \\ &= \frac{NT}{Y}\frac{1}{a(T) + A(T)\omega^2}. \end{aligned} \quad \text{(A5)}$$

An experimentally observable two point density correlation function can be related to the statistical average of the square of the density fluctuation. With a density $\rho(\eta_i)$ for a given sub-volume $d\eta_i$, the two point density correlation G_2 is expressed in the case of $\langle\rho(\eta_1)\rangle = \langle\rho(\eta_2)\rangle = \langle\rho\rangle$ as

$$G_2(\eta_1, \eta_2) = \langle(\rho(\eta_1) - \langle\rho\rangle)(\rho(\eta_2) - \langle\rho\rangle)\rangle, \quad \text{(A6)}$$

where case 1 coinciding with case 2 is excluded to simplify the following discussion. Multiplying both sides of Eq. (A6) by $e^{-i\omega\eta} \equiv e^{-i\omega(\eta_2-\eta_1)}$ and integrating over sub-volume $d\eta_1$ and $d\eta_2$ gives

$$\begin{aligned} Y\int G_2(\eta)e^{-i\omega\eta}d\eta &= \langle|\int(\rho(\eta) - \langle\rho\rangle)e^{-i\omega\eta}d\eta|^2\rangle \\ &= \langle|\phi_\omega|^2\rangle. \end{aligned} \quad \text{(A7)}$$

From Eq. (A5) and (A7), G_2 can be related to the inverse Fourier transformation of the statistical average of $|\phi_\omega|^2$. Therefore in the one-dimensional case G_2 is described as

$$G_2(\eta) = \frac{NT}{2Y^2A(T)}\xi(T)e^{-|\eta|/\xi(T)}, \quad \text{(A8)}$$

where the correlation length $\xi(T)$ is introduced, which is defined as

$$\xi(T)^2 = \frac{A(T)}{a_0|T - T_c|}. \quad \text{(A9)}$$

In general, a singular behavior of $\xi(T)$ as a function of T indicates the critical temperature of the phase transition.

The wave number dependent susceptibility can also be defined from the expansion of the GL free energy based on Eq. (A1) and (A3) as follows,

$$\begin{aligned}\chi_\omega &= -\left(\frac{\partial^2 f}{\partial h^2}\right) = \left(\frac{\partial h}{\partial\phi_\omega}\right)^{-1} \\ &= \left(\frac{\partial^2(\Delta F/Y)}{\partial\phi_\omega^2}\right)^{-1} \\ &= \frac{1}{a_0|T - T_c|(1 + \omega^2\xi(T)^2)}. \end{aligned} \quad \text{(A10)}$$

In the case of the long wavelength limit of $\omega = 0$, the susceptibility can be expressed as,

$$\chi_{\omega=0} = \frac{1}{a_0|T - T_c|} = \frac{2Y^2}{NT}\xi(T)G_2(0). \quad \text{(A11)}$$

In this framework, the ξ and $\chi_{\omega=0}$ diverge at the same temperature.

APPENDIX B: TABLES OF NBD FIT RESULTS

NBD fit results in all window sizes in all centrality bins in Fig. 4. In the following Table III through Table XIV and Table XV through Table XXVII correspond to results in 10% and 5% bin width cases, respectively. $\langle\mu_c\rangle$ and $\langle\mu\rangle$ are weighted means of corrected and uncorrected μ over all window positions respectively. $\langle k_c\rangle$ and $\langle k\rangle$ are weighted means of corrected and uncorrected k over all window positions respectively. Statistical errors on weighted means $\delta\langle k_c\rangle$ (stat) are obtained as explained in Sec. IV F. $\langle\chi^2/NDF\rangle$ is the average of reduced χ^2 of NBD fits over all window positions. $\langle NDF\rangle$ is the average of the degree of freedom of NBD fits over all window positions. Systematic errors $\delta\langle k_c\rangle$ (dead), $\delta\langle k_c\rangle$ (fake) and $\delta\langle k_c\rangle$ (total) are explained in Sec. IV F.

TABLE III: NBD fit results in centrality 0-10%.

$\delta\eta$	$\langle\mu_c\rangle(\langle\mu\rangle)$	$\langle k_c\rangle(\langle k\rangle)$	$\langle\chi^2/NDF\rangle(\langle NDF\rangle)$	$\delta\langle k_c\rangle(dead)$	$\delta\langle k_c\rangle(fake)$	$\delta\langle k_c\rangle(total)$
0.700	77.535(60.011) ± 0.108	114.28(88.45) ± 3.21	0.96(71.0)	±2.89	±2.28	±4.89
0.678	75.445(58.445) ± 0.106	113.11(87.62) ± 3.29	0.89(69.7)	±4.92	±3.31	±6.78
0.656	72.977(56.455) ± 0.103	114.40(88.50) ± 3.38	0.95(68.2)	±4.33	±3.04	±6.28
0.634	70.485(54.450) ± 0.101	114.02(88.08) ± 3.42	0.92(66.7)	±4.54	±3.01	±6.43
0.613	67.998(52.489) ± 0.099	114.44(88.33) ± 3.52	0.94(65.3)	±3.79	±2.31	±5.66
0.591	65.530(50.572) ± 0.096	114.28(88.18) ± 3.60	0.95(63.9)	±3.59	±2.62	±5.72
0.569	63.050(48.609) ± 0.094	114.62(88.35) ± 3.71	0.97(62.3)	±3.88	±2.80	±6.05
0.547	60.569(46.624) ± 0.091	114.27(87.94) ± 3.80	0.96(60.8)	±3.61	±2.98	±6.03
0.525	58.100(44.655) ± 0.089	114.38(87.89) ± 3.92	0.95(59.7)	±3.79	±2.87	±6.16
0.503	55.637(42.682) ± 0.086	114.36(87.70) ± 4.03	0.93(57.8)	±3.64	±3.17	±6.29
0.481	53.164(40.688) ± 0.084	114.41(87.54) ± 4.17	0.94(56.3)	±4.24	±3.40	±6.85
0.459	50.682(38.672) ± 0.081	115.19(87.87) ± 4.35	0.98(54.2)	±4.10	±3.14	±6.75
0.438	48.209(36.654) ± 0.079	114.89(87.33) ± 4.51	0.98(52.4)	±4.49	±3.72	±7.37
0.416	45.743(34.645) ± 0.076	115.05(87.11) ± 4.71	0.98(50.3)	±4.79	±3.49	±7.57
0.394	43.283(32.654) ± 0.074	114.86(86.61) ± 4.90	0.97(48.3)	±4.37	±4.15	±7.77
0.372	40.838(30.677) ± 0.071	115.20(86.46) ± 5.17	1.00(46.2)	±4.22	±4.10	±7.83
0.350	38.424(28.782) ± 0.049	115.87(86.69) ± 3.88	1.04(44.5)	±3.81	±4.22	±6.88
0.328	36.034(27.062) ± 0.047	115.35(86.43) ± 4.04	1.04(42.9)	±4.04	±4.58	±7.32
0.306	33.665(25.363) ± 0.045	114.46(86.00) ± 4.21	1.08(41.2)	±4.28	±4.89	±7.74
0.284	31.288(23.638) ± 0.043	113.91(85.92) ± 4.39	1.09(39.9)	±3.60	±5.13	±7.65
0.263	28.916(21.900) ± 0.041	111.53(84.56) ± 4.51	1.10(37.9)	±3.75	±5.29	±7.90
0.241	26.542(20.145) ± 0.039	109.53(83.35) ± 4.67	1.08(36.3)	±3.71	±5.40	±8.04
0.219	24.155(18.360) ± 0.030	107.67(82.28) ± 4.03	1.11(34.4)	±3.66	±5.96	±8.07
0.197	21.758(16.553) ± 0.028	105.84(80.90) ± 4.29	1.15(32.4)	±3.17	±6.12	±8.12
0.175	19.355(14.723) ± 0.023	102.63(78.59) ± 3.96	1.21(30.1)	±3.59	±6.85	±8.69
0.153	16.948(12.880) ± 0.021	97.91(75.16) ± 4.19	1.25(27.6)	±3.83	±6.93	±8.96
0.131	14.536(11.031) ± 0.017	93.93(72.13) ± 4.01	1.34(24.9)	±3.77	±7.03	±8.93
0.109	12.119(9.172) ± 0.014	87.92(66.93) ± 3.81	1.39(21.9)	±3.48	±7.30	±8.94
0.087	9.695(7.305) ± 0.011	78.94(58.95) ± 3.35	1.34(18.7)	±3.48	±7.34	±8.79
0.066	7.308(5.685) ± 0.008	65.53(49.27) ± 2.87	1.09(15.4)	±4.05	±6.83	±8.45

TABLE IV: NBD fit results in centrality 5-15%.

$\delta\eta$	$\langle\mu_c\rangle(\langle\mu\rangle)$	$\langle k_c\rangle(\langle k\rangle)$	$\langle\chi^2/NDF\rangle(\langle NDF\rangle)$	$\delta\langle k_c\rangle(dead)$	$\delta\langle k_c\rangle(fake)$	$\delta\langle k_c\rangle(total)$
0.700	66.445(51.428) ± 0.098	80.80(62.54) ± 1.92	1.20(68.0)	±2.14	±2.17	±3.60
0.678	64.658(50.089) ± 0.097	80.40(62.28) ± 1.95	1.15(66.4)	±3.40	±1.53	±4.21
0.656	62.535(48.377) ± 0.094	81.17(62.79) ± 1.99	1.20(65.0)	±2.28	±1.11	±3.22
0.634	60.379(46.644) ± 0.092	81.10(62.65) ± 2.02	1.23(64.1)	±2.24	±1.57	±3.40
0.613	58.258(44.970) ± 0.090	80.61(62.21) ± 2.06	1.21(62.4)	±2.75	±1.43	±3.72
0.591	56.156(43.337) ± 0.088	79.66(61.47) ± 2.08	1.12(60.6)	±2.85	±1.50	±3.83
0.569	54.043(41.665) ± 0.085	79.26(61.09) ± 2.12	1.07(59.2)	±2.59	±1.88	±3.83
0.547	51.923(39.968) ± 0.083	78.98(60.79) ± 2.17	1.09(57.4)	±2.90	±1.68	±3.99
0.525	49.809(38.283) ± 0.081	79.14(60.81) ± 2.23	1.11(56.2)	±2.83	±1.88	±4.07
0.503	47.691(36.586) ± 0.078	79.62(61.06) ± 2.32	1.13(54.7)	±2.15	±1.91	±3.69
0.481	45.573(34.878) ± 0.076	79.66(60.95) ± 2.39	1.13(53.0)	±2.35	±1.59	±3.71
0.459	43.446(33.150) ± 0.073	80.40(61.33) ± 2.48	1.18(51.3)	±2.25	±1.70	±3.76
0.438	41.327(31.420) ± 0.071	79.99(60.80) ± 2.56	1.15(49.4)	±2.84	±2.29	±4.46
0.416	39.211(29.696) ± 0.069	80.34(60.83) ± 2.67	1.18(47.7)	±2.98	±2.03	±4.49
0.394	37.107(27.993) ± 0.067	80.40(60.62) ± 2.79	1.15(45.9)	±3.24	±2.36	±4.88
0.372	35.007(26.295) ± 0.064	80.45(60.38) ± 2.92	1.18(43.9)	±3.19	±2.29	±4.89
0.350	32.938(24.672) ± 0.044	80.58(60.28) ± 2.17	1.21(42.1)	±3.22	±2.23	±4.48
0.328	30.889(23.196) ± 0.042	80.09(60.08) ± 2.25	1.22(40.3)	±3.29	±2.71	±4.82
0.306	28.861(21.741) ± 0.040	79.49(59.81) ± 2.33	1.22(38.6)	±3.21	±2.56	±4.73
0.284	26.832(20.270) ± 0.038	79.11(59.73) ± 2.44	1.24(37.0)	±2.85	±2.87	±4.72
0.263	24.795(18.778) ± 0.036	78.06(59.22) ± 2.55	1.23(35.3)	±3.01	±3.26	±5.12
0.241	22.758(17.270) ± 0.035	77.16(58.82) ± 2.68	1.22(33.8)	±2.93	±3.39	±5.22
0.219	20.708(15.737) ± 0.026	76.33(58.44) ± 2.32	1.27(32.1)	±2.56	±3.09	±4.64
0.197	18.654(14.187) ± 0.025	75.26(57.80) ± 2.47	1.29(30.2)	±2.84	±3.67	±5.26
0.175	16.591(12.614) ± 0.020	73.89(56.91) ± 2.30	1.36(28.1)	±2.74	±3.58	±5.06
0.153	14.526(11.035) ± 0.019	71.68(55.18) ± 2.44	1.41(25.9)	±2.84	±3.97	±5.46
0.131	12.458(9.451) ± 0.015	69.08(53.03) ± 2.31	1.47(23.1)	±2.81	±4.10	±5.48
0.109	10.385(7.857) ± 0.013	65.32(49.65) ± 2.23	1.46(20.3)	±2.92	±4.28	±5.64
0.087	8.306(6.253) ± 0.010	59.45(44.57) ± 2.03	1.29(17.4)	±2.58	±4.32	±5.43
0.066	6.262(4.870) ± 0.007	51.33(38.86) ± 1.88	0.89(14.4)	±2.75	±4.18	±5.34

TABLE V: NBD fit results in centrality 10-20%.

$\delta\eta$	$\langle\mu_c\rangle(\langle\mu\rangle)$	$\langle k_c\rangle(\langle k\rangle)$	$\langle\chi^2/NDF\rangle(\langle NDF\rangle)$	$\delta\langle k_c\rangle(dead)$	$\delta\langle k_c\rangle(fake)$	$\delta\langle k_c\rangle(total)$
0.700	55.290(42.794) ± 0.090	63.58(49.21) ± 1.47	1.14(64.0)	±0.37	±0.57	±1.62
0.678	53.832(41.701) ± 0.089	62.10(48.11) ± 1.46	0.93(63.1)	±2.48	±2.60	±3.88
0.656	52.092(40.299) ± 0.087	61.78(47.79) ± 1.48	0.88(62.3)	±2.34	±1.54	±3.17
0.634	50.301(38.858) ± 0.085	61.91(47.82) ± 1.51	0.90(60.3)	±2.06	±1.23	±2.83
0.613	48.533(37.463) ± 0.082	61.80(47.70) ± 1.54	0.88(58.5)	±2.10	±1.09	±2.83
0.591	46.769(36.093) ± 0.080	62.00(47.85) ± 1.58	0.90(57.9)	±1.74	±1.21	±2.64
0.569	45.006(34.698) ± 0.078	61.89(47.71) ± 1.61	0.87(56.6)	±1.77	±1.06	±2.62
0.547	43.255(33.296) ± 0.076	61.70(47.49) ± 1.65	0.88(55.1)	±1.80	±1.34	±2.78
0.525	41.499(31.895) ± 0.074	61.86(47.55) ± 1.70	0.89(53.8)	±1.95	±1.21	±2.86
0.503	39.742(30.488) ± 0.072	61.94(47.51) ± 1.75	0.90(52.4)	±1.89	±1.38	±2.92
0.481	37.976(29.063) ± 0.070	61.92(47.38) ± 1.80	0.90(50.8)	±1.84	±1.26	±2.87
0.459	36.206(27.625) ± 0.067	61.91(47.24) ± 1.85	0.91(48.8)	±1.84	±1.46	±2.99
0.438	34.435(26.179) ± 0.065	61.83(47.01) ± 1.91	0.91(47.2)	±1.91	±1.55	±3.12
0.416	32.667(24.739) ± 0.063	62.02(46.98) ± 1.99	0.95(45.6)	±1.96	±1.63	±3.23
0.394	30.908(23.315) ± 0.061	62.18(46.92) ± 2.07	1.00(43.8)	±2.02	±1.58	±3.30
0.372	29.156(21.898) ± 0.059	62.35(46.85) ± 2.16	1.02(42.1)	±2.14	±1.69	±3.48
0.350	27.434(20.547) ± 0.040	62.21(46.61) ± 1.59	1.02(40.4)	±2.30	±1.77	±3.31
0.328	25.727(19.316) ± 0.038	61.90(46.54) ± 1.64	1.06(38.6)	±2.05	±1.66	±3.11
0.306	24.039(18.105) ± 0.037	61.43(46.42) ± 1.71	1.09(36.8)	±2.09	±1.68	±3.17
0.284	22.347(16.876) ± 0.035	60.84(46.18) ± 1.77	1.10(35.1)	±2.30	±1.84	±3.44
0.263	20.653(15.635) ± 0.033	60.20(45.91) ± 1.85	1.12(33.3)	±2.19	±1.93	±3.45
0.241	18.956(14.380) ± 0.032	59.81(45.79) ± 1.95	1.19(31.6)	±2.27	±1.91	±3.54
0.219	17.251(13.105) ± 0.024	59.09(45.44) ± 1.68	1.22(29.7)	±2.19	±2.04	±3.43
0.197	15.537(11.813) ± 0.023	58.31(44.99) ± 1.78	1.25(27.6)	±2.23	±2.11	±3.55
0.175	13.816(10.501) ± 0.018	57.38(44.38) ± 1.65	1.31(25.5)	±1.84	±2.17	±3.29
0.153	12.090(9.179) ± 0.017	55.59(43.04) ± 1.75	1.33(23.0)	±1.77	±2.18	±3.31
0.131	10.367(7.858) ± 0.014	52.81(40.76) ± 1.63	1.27(20.6)	±1.83	±2.31	±3.36
0.109	8.639(6.528) ± 0.011	49.83(38.38) ± 1.57	1.14(18.2)	±1.85	±2.55	±3.52
0.087	6.909(5.194) ± 0.009	46.30(35.28) ± 1.45	0.97(15.6)	±1.82	±2.85	±3.68
0.066	5.215(4.052) ± 0.007	42.21(32.18) ± 1.43	0.75(13.0)	±2.04	±2.90	±3.82

TABLE VI: NBD fit results in centrality 15-25%.

$\delta\eta$	$\langle\mu_c\rangle(\langle\mu\rangle)$	$\langle k_c\rangle(\langle k\rangle)$	$\langle\chi^2/NDF\rangle(\langle NDF\rangle)$	$\delta\langle k_c\rangle(dead)$	$\delta\langle k_c\rangle(fake)$	$\delta\langle k_c\rangle(total)$
0.700	45.868(35.502) ± 0.082	53.43(41.35) ± 1.25	1.06(57.0)	±1.83	±1.78	±2.85
0.678	44.657(34.594) ± 0.080	53.48(41.43) ± 1.29	0.95(55.3)	±1.49	±0.53	±2.04
0.656	43.211(33.428) ± 0.078	53.45(41.35) ± 1.31	0.98(54.2)	±1.53	±0.71	±2.14
0.634	41.737(32.242) ± 0.076	53.70(41.48) ± 1.35	0.96(53.0)	±1.43	±0.58	±2.05
0.613	40.288(31.098) ± 0.075	53.41(41.23) ± 1.38	0.92(51.2)	±1.94	±1.12	±2.63
0.591	38.829(29.965) ± 0.073	53.66(41.42) ± 1.42	0.96(50.3)	±1.71	±0.70	±2.33
0.569	37.368(28.808) ± 0.071	53.48(41.23) ± 1.45	0.94(49.0)	±1.76	±0.82	±2.42
0.547	35.911(27.642) ± 0.069	53.32(41.04) ± 1.48	0.91(47.6)	±1.77	±0.88	±2.47
0.525	34.454(26.481) ± 0.067	53.41(41.05) ± 1.52	0.95(46.1)	±1.75	±0.76	±2.44
0.503	32.995(25.311) ± 0.065	53.58(41.11) ± 1.56	1.02(44.9)	±1.50	±0.81	±2.31
0.481	31.532(24.131) ± 0.063	53.73(41.13) ± 1.61	1.02(44.0)	±1.50	±0.66	±2.29
0.459	30.062(22.936) ± 0.061	53.65(40.95) ± 1.65	1.02(42.8)	±1.57	±0.86	±2.44
0.438	28.591(21.736) ± 0.059	53.69(40.84) ± 1.71	1.03(41.4)	±1.70	±0.87	±2.57
0.416	27.125(20.541) ± 0.057	53.76(40.75) ± 1.78	1.04(40.0)	±1.71	±0.84	±2.61
0.394	25.664(19.358) ± 0.055	53.81(40.64) ± 1.84	1.03(38.5)	±1.78	±1.07	±2.78
0.372	24.206(18.179) ± 0.053	54.03(40.64) ± 1.93	1.05(37.1)	±1.71	±1.02	±2.77
0.350	22.778(17.058) ± 0.036	54.05(40.55) ± 1.42	1.09(35.7)	±1.94	±1.07	±2.63
0.328	21.359(16.035) ± 0.035	53.79(40.53) ± 1.48	1.12(34.5)	±1.74	±1.02	±2.50
0.306	19.955(15.027) ± 0.033	53.36(40.43) ± 1.54	1.14(33.2)	±1.74	±1.09	±2.57
0.284	18.552(14.008) ± 0.032	52.52(40.03) ± 1.59	1.16(31.7)	±1.78	±1.17	±2.66
0.263	17.146(12.979) ± 0.030	51.86(39.73) ± 1.66	1.19(29.9)	±1.63	±1.17	±2.60
0.241	15.736(11.936) ± 0.029	51.03(39.31) ± 1.74	1.25(28.0)	±1.53	±1.28	±2.65
0.219	14.320(10.876) ± 0.022	49.80(38.58) ± 1.48	1.26(26.0)	±1.69	±1.32	±2.60
0.197	12.897(9.802) ± 0.021	48.78(37.96) ± 1.57	1.26(24.1)	±1.43	±1.39	±2.53
0.175	11.465(8.711) ± 0.017	47.43(37.04) ± 1.43	1.26(22.3)	±1.39	±1.30	±2.38
0.153	10.030(7.612) ± 0.015	45.48(35.65) ± 1.51	1.21(20.2)	±1.13	±1.41	±2.36
0.131	8.597(6.513) ± 0.013	43.13(33.84) ± 1.41	1.06(18.1)	±1.27	±1.55	±2.45
0.109	7.163(5.409) ± 0.011	40.33(31.64) ± 1.34	0.79(15.9)	±1.21	±1.67	±2.45
0.087	5.730(4.304) ± 0.008	37.88(29.64) ± 1.27	0.64(13.7)	±1.15	±1.77	±2.47
0.066	4.327(3.360) ± 0.006	35.48(27.59) ± 1.28	0.54(11.6)	±1.20	±1.96	±2.63

TABLE VII: NBD fit results in centrality 20-30%.

$\delta\eta$	$\langle\mu_c\rangle(\langle\mu\rangle)$	$\langle k_c\rangle(\langle k\rangle)$	$\langle\chi^2/NDF\rangle(\langle NDF\rangle)$	$\delta\langle k_c\rangle(dead)$	$\delta\langle k_c\rangle(fake)$	$\delta\langle k_c\rangle(total)$
0.700	37.610(29.110) ± 0.073	47.51(36.77) ± 1.17	0.82(53.0)	±1.28	±0.76	±1.89
0.678	36.606(28.358) ± 0.072	47.66(36.92) ± 1.20	0.86(51.7)	±1.61	±0.68	±2.12
0.656	35.403(27.388) ± 0.070	47.76(36.94) ± 1.22	0.83(51.4)	±1.10	±0.43	±1.70
0.634	34.199(26.419) ± 0.069	47.45(36.66) ± 1.24	0.83(50.2)	±1.54	±0.65	±2.08
0.613	33.002(25.474) ± 0.067	47.80(36.90) ± 1.27	0.97(49.3)	±0.99	±0.68	±1.75
0.591	31.812(24.550) ± 0.065	47.37(36.56) ± 1.28	0.96(48.6)	±1.29	±0.62	±1.92
0.569	30.609(23.598) ± 0.063	47.42(36.56) ± 1.31	0.93(47.7)	±1.12	±0.51	±1.80
0.547	29.413(22.641) ± 0.062	47.14(36.29) ± 1.34	0.92(46.0)	±1.26	±0.68	±1.96
0.525	28.218(21.688) ± 0.060	47.13(36.23) ± 1.37	0.94(44.8)	±1.38	±0.66	±2.05
0.503	27.021(20.729) ± 0.058	47.16(36.19) ± 1.41	0.98(43.6)	±1.29	±0.53	±1.98
0.481	25.823(19.762) ± 0.057	47.14(36.08) ± 1.45	0.98(42.2)	±1.40	±0.52	±2.08
0.459	24.623(18.787) ± 0.055	47.14(35.98) ± 1.50	0.98(41.1)	±1.37	±0.57	±2.11
0.438	23.421(17.806) ± 0.053	46.88(35.66) ± 1.54	0.95(39.4)	±1.53	±0.68	±2.28
0.416	22.218(16.826) ± 0.051	47.13(35.72) ± 1.61	1.02(38.0)	±1.42	±0.55	±2.21
0.394	21.024(15.858) ± 0.050	46.86(35.38) ± 1.67	0.99(36.6)	±1.61	±0.68	±2.42
0.372	19.831(14.894) ± 0.048	46.92(35.28) ± 1.74	1.00(35.1)	±1.60	±0.78	±2.49
0.350	18.658(13.973) ± 0.033	46.79(35.08) ± 1.29	1.02(33.7)	±1.63	±0.83	±2.23
0.328	17.499(13.138) ± 0.031	46.40(34.90) ± 1.33	1.02(32.1)	±1.63	±0.79	±2.25
0.306	16.350(12.314) ± 0.030	46.22(34.90) ± 1.40	1.07(30.6)	±1.72	±0.73	±2.33
0.284	15.201(11.480) ± 0.029	45.61(34.60) ± 1.45	1.06(29.0)	±1.56	±0.82	±2.28
0.263	14.048(10.636) ± 0.027	44.99(34.29) ± 1.51	1.06(27.4)	±1.65	±0.90	±2.41
0.241	12.892(9.781) ± 0.026	44.22(33.84) ± 1.58	1.07(25.6)	±1.54	±0.91	±2.39
0.219	11.729(8.913) ± 0.020	43.26(33.22) ± 1.34	1.05(24.0)	±1.36	±0.93	±2.13
0.197	10.561(8.032) ± 0.019	42.28(32.55) ± 1.41	1.05(22.4)	±1.30	±0.95	±2.14
0.175	9.389(7.139) ± 0.015	41.04(31.68) ± 1.29	0.96(20.4)	±1.26	±0.96	±2.04
0.153	8.216(6.239) ± 0.014	39.50(30.60) ± 1.36	0.83(18.6)	±1.18	±1.13	±2.13
0.131	7.045(5.342) ± 0.012	38.08(29.47) ± 1.31	0.68(16.6)	±1.07	±1.20	±2.08
0.109	5.871(4.439) ± 0.009	36.53(28.20) ± 1.30	0.54(14.7)	±1.08	±1.31	±2.14
0.087	4.697(3.532) ± 0.007	35.06(27.06) ± 1.31	0.51(12.4)	±1.03	±1.57	±2.29
0.066	3.547(2.756) ± 0.005	32.64(25.34) ± 1.37	0.46(10.4)	±1.02	±1.72	±2.42

TABLE VIII: NBD fit results in centrality 25-35%.

$\delta\eta$	$\langle\mu_c\rangle(\langle\mu\rangle)$	$\langle k_c\rangle(\langle k\rangle)$	$\langle\chi^2/NDF\rangle(\langle NDF\rangle)$	$\delta\langle k_c\rangle(dead)$	$\delta\langle k_c\rangle(fake)$	$\delta\langle k_c\rangle(total)$
0.700	30.796(23.836) ± 0.065	41.09(31.80) ± 1.05	0.77(48.0)	±1.99	±0.38	±2.28
0.678	29.940(23.193) ± 0.063	41.40(32.07) ± 1.06	0.83(48.9)	±1.53	±0.13	±1.87
0.656	28.970(22.412) ± 0.062	41.18(31.85) ± 1.07	0.81(47.9)	±1.52	±0.55	±1.94
0.634	27.967(21.605) ± 0.060	41.07(31.73) ± 1.09	0.84(46.8)	±1.36	±0.47	±1.81
0.613	26.977(20.823) ± 0.059	40.97(31.62) ± 1.11	0.85(45.4)	±1.15	±0.55	±1.69
0.591	26.003(20.068) ± 0.058	40.72(31.42) ± 1.12	0.88(44.1)	±1.23	±0.36	±1.71
0.569	25.020(19.289) ± 0.056	40.64(31.33) ± 1.15	0.89(42.6)	±1.43	±0.53	±1.91
0.547	24.036(18.502) ± 0.055	40.41(31.11) ± 1.17	0.91(41.1)	±1.35	±0.55	±1.87
0.525	23.058(17.722) ± 0.053	40.37(31.03) ± 1.20	0.91(40.0)	±1.37	±0.44	±1.87
0.503	22.086(16.943) ± 0.052	40.25(30.88) ± 1.23	0.90(38.8)	±1.54	±0.55	±2.05
0.481	21.108(16.155) ± 0.050	40.05(30.66) ± 1.26	0.91(37.2)	±1.56	±0.48	±2.07
0.459	20.126(15.356) ± 0.049	40.00(30.53) ± 1.30	0.92(35.9)	±1.59	±0.39	±2.09
0.438	19.143(14.554) ± 0.047	39.77(30.26) ± 1.34	0.92(34.6)	±1.62	±0.42	±2.15
0.416	18.163(13.755) ± 0.046	39.51(29.96) ± 1.38	0.88(33.3)	±1.70	±0.52	±2.25
0.394	17.184(12.962) ± 0.044	39.36(29.73) ± 1.44	0.91(31.8)	±1.72	±0.50	±2.29
0.372	16.206(12.172) ± 0.043	39.43(29.67) ± 1.50	0.95(30.6)	±1.64	±0.43	±2.27
0.350	15.249(11.420) ± 0.029	39.31(29.50) ± 1.11	0.98(29.2)	±1.63	±0.51	±2.04
0.328	14.299(10.736) ± 0.028	38.92(29.31) ± 1.14	1.00(27.9)	±1.55	±0.53	±2.00
0.306	13.362(10.063) ± 0.027	38.24(28.93) ± 1.18	0.97(26.5)	±1.56	±0.56	±2.04
0.284	12.422(9.381) ± 0.026	37.66(28.62) ± 1.22	0.95(25.2)	±1.48	±0.63	±2.02
0.263	11.476(8.689) ± 0.024	37.27(28.42) ± 1.28	0.97(23.9)	±1.35	±0.59	±1.95
0.241	10.531(7.990) ± 0.023	36.55(27.96) ± 1.33	0.91(22.4)	±1.35	±0.60	±1.99
0.219	9.581(7.281) ± 0.018	35.75(27.42) ± 1.13	0.78(21.0)	±1.21	±0.67	±1.78
0.197	8.626(6.560) ± 0.017	35.01(26.95) ± 1.19	0.73(19.3)	±1.15	±0.74	±1.81
0.175	7.670(5.832) ± 0.013	34.26(26.41) ± 1.09	0.63(17.6)	±1.20	±0.74	±1.78
0.153	6.712(5.099) ± 0.013	33.65(25.96) ± 1.19	0.59(16.0)	±1.12	±0.82	±1.82
0.131	5.756(4.365) ± 0.010	32.98(25.42) ± 1.16	0.53(14.3)	±0.98	±0.85	±1.74
0.109	4.800(3.629) ± 0.009	31.80(24.50) ± 1.17	0.48(12.4)	±1.01	±0.95	±1.82
0.087	3.841(2.888) ± 0.006	30.92(23.78) ± 1.17	0.54(10.7)	±0.94	±1.11	±1.87
0.066	2.902(2.255) ± 0.005	28.55(22.23) ± 1.20	0.47(9.0)	±0.98	±1.24	±1.98

TABLE IX: NBD fit results in centrality 30-40%.

$\delta\eta$	$\langle\mu_c\rangle(\langle\mu\rangle)$	$\langle k_c\rangle(\langle k\rangle)$	$\langle\chi^2/NDF\rangle(\langle NDF\rangle)$	$\delta\langle k_c\rangle(dead)$	$\delta\langle k_c\rangle(fake)$	$\delta\langle k_c\rangle(total)$
0.700	24.860(19.241) ± 0.058	34.21(26.48) ± 0.88	0.75(47.0)	±1.14	±0.33	±1.47
0.678	24.177(18.729) ± 0.057	34.00(26.34) ± 0.88	0.77(45.9)	±1.12	±0.30	±1.46
0.656	23.382(18.088) ± 0.055	33.88(26.21) ± 0.90	0.81(44.2)	±0.91	±0.29	±1.31
0.634	22.573(17.438) ± 0.054	33.73(26.06) ± 0.91	0.90(42.5)	±1.10	±0.25	±1.45
0.613	21.776(16.808) ± 0.053	33.63(25.96) ± 0.93	0.94(40.9)	±1.08	±0.27	±1.44
0.591	20.986(16.195) ± 0.051	33.54(25.89) ± 0.94	0.92(39.8)	±0.97	±0.25	±1.38
0.569	20.198(15.571) ± 0.050	33.46(25.80) ± 0.97	0.97(38.4)	±1.04	±0.26	±1.44
0.547	19.406(14.937) ± 0.049	33.43(25.74) ± 0.99	1.01(37.2)	±1.04	±0.24	±1.45
0.525	18.616(14.307) ± 0.048	33.48(25.74) ± 1.02	1.03(36.0)	±1.04	±0.25	±1.48
0.503	17.830(13.678) ± 0.046	33.37(25.61) ± 1.05	1.06(34.7)	±1.07	±0.28	±1.52
0.481	17.040(13.040) ± 0.045	33.31(25.51) ± 1.08	1.03(33.4)	±1.11	±0.28	±1.58
0.459	16.246(12.395) ± 0.043	33.30(25.43) ± 1.12	1.04(32.2)	±1.03	±0.28	±1.55
0.438	15.451(11.746) ± 0.042	33.14(25.23) ± 1.16	1.03(31.0)	±1.09	±0.34	±1.63
0.416	14.662(11.103) ± 0.041	32.95(24.99) ± 1.20	0.97(29.7)	±1.18	±0.38	±1.73
0.394	13.869(10.461) ± 0.040	32.84(24.83) ± 1.25	0.99(28.4)	±1.21	±0.33	±1.77
0.372	13.081(9.824) ± 0.038	32.69(24.61) ± 1.30	1.00(26.8)	±1.08	±0.36	±1.73
0.350	12.306(9.216) ± 0.026	32.49(24.40) ± 0.95	1.00(25.5)	±1.05	±0.35	±1.46
0.328	11.540(8.663) ± 0.025	31.92(24.08) ± 0.98	0.99(24.2)	±1.05	±0.36	±1.48
0.306	10.781(8.119) ± 0.024	31.35(23.78) ± 1.00	0.94(23.1)	±1.05	±0.36	±1.49
0.284	10.020(7.565) ± 0.023	30.76(23.49) ± 1.04	0.91(22.0)	±1.01	±0.35	±1.49
0.263	9.258(7.008) ± 0.022	30.22(23.20) ± 1.07	0.83(20.8)	±0.93	±0.36	±1.46
0.241	8.494(6.443) ± 0.021	29.75(22.94) ± 1.12	0.77(19.5)	±0.91	±0.39	±1.49
0.219	7.727(5.870) ± 0.016	29.20(22.62) ± 0.95	0.70(18.3)	±0.85	±0.37	±1.33
0.197	6.958(5.290) ± 0.015	28.62(22.29) ± 1.01	0.65(17.0)	±0.76	±0.38	±1.32
0.175	6.187(4.702) ± 0.012	27.94(21.88) ± 0.93	0.59(15.5)	±0.83	±0.46	±1.33
0.153	5.416(4.112) ± 0.011	27.29(21.40) ± 1.00	0.50(14.0)	±0.84	±0.56	±1.42
0.131	4.645(3.520) ± 0.009	26.74(20.98) ± 0.99	0.50(12.5)	±0.81	±0.60	±1.41
0.109	3.873(2.926) ± 0.008	25.80(20.22) ± 1.01	0.50(10.9)	±0.86	±0.66	±1.48
0.087	3.098(2.328) ± 0.006	24.72(19.40) ± 1.02	0.54(9.4)	±0.75	±0.74	±1.46
0.066	2.341(1.819) ± 0.004	22.77(17.95) ± 1.02	0.49(8.0)	±0.64	±0.81	±1.45

TABLE X: NBD fit results in centrality 35-45%.

$\delta\eta$	$\langle\mu_c\rangle(\langle\mu\rangle)$	$\langle k_c\rangle(\langle k\rangle)$	$\langle\chi^2/NDF\rangle(\langle NDF\rangle)$	$\delta\langle k_c\rangle(dead)$	$\delta\langle k_c\rangle(fake)$	$\delta\langle k_c\rangle(total)$
0.700	19.726(15.268) ± 0.051	29.23(22.62) ± 0.80	1.12(40.0)	±0.69	±0.09	±1.06
0.678	19.191(14.867) ± 0.050	29.24(22.65) ± 0.81	1.02(39.0)	±0.58	±0.17	±1.01
0.656	18.568(14.364) ± 0.049	29.05(22.47) ± 0.82	0.98(38.2)	±0.76	±0.16	±1.13
0.634	17.920(13.844) ± 0.048	29.04(22.43) ± 0.83	1.09(37.1)	±0.73	±0.13	±1.12
0.613	17.291(13.348) ± 0.046	28.91(22.31) ± 0.85	1.06(36.2)	±0.77	±0.10	±1.15
0.591	16.672(12.867) ± 0.045	28.64(22.10) ± 0.86	1.04(35.3)	±0.86	±0.20	±1.23
0.569	16.044(12.369) ± 0.044	28.57(22.02) ± 0.88	1.06(34.2)	±0.79	±0.18	±1.20
0.547	15.417(11.867) ± 0.043	28.48(21.92) ± 0.90	1.07(33.3)	±0.91	±0.24	±1.30
0.525	14.789(11.366) ± 0.042	28.48(21.89) ± 0.92	1.12(32.2)	±0.88	±0.21	±1.29
0.503	14.165(10.866) ± 0.041	28.36(21.76) ± 0.94	1.10(31.2)	±0.82	±0.21	±1.26
0.481	13.537(10.360) ± 0.040	28.27(21.64) ± 0.97	1.11(29.9)	±0.85	±0.20	±1.31
0.459	12.908(9.849) ± 0.039	28.14(21.47) ± 1.00	1.11(28.8)	±0.92	±0.21	±1.38
0.438	12.276(9.334) ± 0.037	28.00(21.28) ± 1.03	1.10(27.7)	±0.88	±0.23	±1.37
0.416	11.648(8.822) ± 0.036	27.82(21.07) ± 1.06	1.08(26.6)	±0.89	±0.23	±1.40
0.394	11.019(8.313) ± 0.035	27.61(20.83) ± 1.09	1.04(25.5)	±0.96	±0.26	±1.47
0.372	10.391(7.805) ± 0.034	27.49(20.65) ± 1.13	0.98(24.5)	±0.85	±0.26	±1.44
0.350	9.774(7.322) ± 0.023	27.32(20.46) ± 0.83	0.92(23.4)	±0.81	±0.21	±1.18
0.328	9.165(6.883) ± 0.022	26.94(20.23) ± 0.85	0.89(22.4)	±0.75	±0.21	±1.15
0.306	8.562(6.451) ± 0.021	26.60(20.05) ± 0.87	0.86(21.4)	±0.72	±0.16	±1.14
0.284	7.959(6.013) ± 0.020	26.19(19.83) ± 0.90	0.82(20.2)	±0.73	±0.21	±1.18
0.263	7.353(5.569) ± 0.019	25.80(19.62) ± 0.93	0.75(19.3)	±0.73	±0.22	±1.21
0.241	6.748(5.122) ± 0.018	25.24(19.28) ± 0.97	0.65(18.3)	±0.80	±0.29	±1.29
0.219	6.138(4.666) ± 0.014	24.84(19.05) ± 0.83	0.63(17.1)	±0.61	±0.29	±1.07
0.197	5.527(4.205) ± 0.013	24.45(18.82) ± 0.88	0.61(15.9)	±0.62	±0.28	±1.11
0.175	4.915(3.739) ± 0.011	24.05(18.53) ± 0.81	0.62(14.7)	±0.55	±0.30	±1.03
0.153	4.303(3.270) ± 0.010	23.55(18.15) ± 0.88	0.57(13.3)	±0.60	±0.37	±1.13
0.131	3.691(2.801) ± 0.008	22.88(17.57) ± 0.85	0.53(11.8)	±0.59	±0.38	±1.11
0.109	3.076(2.328) ± 0.007	22.21(16.99) ± 0.88	0.56(10.4)	±0.51	±0.41	±1.10
0.087	2.461(1.851) ± 0.005	21.27(16.15) ± 0.89	0.61(8.9)	±0.56	±0.47	±1.16
0.066	1.859(1.445) ± 0.004	19.60(14.74) ± 0.92	0.59(7.4)	±0.70	±0.52	±1.27

TABLE XI: NBD fit results in centrality 40-50%.

$\delta\eta$	$\langle\mu_c\rangle(\langle\mu\rangle)$	$\langle k_c\rangle(\langle k\rangle)$	$\langle\chi^2/NDF\rangle(\langle NDF\rangle)$	$\delta\langle k_c\rangle(dead)$	$\delta\langle k_c\rangle(fake)$	$\delta\langle k_c\rangle(total)$
0.700	15.446(11.955) ± 0.044	23.99(18.57) ± 0.65	1.07(36.0)	±1.02	±0.17	±1.22
0.678	15.032(11.644) ± 0.043	23.87(18.49) ± 0.66	1.08(35.1)	±0.64	±0.18	±0.93
0.656	14.534(11.243) ± 0.042	24.03(18.59) ± 0.68	1.24(34.0)	±0.61	±0.06	±0.91
0.634	14.033(10.841) ± 0.041	24.11(18.63) ± 0.69	1.25(33.2)	±0.78	±0.16	±1.06
0.613	13.547(10.457) ± 0.041	23.98(18.51) ± 0.71	1.18(32.4)	±0.77	±0.17	±1.06
0.591	13.055(10.075) ± 0.040	23.97(18.50) ± 0.73	1.15(31.6)	±0.80	±0.16	±1.09
0.569	12.561(9.684) ± 0.038	23.89(18.42) ± 0.74	1.16(30.8)	±0.68	±0.14	±1.02
0.547	12.072(9.293) ± 0.037	23.70(18.24) ± 0.76	1.09(30.2)	±0.74	±0.14	±1.07
0.525	11.583(8.903) ± 0.037	23.65(18.17) ± 0.78	1.02(29.3)	±0.63	±0.12	±1.01
0.503	11.093(8.510) ± 0.036	23.66(18.15) ± 0.81	1.05(28.1)	±0.65	±0.15	±1.05
0.481	10.600(8.112) ± 0.035	23.64(18.09) ± 0.83	1.00(27.3)	±0.66	±0.17	±1.08
0.459	10.106(7.711) ± 0.034	23.56(17.98) ± 0.86	0.95(26.2)	±0.58	±0.16	±1.05
0.438	9.610(7.306) ± 0.033	23.42(17.81) ± 0.89	0.86(25.2)	±0.60	±0.14	±1.08
0.416	9.116(6.904) ± 0.032	23.27(17.62) ± 0.92	0.80(23.9)	±0.67	±0.18	±1.15
0.394	8.620(6.503) ± 0.030	23.36(17.62) ± 0.96	0.81(22.9)	±0.55	±0.17	±1.12
0.372	8.131(6.107) ± 0.029	23.21(17.44) ± 1.00	0.72(22.0)	±0.62	±0.18	±1.19
0.350	7.652(5.731) ± 0.020	22.92(17.18) ± 0.73	0.64(20.9)	±0.77	±0.24	±1.08
0.328	7.176(5.388) ± 0.019	22.61(17.05) ± 0.76	0.63(19.8)	±0.74	±0.21	±1.08
0.306	6.706(5.050) ± 0.018	22.30(16.92) ± 0.78	0.62(18.8)	±0.70	±0.20	±1.07
0.284	6.235(4.708) ± 0.018	22.05(16.82) ± 0.81	0.60(18.0)	±0.65	±0.20	±1.06
0.263	5.762(4.362) ± 0.017	21.72(16.65) ± 0.85	0.59(17.0)	±0.61	±0.22	±1.06
0.241	5.287(4.011) ± 0.016	21.38(16.47) ± 0.89	0.60(16.0)	±0.55	±0.23	±1.07
0.219	4.811(3.656) ± 0.012	20.89(16.16) ± 0.76	0.57(14.9)	±0.58	±0.24	±0.98
0.197	4.333(3.295) ± 0.012	20.52(15.95) ± 0.81	0.53(13.9)	±0.51	±0.25	±0.99
0.175	3.852(2.929) ± 0.009	20.17(15.72) ± 0.76	0.54(12.8)	±0.49	±0.28	±0.94
0.153	3.372(2.561) ± 0.009	19.78(15.44) ± 0.82	0.51(11.6)	±0.45	±0.28	±0.98
0.131	2.891(2.192) ± 0.007	19.34(15.10) ± 0.81	0.49(10.6)	±0.43	±0.28	±0.96
0.109	2.410(1.821) ± 0.006	18.81(14.69) ± 0.85	0.46(9.3)	±0.36	±0.33	±0.98
0.087	1.928(1.449) ± 0.004	18.14(14.19) ± 0.87	0.48(7.9)	±0.38	±0.35	±1.01
0.066	1.456(1.131) ± 0.004	17.03(13.51) ± 0.91	0.48(6.6)	±0.32	±0.35	±1.03

TABLE XII: NBD fit results in centrality 45-55%.

$\delta\eta$	$\langle\mu_c\rangle(\langle\mu\rangle)$	$\langle k_c\rangle(\langle k\rangle)$	$\langle\chi^2/NDF\rangle(\langle NDF\rangle)$	$\delta\langle k_c\rangle(dead)$	$\delta\langle k_c\rangle(fake)$	$\delta\langle k_c\rangle(total)$
0.700	11.838(9.163) ± 0.038	20.15(15.59) ± 0.61	1.14(28.0)	±0.71	±0.06	±0.94
0.678	11.517(8.922) ± 0.037	20.06(15.54) ± 0.61	1.10(27.9)	±0.60	±0.03	±0.86
0.656	11.142(8.620) ± 0.036	19.94(15.43) ± 0.62	1.10(26.6)	±0.48	±0.08	±0.79
0.634	10.759(8.311) ± 0.035	19.94(15.40) ± 0.64	1.08(25.8)	±0.47	±0.11	±0.80
0.613	10.380(8.013) ± 0.035	19.99(15.43) ± 0.65	1.06(24.9)	±0.51	±0.08	±0.83
0.591	10.005(7.721) ± 0.034	19.95(15.39) ± 0.67	1.06(24.1)	±0.41	±0.11	±0.79
0.569	9.629(7.424) ± 0.033	19.85(15.30) ± 0.68	1.05(23.2)	±0.44	±0.10	±0.82
0.547	9.254(7.123) ± 0.032	19.76(15.21) ± 0.70	1.04(22.5)	±0.47	±0.12	±0.85
0.525	8.879(6.824) ± 0.031	19.73(15.16) ± 0.72	1.02(21.8)	±0.42	±0.11	±0.84
0.503	8.505(6.525) ± 0.030	19.69(15.10) ± 0.74	0.96(21.4)	±0.42	±0.13	±0.86
0.481	8.130(6.222) ± 0.030	19.63(15.02) ± 0.76	0.89(20.7)	±0.44	±0.14	±0.89
0.459	7.751(5.915) ± 0.029	19.62(14.97) ± 0.79	0.77(20.1)	±0.49	±0.14	±0.94
0.438	7.370(5.604) ± 0.028	19.66(14.95) ± 0.82	0.66(19.6)	±0.49	±0.14	±0.96
0.416	6.991(5.295) ± 0.027	19.74(14.95) ± 0.85	0.63(18.8)	±0.49	±0.16	±1.00
0.394	6.612(4.988) ± 0.026	19.80(14.94) ± 0.89	0.62(18.1)	±0.55	±0.17	±1.06
0.372	6.236(4.684) ± 0.025	19.79(14.86) ± 0.93	0.58(17.3)	±0.56	±0.17	±1.10
0.350	5.868(4.395) ± 0.017	19.74(14.79) ± 0.69	0.58(16.7)	±0.55	±0.20	±0.91
0.328	5.502(4.131) ± 0.017	19.58(14.75) ± 0.72	0.62(16.1)	±0.52	±0.21	±0.91
0.306	5.141(3.872) ± 0.016	19.30(14.66) ± 0.74	0.62(15.5)	±0.51	±0.19	±0.92
0.284	4.780(3.610) ± 0.015	18.97(14.51) ± 0.78	0.59(14.9)	±0.47	±0.17	±0.93
0.263	4.418(3.345) ± 0.015	18.76(14.44) ± 0.82	0.61(14.2)	±0.48	±0.21	±0.97
0.241	4.056(3.077) ± 0.014	18.53(14.33) ± 0.87	0.59(13.6)	±0.48	±0.19	±1.01
0.219	3.689(2.803) ± 0.011	18.38(14.30) ± 0.76	0.61(13.0)	±0.49	±0.19	±0.93
0.197	3.321(2.526) ± 0.010	18.29(14.30) ± 0.83	0.60(12.2)	±0.44	±0.20	±0.96
0.175	2.953(2.244) ± 0.008	18.03(14.17) ± 0.79	0.56(11.4)	±0.52	±0.20	±0.97
0.153	2.583(1.962) ± 0.007	17.80(14.06) ± 0.89	0.55(10.4)	±0.46	±0.22	±1.02
0.131	2.215(1.678) ± 0.006	17.55(13.94) ± 0.92	0.57(9.3)	±0.34	±0.24	±1.00
0.109	1.846(1.394) ± 0.005	17.10(13.66) ± 0.98	0.56(8.2)	±0.34	±0.29	±1.08
0.087	1.477(1.109) ± 0.004	16.55(13.29) ± 1.05	0.51(7.0)	±0.29	±0.27	±1.12
0.066	1.117(0.875) ± 0.003	16.05(12.98) ± 1.09	0.51(5.8)	±0.26	±0.34	±1.17

TABLE XIII: NBD fit results in centrality 50-60%.

$\delta\eta$	$\langle\mu_c\rangle(\langle\mu\rangle)$	$\langle k_c\rangle(\langle k\rangle)$	$\langle\chi^2/NDF\rangle(\langle NDF\rangle)$	$\delta\langle k_c\rangle(dead)$	$\delta\langle k_c\rangle(fake)$	$\delta\langle k_c\rangle(total)$
0.700	4.508(3.489) ± 0.023	8.89(6.88) ± 0.29	0.90(15.0)	±0.21	±0.01	±0.35
0.678	4.387(3.398) ± 0.022	8.85(6.85) ± 0.29	0.90(14.8)	±0.23	±0.01	±0.37
0.656	4.248(3.286) ± 0.022	8.78(6.79) ± 0.29	0.76(14.2)	±0.25	±0.01	±0.39
0.634	4.102(3.169) ± 0.021	8.74(6.75) ± 0.30	0.76(13.9)	±0.26	±0.01	±0.39
0.613	3.954(3.052) ± 0.021	8.81(6.80) ± 0.31	1.14(13.4)	±0.23	±0.01	±0.38
0.591	3.813(2.942) ± 0.020	8.67(6.69) ± 0.31	0.91(13.1)	±0.24	±0.01	±0.39
0.569	3.666(2.827) ± 0.020	8.66(6.67) ± 0.32	0.96(12.9)	±0.27	±0.02	±0.42
0.547	3.518(2.708) ± 0.019	8.78(6.76) ± 0.33	1.19(12.5)	±0.21	±0.01	±0.40
0.525	3.378(2.596) ± 0.019	8.67(6.66) ± 0.34	0.93(12.0)	±0.21	±0.01	±0.40
0.503	3.236(2.482) ± 0.018	8.67(6.65) ± 0.35	0.86(11.8)	±0.25	±0.01	±0.43
0.481	3.091(2.366) ± 0.018	8.71(6.67) ± 0.36	0.88(11.6)	±0.23	±0.02	±0.43
0.459	2.949(2.250) ± 0.017	8.67(6.62) ± 0.37	0.80(11.1)	±0.20	±0.02	±0.42
0.438	2.806(2.133) ± 0.017	8.63(6.56) ± 0.39	0.76(10.5)	±0.20	±0.03	±0.44
0.416	2.664(2.017) ± 0.017	8.58(6.50) ± 0.40	0.65(9.9)	±0.24	±0.03	±0.47
0.394	2.520(1.901) ± 0.016	8.60(6.49) ± 0.42	0.64(9.5)	±0.23	±0.02	±0.48
0.372	2.376(1.785) ± 0.015	8.69(6.54) ± 0.45	0.75(8.9)	±0.26	±0.02	±0.52
0.350	2.236(1.675) ± 0.011	8.77(6.57) ± 0.34	0.73(8.5)	±0.25	±0.02	±0.43
0.328	2.097(1.575) ± 0.010	8.75(6.58) ± 0.36	0.69(8.1)	±0.25	±0.02	±0.44
0.306	1.960(1.476) ± 0.010	8.74(6.61) ± 0.38	0.74(7.6)	±0.22	±0.03	±0.44
0.284	1.822(1.376) ± 0.009	8.71(6.63) ± 0.41	0.75(7.1)	±0.23	±0.03	±0.47
0.263	1.683(1.274) ± 0.009	8.70(6.67) ± 0.44	0.78(6.7)	±0.21	±0.03	±0.49
0.241	1.545(1.172) ± 0.008	8.66(6.67) ± 0.47	0.75(6.3)	±0.19	±0.03	±0.51
0.219	1.407(1.069) ± 0.006	8.55(6.62) ± 0.41	0.70(5.9)	±0.18	±0.03	±0.45
0.197	1.267(0.963) ± 0.006	8.45(6.57) ± 0.45	0.59(5.5)	±0.18	±0.03	±0.48
0.175	1.126(0.856) ± 0.005	8.41(6.59) ± 0.44	0.59(5.2)	±0.15	±0.04	±0.47
0.153	0.986(0.749) ± 0.005	8.31(6.54) ± 0.50	0.58(4.8)	±0.14	±0.05	±0.52
0.131	0.846(0.641) ± 0.004	8.07(6.36) ± 0.52	0.52(4.4)	±0.16	±0.06	±0.55
0.109	0.706(0.534) ± 0.003	7.85(6.21) ± 0.54	0.40(3.8)	±0.08	±0.07	±0.55
0.087	0.565(0.424) ± 0.002	7.86(6.23) ± 0.64	0.58(3.3)	±0.06	±0.09	±0.65
0.066	0.428(0.339) ± 0.002	7.22(5.77) ± 0.64	0.44(2.9)	±0.06	±0.07	±0.65

TABLE XIV: NBD fit results in centrality 55-65%.

$\delta\eta$	$\langle\mu_c\rangle(\langle\mu\rangle)$	$\langle k_c\rangle(\langle k\rangle)$	$\langle\chi^2/NDF\rangle(\langle NDF\rangle)$	$\delta\langle k_c\rangle(dead)$	$\delta\langle k_c\rangle(fake)$	$\delta\langle k_c\rangle(total)$
0.700	3.086(2.389) ± 0.019	5.90(4.56) ± 0.20	0.76(13.0)	±0.25	±0.01	±0.32
0.678	3.000(2.324) ± 0.019	5.88(4.56) ± 0.20	0.79(12.7)	±0.13	±0.01	±0.24
0.656	2.902(2.245) ± 0.018	5.85(4.52) ± 0.20	0.76(12.5)	±0.14	±0.02	±0.24
0.634	2.803(2.166) ± 0.018	5.78(4.46) ± 0.20	0.69(12.2)	±0.14	±0.02	±0.25
0.613	2.703(2.086) ± 0.017	5.80(4.48) ± 0.21	0.78(12.1)	±0.07	±0.02	±0.22
0.591	2.607(2.012) ± 0.017	5.76(4.45) ± 0.21	0.70(11.3)	±0.14	±0.02	±0.25
0.569	2.508(1.934) ± 0.017	5.76(4.44) ± 0.22	0.62(10.9)	±0.13	±0.02	±0.25
0.547	2.410(1.855) ± 0.016	5.75(4.43) ± 0.23	0.55(10.3)	±0.12	±0.04	±0.26
0.525	2.313(1.777) ± 0.016	5.75(4.42) ± 0.23	0.50(9.9)	±0.16	±0.04	±0.28
0.503	2.215(1.699) ± 0.015	5.76(4.42) ± 0.24	0.47(9.6)	±0.16	±0.01	±0.29
0.481	2.117(1.620) ± 0.015	5.79(4.43) ± 0.25	0.49(9.2)	±0.16	±0.01	±0.30
0.459	2.018(1.540) ± 0.015	5.78(4.41) ± 0.26	0.49(8.9)	±0.16	±0.01	±0.30
0.438	1.919(1.459) ± 0.014	5.79(4.40) ± 0.27	0.50(8.8)	±0.17	±0.02	±0.32
0.416	1.820(1.378) ± 0.014	5.81(4.40) ± 0.28	0.52(8.6)	±0.20	±0.03	±0.34
0.394	1.721(1.298) ± 0.013	5.84(4.41) ± 0.30	0.53(8.4)	±0.15	±0.02	±0.34
0.372	1.623(1.219) ± 0.013	5.84(4.39) ± 0.32	0.54(7.8)	±0.18	±0.01	±0.36
0.350	1.527(1.144) ± 0.009	5.87(4.41) ± 0.24	0.52(7.6)	±0.21	±0.01	±0.32
0.328	1.432(1.075) ± 0.008	5.86(4.42) ± 0.25	0.49(7.4)	±0.24	±0.02	±0.34
0.306	1.339(1.008) ± 0.008	5.85(4.43) ± 0.27	0.48(7.2)	±0.21	±0.02	±0.34
0.284	1.244(0.940) ± 0.008	5.85(4.45) ± 0.28	0.52(6.9)	±0.21	±0.02	±0.35
0.263	1.150(0.871) ± 0.007	5.85(4.48) ± 0.31	0.59(6.5)	±0.14	±0.02	±0.34
0.241	1.056(0.801) ± 0.007	5.83(4.49) ± 0.33	0.59(6.2)	±0.11	±0.02	±0.35
0.219	0.961(0.730) ± 0.005	5.81(4.50) ± 0.29	0.62(5.9)	±0.10	±0.03	±0.31
0.197	0.866(0.658) ± 0.005	5.73(4.46) ± 0.32	0.57(5.5)	±0.10	±0.03	±0.34
0.175	0.770(0.585) ± 0.004	5.72(4.46) ± 0.32	0.54(5.2)	±0.10	±0.04	±0.33
0.153	0.674(0.511) ± 0.004	5.67(4.44) ± 0.36	0.53(4.8)	±0.09	±0.06	±0.38
0.131	0.578(0.438) ± 0.003	5.50(4.32) ± 0.36	0.40(4.5)	±0.05	±0.07	±0.37
0.109	0.482(0.364) ± 0.003	5.31(4.18) ± 0.39	0.51(4.0)	±0.05	±0.10	±0.41
0.087	0.386(0.292) ± 0.002	4.90(3.89) ± 0.43	0.54(3.6)	±0.05	±0.02	±0.43
0.066	0.292(0.232) ± 0.002	4.56(3.63) ± 0.44	0.57(3.1)	±0.05	±0.05	±0.45

TABLE XV: NBD fit results in centrality 0-5%.

$\delta\eta$	$\langle\mu_c\rangle(\langle\mu\rangle)$	$\langle k_c\rangle(\langle k\rangle)$	$\langle\chi^2/NDF\rangle(\langle NDF\rangle)$	$\delta\langle k_c\rangle(dead)$	$\delta\langle k_c\rangle(fake)$	$\delta\langle k_c\rangle(total)$
0.700	84.371(65.303) ± 0.148	341.22(264.10) ± 31.75	0.54(58.0)	±54.10	±6.72	±63.09
0.678	82.149(63.638) ± 0.144	359.73(278.66) ± 35.51	0.58(57.8)	±29.67	±26.46	±53.31
0.656	79.451(61.463) ± 0.141	369.96(286.25) ± 37.82	0.66(56.4)	±13.85	±14.18	±42.69
0.634	76.740(59.282) ± 0.138	370.46(286.18) ± 38.62	0.63(55.4)	±19.09	±14.98	±45.61
0.613	74.027(57.142) ± 0.135	372.37(287.35) ± 40.79	0.62(54.7)	±13.54	±15.22	±45.60
0.591	71.331(55.050) ± 0.133	374.07(288.55) ± 42.84	0.64(53.6)	±13.41	±17.15	±48.06
0.569	68.629(52.910) ± 0.130	374.10(288.36) ± 44.31	0.64(52.7)	±18.44	±19.49	±51.80
0.547	65.925(50.747) ± 0.127	367.65(282.90) ± 44.42	0.64(52.2)	±16.76	±24.95	±53.63
0.525	63.249(48.612) ± 0.124	368.12(282.88) ± 46.12	0.68(51.2)	±16.19	±24.02	±54.46
0.503	60.566(46.465) ± 0.121	364.03(279.07) ± 46.64	0.65(50.2)	±15.42	±23.48	±54.45
0.481	57.877(44.295) ± 0.118	362.25(277.19) ± 48.15	0.65(49.0)	±12.93	±24.16	±55.40
0.459	55.171(42.098) ± 0.115	363.40(277.12) ± 50.80	0.66(47.9)	±13.82	±20.65	±56.55
0.438	52.479(39.900) ± 0.112	355.07(269.86) ± 51.95	0.64(46.5)	±9.95	±25.57	±58.75
0.416	49.791(37.710) ± 0.109	352.80(267.18) ± 54.68	0.66(45.2)	±14.68	±26.89	±62.68
0.394	47.118(35.547) ± 0.106	349.73(263.69) ± 57.42	0.64(43.6)	±13.29	±32.16	±67.14
0.372	44.456(33.395) ± 0.103	347.01(260.24) ± 64.15	0.65(42.1)	±3.82	±30.09	±70.96
0.350	41.832(31.335) ± 0.070	340.53(254.77) ± 52.65	0.67(40.6)	±11.74	±34.67	±64.13
0.328	39.229(29.465) ± 0.068	340.79(254.20) ± 55.01	0.65(39.4)	±2.10	±27.89	±61.72
0.306	36.653(27.626) ± 0.065	332.14(246.66) ± 60.16	0.68(37.9)	±12.90	±31.13	±68.95
0.284	34.073(25.755) ± 0.062	333.98(247.30) ± 64.64	0.69(37.0)	±1.38	±33.33	±72.74
0.263	31.493(23.870) ± 0.060	313.43(230.73) ± 62.92	0.69(35.2)	±1.26	±26.90	±68.44
0.241	28.903(21.959) ± 0.057	294.86(214.95) ± 59.84	0.68(33.5)	±2.22	±32.24	±68.01
0.219	26.305(20.020) ± 0.044	278.11(200.81) ± 51.12	0.69(31.9)	±3.21	±29.02	±58.87
0.197	23.677(18.009) ± 0.042	253.36(181.02) ± 56.29	0.71(30.2)	±6.54	±23.20	±61.24
0.175	21.066(16.025) ± 0.034	232.35(165.72) ± 50.48	0.73(28.3)	±3.92	±24.00	±56.04
0.153	18.425(13.948) ± 0.032	199.21(140.84) ± 48.99	0.75(26.2)	±8.99	±17.20	±52.70
0.131	15.807(11.964) ± 0.026	181.55(126.91) ± 37.35	0.80(24.2)	±10.43	±17.64	±42.61
0.109	13.174(9.949) ± 0.022	157.69(108.85) ± 28.73	0.83(21.4)	±3.79	±14.86	±32.57
0.087	10.522(7.808) ± 0.017	125.65(86.76) ± 21.21	0.80(18.2)	±3.14	±11.02	±24.10
0.066	7.947(6.122) ± 0.013	97.74(67.60) ± 13.55	0.73(15.1)	±8.30	±9.98	±18.77

TABLE XVI: NBD fit results in centrality 5-10%.

$\delta\eta$	$\langle\mu_c\rangle(\langle\mu\rangle)$	$\langle k_c\rangle(\langle k\rangle)$	$\langle\chi^2/NDF\rangle(\langle NDF\rangle)$	$\delta\langle k_c\rangle(dead)$	$\delta\langle k_c\rangle(fake)$	$\delta\langle k_c\rangle(total)$
0.700	72.246(55.918) ± 0.126	187.62(145.22) ± 10.56	0.80(61.0)	±1.88	±9.61	±14.40
0.678	70.291(54.452) ± 0.124	185.02(143.32) ± 10.61	0.68(61.3)	±10.46	±6.69	±16.33
0.656	67.996(52.602) ± 0.121	188.09(145.50) ± 11.00	0.71(59.8)	±4.99	±4.56	±12.91
0.634	65.656(50.720) ± 0.119	188.72(145.76) ± 11.29	0.76(59.0)	±2.81	±6.48	±13.32
0.613	63.346(48.897) ± 0.116	186.50(143.95) ± 11.39	0.79(57.0)	±4.55	±6.31	±13.79
0.591	61.055(47.118) ± 0.114	185.01(142.75) ± 11.53	0.76(55.6)	±6.00	±5.32	±14.04
0.569	58.752(45.296) ± 0.111	184.61(142.29) ± 11.90	0.76(54.0)	±4.96	±7.98	±15.16
0.547	56.443(43.447) ± 0.108	183.38(141.14) ± 12.28	0.78(52.2)	±5.40	±8.57	±15.92
0.525	54.144(41.614) ± 0.106	183.73(141.18) ± 12.87	0.78(51.2)	±5.90	±8.41	±16.47
0.503	51.839(39.768) ± 0.103	186.84(143.32) ± 13.65	0.81(49.4)	±3.47	±7.23	±15.83
0.481	49.534(37.909) ± 0.100	187.11(143.19) ± 14.16	0.84(47.9)	±3.90	±7.38	±16.44
0.459	47.220(36.030) ± 0.097	189.72(144.71) ± 15.07	0.88(46.3)	±2.39	±7.36	±16.94
0.438	44.921(34.153) ± 0.095	187.66(142.61) ± 15.56	0.85(44.6)	±8.12	±10.08	±20.24
0.416	42.618(32.277) ± 0.092	188.72(142.85) ± 16.50	0.86(43.1)	±7.80	±7.74	±19.83
0.394	40.328(30.425) ± 0.089	186.94(140.87) ± 17.11	0.82(41.6)	±5.86	±9.43	±20.40
0.372	38.053(28.585) ± 0.086	186.28(139.66) ± 18.10	0.85(39.9)	±7.17	±9.93	±21.86
0.350	35.798(26.815) ± 0.059	187.25(139.96) ± 13.64	0.89(38.5)	±5.58	±9.02	±17.28
0.328	33.572(25.212) ± 0.057	184.92(138.46) ± 14.19	0.89(37.3)	±5.46	±12.28	±19.55
0.306	31.368(23.631) ± 0.055	182.12(136.56) ± 14.59	0.91(36.0)	±5.25	±11.88	±19.53
0.284	29.158(22.030) ± 0.052	178.29(134.27) ± 14.70	0.89(34.6)	±4.86	±13.82	±20.75
0.263	26.943(20.408) ± 0.050	173.07(131.50) ± 15.26	0.91(33.1)	±5.84	±15.75	±22.69
0.241	24.731(18.770) ± 0.048	169.01(129.45) ± 15.73	0.88(32.1)	±6.53	±15.73	±23.19
0.219	22.501(17.102) ± 0.037	167.76(129.28) ± 13.97	0.94(30.7)	±3.27	±12.91	±19.31
0.197	20.271(15.421) ± 0.035	160.25(123.65) ± 14.29	0.94(29.1)	±5.43	±15.13	±21.52
0.175	18.030(13.713) ± 0.028	152.49(118.31) ± 13.95	0.99(27.4)	±5.87	±13.32	±20.16
0.153	15.787(11.998) ± 0.026	144.71(112.06) ± 13.58	1.00(25.4)	±5.81	±15.35	±21.30
0.131	13.540(10.276) ± 0.022	137.12(106.29) ± 12.40	1.05(22.9)	±5.42	±14.45	±19.80
0.109	11.289(8.548) ± 0.018	122.24(92.30) ± 10.92	1.09(20.3)	±6.77	±14.31	±19.23
0.087	9.029(6.805) ± 0.014	99.52(72.96) ± 9.30	1.03(17.2)	±5.46	±10.51	±15.06
0.066	6.807(5.296) ± 0.011	75.37(54.94) ± 6.89	0.81(14.2)	±6.29	±8.08	±12.34

TABLE XVII: NBD fit results in centrality 10-15%.

$\delta\eta$	$\langle\mu_c\rangle(\langle\mu\rangle)$	$\langle k_c\rangle(\langle k\rangle)$	$\langle\chi^2/NDF\rangle(\langle NDF\rangle)$	$\delta\langle k_c\rangle(dead)$	$\delta\langle k_c\rangle(fake)$	$\delta\langle k_c\rangle(total)$
0.700	60.607(46.909) ± 0.119	129.59(100.31) ± 6.29	0.80(58.0)	±1.29	±1.51	±6.60
0.678	59.026(45.725) ± 0.118	123.34(95.54) ± 6.09	0.76(56.6)	±4.71	±9.77	±12.44
0.656	57.108(44.179) ± 0.116	121.44(93.94) ± 6.08	0.70(55.3)	±5.55	±4.90	±9.58
0.634	55.139(42.596) ± 0.113	121.88(94.14) ± 6.24	0.70(54.2)	±4.92	±3.01	±8.50
0.613	53.198(41.064) ± 0.111	120.98(93.37) ± 6.33	0.69(52.9)	±5.23	±2.63	±8.62
0.591	51.256(39.556) ± 0.108	120.49(92.96) ± 6.46	0.71(52.2)	±3.80	±3.87	±8.44
0.569	49.321(38.025) ± 0.106	119.78(92.31) ± 6.58	0.70(51.3)	±3.61	±2.65	±7.95
0.547	47.393(36.482) ± 0.103	117.86(90.68) ± 6.62	0.71(50.1)	±3.12	±3.60	±8.15
0.525	45.463(34.943) ± 0.101	117.65(90.38) ± 6.79	0.71(49.2)	±3.77	±3.44	±8.49
0.503	43.535(33.398) ± 0.098	117.79(90.32) ± 7.03	0.71(48.2)	±3.47	±4.14	±8.87
0.481	41.602(31.839) ± 0.095	118.04(90.30) ± 7.29	0.71(46.9)	±3.18	±3.55	±8.71
0.459	39.668(30.267) ± 0.092	118.96(90.76) ± 7.64	0.73(45.2)	±3.46	±4.65	±9.59
0.438	37.729(28.684) ± 0.090	118.41(90.03) ± 7.87	0.72(44.0)	±3.52	±4.95	±9.94
0.416	35.787(27.104) ± 0.087	118.19(89.52) ± 8.24	0.74(42.5)	±4.23	±5.06	±10.56
0.394	33.864(25.547) ± 0.084	118.35(89.25) ± 8.67	0.76(41.1)	±4.60	±4.92	±10.98
0.372	31.943(23.994) ± 0.082	118.19(88.71) ± 9.20	0.75(39.6)	±4.92	±5.31	±11.70
0.350	30.061(22.517) ± 0.056	117.56(87.92) ± 6.85	0.75(38.1)	±4.91	±5.85	±10.26
0.328	28.191(21.172) ± 0.053	117.37(87.84) ± 7.21	0.78(36.3)	±5.14	±5.41	±10.38
0.306	26.340(19.845) ± 0.051	117.25(87.95) ± 7.59	0.78(34.7)	±4.90	±5.07	±10.36
0.284	24.493(18.509) ± 0.049	117.01(87.82) ± 8.16	0.82(33.5)	±4.41	±5.83	±10.96
0.263	22.636(17.150) ± 0.047	114.86(86.40) ± 8.44	0.80(31.8)	±5.74	±5.96	±11.82
0.241	20.776(15.774) ± 0.044	114.37(86.11) ± 8.95	0.82(30.3)	±5.34	±6.20	±12.13
0.219	18.905(14.375) ± 0.034	112.39(84.83) ± 7.68	0.82(28.8)	±5.37	±7.32	±11.89
0.197	17.029(12.958) ± 0.033	111.32(84.34) ± 8.15	0.83(26.9)	±6.15	±7.47	±12.66
0.175	15.142(11.519) ± 0.026	109.44(83.15) ± 7.72	0.88(25.1)	±5.22	±7.32	±11.85
0.153	13.253(10.073) ± 0.024	106.03(80.26) ± 8.35	0.94(23.0)	±4.18	±6.94	±11.64
0.131	11.367(8.626) ± 0.020	96.68(72.34) ± 7.60	0.94(20.5)	±4.30	±7.09	±11.25
0.109	9.474(7.170) ± 0.017	88.58(65.38) ± 7.20	0.87(18.1)	±3.97	±8.10	±11.54
0.087	7.575(5.704) ± 0.013	77.55(55.69) ± 6.79	0.81(15.6)	±3.54	±7.64	±10.82
0.066	5.714(4.443) ± 0.010	64.41(47.02) ± 6.22	0.63(12.8)	±4.49	±6.13	±9.82

TABLE XVIII: NBD fit results in centrality 15-20%.

$\delta\eta$	$\langle\mu_c\rangle(\langle\mu\rangle)$	$\langle k_c\rangle(\langle k\rangle)$	$\langle\chi^2/NDF\rangle(\langle NDF\rangle)$	$\delta\langle k_c\rangle(dead)$	$\delta\langle k_c\rangle(fake)$	$\delta\langle k_c\rangle(total)$
0.700	50.243(38.888) ± 0.109	95.08(73.59) ± 4.42	0.79(53.0)	±4.84	±6.50	±9.23
0.678	48.892(37.875) ± 0.106	95.76(74.18) ± 4.54	0.67(52.4)	±3.20	±1.41	±5.73
0.656	47.301(36.592) ± 0.104	95.63(73.98) ± 4.65	0.75(51.2)	±2.80	±1.66	±5.68
0.634	45.685(35.292) ± 0.102	95.70(73.94) ± 4.78	0.71(49.2)	±2.09	±1.96	±5.57
0.613	44.087(34.031) ± 0.100	94.78(73.17) ± 4.87	0.71(47.7)	±3.79	±3.17	±6.94
0.591	42.483(32.785) ± 0.097	95.97(74.07) ± 5.05	0.70(47.1)	±2.95	±1.99	±6.18
0.569	40.884(31.519) ± 0.095	96.10(74.10) ± 5.22	0.69(46.1)	±2.66	±2.10	±6.22
0.547	39.301(30.251) ± 0.092	95.92(73.85) ± 5.36	0.70(44.8)	±3.31	±2.60	±6.82
0.525	37.708(28.981) ± 0.090	96.52(74.20) ± 5.57	0.71(43.6)	±3.47	±1.98	±6.85
0.503	36.108(27.700) ± 0.088	96.81(74.28) ± 5.77	0.75(42.5)	±2.84	±2.39	±6.86
0.481	34.505(26.406) ± 0.085	96.51(73.88) ± 5.92	0.73(41.4)	±2.38	±1.88	±6.65
0.459	32.897(25.100) ± 0.083	95.50(72.89) ± 6.03	0.73(40.1)	±2.67	±2.54	±7.07
0.438	31.285(23.784) ± 0.081	95.28(72.47) ± 6.24	0.77(38.6)	±2.78	±2.27	±7.19
0.416	29.677(22.474) ± 0.078	95.11(72.09) ± 6.45	0.78(37.3)	±3.02	±2.26	±7.47
0.394	28.079(21.180) ± 0.076	94.76(71.57) ± 6.69	0.78(35.9)	±2.98	±3.07	±7.94
0.372	26.483(19.889) ± 0.073	95.08(71.55) ± 7.04	0.81(34.6)	±2.59	±2.66	±7.96
0.350	24.918(18.661) ± 0.050	94.28(70.78) ± 5.11	0.80(33.3)	±3.11	±2.66	±6.55
0.328	23.365(17.541) ± 0.048	92.98(70.16) ± 5.28	0.82(32.3)	±2.56	±2.78	±6.50
0.306	21.831(16.441) ± 0.046	91.68(69.59) ± 5.47	0.84(31.2)	±2.32	±3.06	±6.69
0.284	20.294(15.325) ± 0.044	89.06(68.15) ± 5.60	0.85(29.8)	±2.62	±3.13	±6.93
0.263	18.754(14.199) ± 0.042	87.46(67.23) ± 5.76	0.85(28.5)	±2.47	±2.87	±6.90
0.241	17.215(13.060) ± 0.040	86.16(66.47) ± 6.04	0.88(27.0)	±2.30	±3.25	±7.23
0.219	15.665(11.902) ± 0.031	83.50(64.86) ± 5.15	0.90(25.4)	±3.27	±3.46	±7.01
0.197	14.110(10.728) ± 0.029	81.20(63.31) ± 5.36	0.88(23.7)	±2.47	±3.88	±7.06
0.175	12.547(9.540) ± 0.024	79.16(61.58) ± 4.86	0.93(21.9)	±2.06	±3.41	±6.28
0.153	10.977(8.337) ± 0.022	73.67(57.42) ± 4.99	0.91(19.8)	±1.63	±3.89	±6.53
0.131	9.409(7.133) ± 0.018	67.77(52.73) ± 4.44	0.83(17.8)	±2.00	±3.98	±6.29
0.109	7.840(5.924) ± 0.015	61.02(47.54) ± 4.01	0.74(15.6)	±1.99	±4.09	±6.06
0.087	6.271(4.713) ± 0.012	54.47(42.05) ± 3.54	0.63(13.4)	±1.64	±3.81	±5.46
0.066	4.734(3.678) ± 0.009	47.73(35.64) ± 3.59	0.58(11.3)	±2.06	±3.33	±5.31

TABLE XIX: NBD fit results in centrality 20-25%.

$\delta\eta$	$\langle\mu_c\rangle(\langle\mu\rangle)$	$\langle k_c\rangle(\langle k\rangle)$	$\langle\chi^2/NDF\rangle(\langle NDF\rangle)$	$\delta\langle k_c\rangle(dead)$	$\delta\langle k_c\rangle(fake)$	$\delta\langle k_c\rangle(total)$
0.700	41.340(31.997) ± 0.101	80.17(62.05) ± 3.85	0.71(48.0)	±1.34	±1.27	±4.27
0.678	40.233(31.167) ± 0.099	80.14(62.08) ± 3.92	0.67(47.2)	±3.19	±1.69	±5.33
0.656	38.920(30.109) ± 0.096	81.43(63.00) ± 4.07	0.68(46.9)	±1.52	±0.92	±4.44
0.634	37.606(29.051) ± 0.094	81.18(62.71) ± 4.17	0.68(45.8)	±3.68	±1.51	±5.76
0.613	36.282(28.006) ± 0.092	82.48(63.67) ± 4.38	0.78(44.7)	±1.90	±1.68	±5.07
0.591	34.986(27.000) ± 0.090	81.78(63.12) ± 4.43	0.76(44.2)	±2.76	±1.37	±5.39
0.569	33.656(25.947) ± 0.088	81.76(63.04) ± 4.53	0.75(43.4)	±1.38	±1.07	±4.86
0.547	32.342(24.895) ± 0.086	81.09(62.42) ± 4.60	0.68(42.5)	±1.91	±1.56	±5.22
0.525	31.029(23.848) ± 0.083	81.53(62.67) ± 4.76	0.72(41.5)	±1.98	±1.63	±5.40
0.503	29.714(22.794) ± 0.081	81.92(62.85) ± 4.93	0.77(40.5)	±1.94	±1.10	±5.41
0.481	28.395(21.731) ± 0.079	82.20(62.93) ± 5.11	0.77(39.3)	±2.21	±1.08	±5.67
0.459	27.071(20.654) ± 0.077	82.39(62.89) ± 5.33	0.79(38.3)	±2.25	±1.31	±5.93
0.438	25.754(19.579) ± 0.074	81.71(62.18) ± 5.47	0.78(37.1)	±2.79	±1.73	±6.38
0.416	24.428(18.499) ± 0.072	82.61(62.66) ± 5.83	0.82(35.8)	±2.05	±1.10	±6.28
0.394	23.116(17.436) ± 0.070	81.91(61.93) ± 6.04	0.78(34.6)	±2.84	±1.75	±6.90
0.372	21.803(16.374) ± 0.068	82.06(61.77) ± 6.34	0.78(33.3)	±2.84	±1.94	±7.21
0.350	20.516(15.364) ± 0.046	82.29(61.74) ± 4.77	0.82(32.1)	±3.10	±2.13	±6.08
0.328	19.244(14.448) ± 0.044	81.98(61.71) ± 4.99	0.82(30.8)	±2.85	±2.02	±6.09
0.306	17.979(13.542) ± 0.043	81.64(61.65) ± 5.26	0.82(29.7)	±3.02	±1.98	±6.38
0.284	16.715(12.625) ± 0.041	80.08(60.81) ± 5.43	0.83(28.4)	±2.99	±2.30	±6.61
0.263	15.448(11.697) ± 0.039	78.84(60.25) ± 5.73	0.84(26.9)	±3.19	±2.34	±6.96
0.241	14.177(10.756) ± 0.037	77.06(59.22) ± 5.98	0.86(25.2)	±2.73	±2.06	±6.89
0.219	12.899(9.802) ± 0.029	74.63(57.61) ± 5.08	0.88(23.8)	±2.84	±2.57	±6.36
0.197	11.616(8.833) ± 0.027	72.40(56.12) ± 5.38	0.92(22.1)	±2.12	±2.05	±6.13
0.175	10.327(7.850) ± 0.022	68.48(53.34) ± 4.75	0.88(20.2)	±2.15	±2.18	±5.65
0.153	9.035(6.859) ± 0.021	62.87(49.41) ± 4.84	0.82(18.3)	±2.09	±2.55	±5.85
0.131	7.744(5.870) ± 0.017	58.29(45.68) ± 4.29	0.71(16.3)	±2.05	±2.65	±5.45
0.109	6.452(4.877) ± 0.014	54.02(41.89) ± 4.10	0.58(14.5)	±1.91	±2.54	±5.19
0.087	5.160(3.881) ± 0.011	49.72(38.24) ± 4.19	0.49(12.2)	±1.74	±2.92	±5.40
0.066	3.895(3.027) ± 0.008	44.74(34.54) ± 4.38	0.49(10.2)	±1.45	±3.09	±5.55

TABLE XX: NBD fit results in centrality 25-30%.

$\delta\eta$	$\langle\mu_c\rangle(\langle\mu\rangle)$	$\langle k_c\rangle(\langle k\rangle)$	$\langle\chi^2/NDF\rangle(\langle NDF\rangle)$	$\delta\langle k_c\rangle(dead)$	$\delta\langle k_c\rangle(fake)$	$\delta\langle k_c\rangle(total)$
0.700	33.991(26.309) ± 0.090	67.99(52.63) ± 3.18	0.56(44.0)	±2.58	±0.80	±4.17
0.678	33.067(25.615) ± 0.088	68.77(53.27) ± 3.29	0.61(44.0)	±2.56	±0.05	±4.17
0.656	31.992(24.750) ± 0.086	67.53(52.23) ± 3.30	0.56(43.6)	±3.20	±1.31	±4.78
0.634	30.890(23.863) ± 0.084	67.26(51.95) ± 3.34	0.58(42.8)	±2.31	±1.01	±4.19
0.613	29.811(23.012) ± 0.082	67.40(52.02) ± 3.41	0.64(41.9)	±1.64	±1.27	±3.99
0.591	28.732(22.173) ± 0.081	66.18(51.07) ± 3.41	0.65(41.3)	±2.18	±0.79	±4.12
0.569	27.643(21.312) ± 0.079	66.17(51.01) ± 3.50	0.62(40.2)	±2.87	±1.24	±4.69
0.547	26.558(20.443) ± 0.077	65.89(50.72) ± 3.57	0.65(38.9)	±2.32	±1.30	±4.45
0.525	25.479(19.583) ± 0.075	65.64(50.44) ± 3.66	0.66(37.9)	±2.53	±0.86	±4.53
0.503	24.403(18.721) ± 0.073	65.21(50.01) ± 3.75	0.66(37.1)	±3.12	±1.03	±4.99
0.481	23.325(17.852) ± 0.071	64.30(49.19) ± 3.80	0.64(35.9)	±3.10	±0.97	±5.00
0.459	22.243(16.972) ± 0.069	64.65(49.31) ± 3.94	0.67(35.0)	±2.62	±0.71	±4.78
0.438	21.155(16.084) ± 0.067	63.75(48.45) ± 4.03	0.68(33.4)	±2.73	±0.89	±4.95
0.416	20.074(15.204) ± 0.065	63.34(47.95) ± 4.15	0.70(32.4)	±2.72	±1.01	±5.06
0.394	18.991(14.327) ± 0.063	62.47(47.09) ± 4.26	0.69(31.0)	±2.95	±1.01	±5.28
0.372	17.912(13.455) ± 0.061	62.61(47.00) ± 4.49	0.71(29.9)	±2.80	±0.83	±5.35
0.350	16.855(12.625) ± 0.042	62.05(46.45) ± 3.30	0.72(28.7)	±2.34	±0.81	±4.12
0.328	15.805(11.868) ± 0.040	61.38(46.04) ± 3.39	0.72(27.5)	±2.67	±1.02	±4.43
0.306	14.769(11.126) ± 0.038	60.26(45.34) ± 3.48	0.72(26.3)	±2.88	±1.01	±4.63
0.284	13.731(10.376) ± 0.037	59.70(44.97) ± 3.62	0.71(25.1)	±2.44	±1.21	±4.54
0.263	12.685(9.610) ± 0.035	59.20(44.67) ± 3.84	0.74(23.7)	±2.61	±1.06	±4.76
0.241	11.640(8.838) ± 0.033	57.91(43.73) ± 4.00	0.71(22.3)	±2.54	±1.09	±4.86
0.219	10.591(8.054) ± 0.026	56.00(42.22) ± 3.34	0.64(21.0)	±2.38	±1.26	±4.29
0.197	9.535(7.258) ± 0.024	54.60(41.11) ± 3.51	0.67(19.3)	±2.10	±1.43	±4.33
0.175	8.479(6.455) ± 0.020	52.59(39.35) ± 3.21	0.64(17.6)	±2.49	±1.42	±4.30
0.153	7.420(5.643) ± 0.018	51.06(38.08) ± 3.48	0.62(16.0)	±1.76	±1.53	±4.19
0.131	6.363(4.832) ± 0.015	49.16(36.41) ± 3.38	0.56(14.3)	±1.61	±1.59	±4.07
0.109	5.306(4.017) ± 0.013	45.94(33.94) ± 3.32	0.49(12.3)	±1.57	±1.75	±4.07
0.087	4.245(3.196) ± 0.010	43.38(31.95) ± 3.30	0.49(10.5)	±1.68	±2.00	±4.21
0.066	3.205(2.492) ± 0.007	38.41(28.81) ± 3.58	0.47(8.8)	±1.46	±2.20	±4.45

TABLE XXI: NBD fit results in centrality 30-35%.

$\delta\eta$	$\langle\mu_c\rangle(\langle\mu\rangle)$	$\langle k_c\rangle(\langle k\rangle)$	$\langle\chi^2/NDF\rangle(\langle NDF\rangle)$	$\delta\langle k_c\rangle(dead)$	$\delta\langle k_c\rangle(fake)$	$\delta\langle k_c\rangle(total)$
0.700	27.652(21.402) ± 0.079	58.33(45.15) ± 2.86	0.67(41.0)	±3.24	±0.86	±4.41
0.678	26.900(20.838) ± 0.078	57.89(44.85) ± 2.86	0.60(40.9)	±2.95	±0.85	±4.20
0.656	26.016(20.126) ± 0.076	57.99(44.86) ± 2.94	0.63(39.6)	±2.17	±0.88	±3.75
0.634	25.115(19.401) ± 0.074	57.51(44.43) ± 2.98	0.66(38.4)	±2.60	±0.72	±4.02
0.613	24.225(18.699) ± 0.073	56.95(43.97) ± 3.03	0.67(37.0)	±2.60	±0.86	±4.09
0.591	23.345(18.015) ± 0.071	56.94(43.95) ± 3.10	0.70(36.3)	±2.27	±0.77	±3.92
0.569	22.464(17.318) ± 0.070	56.67(43.71) ± 3.17	0.74(35.0)	±1.78	±0.77	±3.72
0.547	21.583(16.613) ± 0.068	55.99(43.12) ± 3.22	0.71(33.9)	±2.04	±0.69	±3.87
0.525	20.702(15.911) ± 0.066	56.01(43.07) ± 3.34	0.73(33.0)	±2.00	±0.70	±3.96
0.503	19.828(15.210) ± 0.065	55.63(42.71) ± 3.44	0.76(31.8)	±1.94	±0.84	±4.03
0.481	18.948(14.500) ± 0.063	55.29(42.37) ± 3.57	0.72(30.9)	±2.25	±0.85	±4.30
0.459	18.064(13.781) ± 0.061	55.70(42.57) ± 3.73	0.77(30.1)	±1.76	±0.78	±4.20
0.438	17.181(13.060) ± 0.059	54.86(41.80) ± 3.89	0.79(29.1)	±2.03	±1.04	±4.51
0.416	16.302(12.344) ± 0.058	53.65(40.75) ± 3.97	0.68(28.0)	±2.50	±1.08	±4.82
0.394	15.419(11.629) ± 0.056	53.33(40.40) ± 4.19	0.74(26.8)	±2.48	±0.99	±4.97
0.372	14.543(10.920) ± 0.054	52.71(39.80) ± 4.38	0.75(25.4)	±2.14	±0.93	±4.96
0.350	13.684(10.246) ± 0.037	52.57(39.60) ± 3.27	0.78(24.3)	±2.15	±0.93	±4.02
0.328	12.833(9.633) ± 0.035	51.53(38.93) ± 3.35	0.81(23.0)	±2.25	±0.95	±4.14
0.306	11.991(9.029) ± 0.034	49.87(37.95) ± 3.43	0.77(22.0)	±2.29	±0.94	±4.23
0.284	11.146(8.415) ± 0.033	48.20(36.98) ± 3.59	0.76(20.9)	±2.06	±0.89	±4.23
0.263	10.299(7.796) ± 0.031	47.05(36.22) ± 3.67	0.71(19.7)	±1.60	±0.93	±4.11
0.241	9.450(7.169) ± 0.030	45.91(35.45) ± 3.79	0.69(18.6)	±1.51	±0.93	±4.18
0.219	8.597(6.532) ± 0.023	44.64(34.66) ± 3.18	0.62(17.5)	±1.43	±1.00	±3.62
0.197	7.740(5.885) ± 0.022	43.61(34.05) ± 3.30	0.57(16.3)	±1.22	±1.01	±3.66
0.175	6.881(5.231) ± 0.018	42.44(33.32) ± 3.04	0.50(14.9)	±1.36	±1.10	±3.51
0.153	6.023(4.574) ± 0.016	41.28(32.47) ± 3.26	0.45(13.6)	±1.39	±1.27	±3.76
0.131	5.165(3.914) ± 0.013	40.29(31.79) ± 3.21	0.45(12.2)	±1.33	±1.30	±3.71
0.109	4.306(3.253) ± 0.011	38.26(30.17) ± 3.27	0.46(10.7)	±1.62	±1.28	±3.87
0.087	3.445(2.587) ± 0.009	35.11(27.79) ± 3.39	0.51(9.2)	±1.18	±1.41	±3.86
0.066	2.606(2.037) ± 0.006	30.96(24.26) ± 3.44	0.54(7.9)	±1.25	±1.14	±3.83

TABLE XXII: NBD fit results in centrality 35-40%.

$\delta\eta$	$\langle\mu_c\rangle(\langle\mu\rangle)$	$\langle k_c\rangle(\langle k\rangle)$	$\langle\chi^2/NDF\rangle(\langle NDF\rangle)$	$\delta\langle k_c\rangle(dead)$	$\delta\langle k_c\rangle(fake)$	$\delta\langle k_c\rangle(total)$
0.700	21.970(17.005) ± 0.071	47.25(36.57) ± 2.31	0.79(38.0)	±0.68	±0.60	±2.48
0.678	21.372(16.556) ± 0.070	47.47(36.77) ± 2.32	0.69(37.7)	±0.44	±0.02	±2.36
0.656	20.684(16.001) ± 0.068	46.97(36.33) ± 2.33	0.71(37.1)	±0.92	±0.23	±2.51
0.634	19.964(15.423) ± 0.067	46.50(35.92) ± 2.35	0.79(36.0)	±0.86	±0.30	±2.52
0.613	19.253(14.862) ± 0.065	46.36(35.78) ± 2.40	0.86(34.6)	±0.91	±0.15	±2.57
0.591	18.572(14.333) ± 0.064	45.46(35.08) ± 2.41	0.82(33.4)	±1.16	±0.36	±2.70
0.569	17.877(13.783) ± 0.063	45.55(35.11) ± 2.48	0.83(32.5)	±1.22	±0.37	±2.79
0.547	17.176(13.221) ± 0.061	45.52(35.05) ± 2.54	0.83(31.7)	±1.26	±0.44	±2.87
0.525	16.475(12.662) ± 0.059	45.45(34.94) ± 2.63	0.87(30.7)	±1.09	±0.34	±2.87
0.503	15.778(12.104) ± 0.058	45.41(34.85) ± 2.70	0.87(29.8)	±0.92	±0.22	±2.86
0.481	15.082(11.542) ± 0.057	44.90(34.38) ± 2.77	0.84(28.6)	±1.02	±0.36	±2.97
0.459	14.380(10.972) ± 0.055	44.50(33.97) ± 2.83	0.81(27.6)	±1.03	±0.31	±3.03
0.438	13.678(10.399) ± 0.053	43.95(33.42) ± 2.91	0.82(26.3)	±1.15	±0.39	±3.15
0.416	12.978(9.829) ± 0.052	43.68(33.09) ± 2.99	0.81(25.4)	±1.16	±0.33	±3.22
0.394	12.280(9.264) ± 0.050	43.03(32.45) ± 3.06	0.79(24.2)	±1.23	±0.41	±3.32
0.372	11.582(8.700) ± 0.049	42.60(31.98) ± 3.17	0.77(23.1)	±1.08	±0.45	±3.38
0.350	10.894(8.161) ± 0.033	42.04(31.45) ± 2.30	0.74(22.0)	±1.00	±0.34	±2.53
0.328	10.213(7.670) ± 0.032	41.13(30.87) ± 2.34	0.72(21.0)	±0.90	±0.35	±2.54
0.306	9.540(7.188) ± 0.031	40.19(30.29) ± 2.39	0.70(20.0)	±0.86	±0.19	±2.55
0.284	8.867(6.699) ± 0.029	39.08(29.61) ± 2.46	0.69(18.9)	±0.92	±0.28	±2.64
0.263	8.191(6.204) ± 0.028	38.50(29.35) ± 2.57	0.67(18.0)	±0.97	±0.34	±2.77
0.241	7.517(5.707) ± 0.027	37.29(28.54) ± 2.64	0.57(17.1)	±1.25	±0.50	±2.97
0.219	6.837(5.198) ± 0.021	36.65(28.17) ± 2.29	0.55(16.1)	±0.92	±0.47	±2.51
0.197	6.155(4.685) ± 0.019	35.93(27.66) ± 2.40	0.55(15.0)	±0.77	±0.51	±2.58
0.175	5.474(4.166) ± 0.016	34.69(26.74) ± 2.20	0.52(13.7)	±0.77	±0.65	±2.43
0.153	4.792(3.644) ± 0.015	33.23(25.56) ± 2.37	0.50(12.4)	±0.86	±0.72	±2.62
0.131	4.111(3.122) ± 0.012	31.76(24.13) ± 2.33	0.48(11.1)	±0.88	±0.72	±2.59
0.109	3.426(2.594) ± 0.010	30.11(22.76) ± 2.52	0.54(9.8)	±0.65	±0.72	±2.69
0.087	2.742(2.069) ± 0.008	28.05(20.82) ± 2.59	0.55(8.3)	±0.86	±0.84	±2.85
0.066	2.070(1.609) ± 0.006	24.89(18.20) ± 2.64	0.54(7.0)	±0.94	±0.95	±2.96

TABLE XXIII: NBD fit results in centrality 40-45%.

$\delta\eta$	$\langle\mu_c\rangle(\langle\mu\rangle)$	$\langle k_c\rangle(\langle k\rangle)$	$\langle\chi^2/NDF\rangle(\langle NDF\rangle)$	$\delta\langle k_c\rangle(dead)$	$\delta\langle k_c\rangle(fake)$	$\delta\langle k_c\rangle(total)$
0.700	17.453(13.508) ± 0.063	37.64(29.13) ± 1.83	0.74(35.0)	±0.40	±0.98	±2.12
0.678	16.988(13.160) ± 0.062	37.36(28.94) ± 1.85	0.74(34.1)	±1.08	±0.27	±2.16
0.656	16.429(12.709) ± 0.061	37.57(29.06) ± 1.91	0.83(33.0)	±0.91	±0.00	±2.12
0.634	15.863(12.255) ± 0.059	37.55(29.01) ± 1.96	0.82(32.2)	±1.54	±0.31	±2.51
0.613	15.315(11.822) ± 0.058	36.88(28.47) ± 1.96	0.76(31.4)	±1.75	±0.34	±2.65
0.591	14.758(11.389) ± 0.057	36.84(28.43) ± 2.00	0.83(30.6)	±1.76	±0.32	±2.68
0.569	14.201(10.948) ± 0.056	36.74(28.32) ± 2.04	0.88(29.8)	±1.32	±0.26	±2.45
0.547	13.652(10.508) ± 0.054	36.19(27.85) ± 2.07	0.85(29.2)	±1.54	±0.32	±2.60
0.525	13.096(10.065) ± 0.053	36.01(27.67) ± 2.12	0.83(28.3)	±1.30	±0.22	±2.50
0.503	12.537(9.618) ± 0.051	36.07(27.66) ± 2.21	0.89(27.1)	±1.25	±0.28	±2.55
0.481	11.980(9.169) ± 0.050	35.96(27.51) ± 2.28	0.91(26.3)	±1.27	±0.33	±2.63
0.459	11.422(8.715) ± 0.049	35.74(27.26) ± 2.36	0.91(25.2)	±1.12	±0.33	±2.63
0.438	10.861(8.258) ± 0.048	35.46(26.95) ± 2.43	0.87(24.2)	±1.08	±0.28	±2.67
0.416	10.302(7.803) ± 0.046	35.19(26.64) ± 2.51	0.89(22.9)	±1.10	±0.38	±2.77
0.394	9.742(7.349) ± 0.045	35.42(26.71) ± 2.63	0.92(22.0)	±0.69	±0.34	±2.74
0.372	9.189(6.902) ± 0.043	35.02(26.31) ± 2.70	0.83(21.1)	±0.86	±0.36	±2.86
0.350	8.649(6.478) ± 0.030	34.15(25.59) ± 1.94	0.73(19.9)	±1.22	±0.51	±2.35
0.328	8.110(6.090) ± 0.029	33.55(25.21) ± 1.99	0.71(19.0)	±1.19	±0.45	±2.36
0.306	7.578(5.708) ± 0.027	33.04(24.89) ± 2.06	0.70(18.0)	±1.22	±0.41	±2.43
0.284	7.044(5.321) ± 0.026	32.48(24.52) ± 2.12	0.67(17.0)	±1.18	±0.43	±2.47
0.263	6.509(4.930) ± 0.025	31.66(23.97) ± 2.17	0.63(16.1)	±1.12	±0.45	±2.48
0.241	5.973(4.533) ± 0.024	30.82(23.44) ± 2.22	0.61(15.1)	±1.00	±0.46	±2.48
0.219	5.435(4.131) ± 0.018	29.59(22.59) ± 1.88	0.58(14.0)	±1.09	±0.45	±2.23
0.197	4.894(3.723) ± 0.017	28.75(22.00) ± 2.00	0.54(13.1)	±0.83	±0.49	±2.22
0.175	4.353(3.311) ± 0.014	28.04(21.41) ± 1.89	0.56(12.1)	±0.90	±0.54	±2.16
0.153	3.811(2.896) ± 0.013	26.88(20.50) ± 2.02	0.50(10.9)	±0.74	±0.51	±2.21
0.131	3.267(2.478) ± 0.011	25.91(19.73) ± 2.01	0.52(9.9)	±0.63	±0.54	±2.18
0.109	2.724(2.060) ± 0.009	24.44(18.61) ± 2.05	0.47(8.7)	±0.38	±0.61	±2.18
0.087	2.179(1.639) ± 0.007	22.93(17.48) ± 2.12	0.55(7.4)	±0.38	±0.55	±2.22
0.066	1.646(1.279) ± 0.005	20.46(15.59) ± 2.26	0.54(6.3)	±0.59	±0.51	±2.39

TABLE XXIV: NBD fit results in centrality 45-50%.

$\delta\eta$	$\langle\mu_c\rangle(\langle\mu\rangle)$	$\langle k_c\rangle(\langle k\rangle)$	$\langle\chi^2/NDF\rangle(\langle NDF\rangle)$	$\delta\langle k_c\rangle(dead)$	$\delta\langle k_c\rangle(fake)$	$\delta\langle k_c\rangle(total)$
0.700	13.493(10.444) ± 0.054	32.22(24.94) ± 1.72	0.77(27.0)	±1.57	±0.13	±2.34
0.678	13.123(10.166) ± 0.053	32.44(25.13) ± 1.74	0.79(26.9)	±1.12	±0.09	±2.07
0.656	12.698(9.823) ± 0.052	32.30(24.99) ± 1.77	0.81(25.6)	±0.70	±0.22	±1.92
0.634	12.261(9.472) ± 0.051	32.54(25.14) ± 1.85	0.89(24.6)	±0.78	±0.32	±2.04
0.613	11.829(9.131) ± 0.050	32.98(25.46) ± 1.94	0.89(23.9)	±0.81	±0.20	±2.11
0.591	11.403(8.800) ± 0.049	33.01(25.47) ± 2.00	0.88(23.1)	±0.56	±0.28	±2.10
0.569	10.976(8.462) ± 0.048	32.73(25.23) ± 2.04	0.84(22.3)	±0.56	±0.24	±2.13
0.547	10.547(8.119) ± 0.046	32.55(25.05) ± 2.09	0.84(21.7)	±0.52	±0.29	±2.18
0.525	10.120(7.778) ± 0.045	32.54(25.00) ± 2.16	0.80(21.0)	±0.30	±0.28	±2.20
0.503	9.694(7.437) ± 0.044	32.48(24.91) ± 2.23	0.76(20.5)	±0.39	±0.31	±2.28
0.481	9.267(7.093) ± 0.043	32.14(24.60) ± 2.28	0.67(19.8)	±0.44	±0.30	±2.34
0.459	8.836(6.742) ± 0.042	31.98(24.40) ± 2.37	0.60(19.1)	±0.57	±0.34	±2.46
0.438	8.403(6.389) ± 0.041	31.90(24.26) ± 2.46	0.55(18.5)	±0.56	±0.36	±2.54
0.416	7.970(6.037) ± 0.039	31.80(24.10) ± 2.56	0.52(17.7)	±0.58	±0.38	±2.65
0.394	7.537(5.686) ± 0.038	31.73(23.97) ± 2.67	0.54(17.1)	±0.79	±0.42	±2.82
0.372	7.108(5.339) ± 0.037	31.47(23.68) ± 2.78	0.53(16.4)	±0.83	±0.37	±2.92
0.350	6.688(5.009) ± 0.025	31.14(23.38) ± 2.05	0.54(15.6)	±0.84	±0.38	±2.25
0.328	6.271(4.709) ± 0.024	30.59(23.16) ± 2.12	0.55(15.0)	±0.77	±0.37	±2.29
0.306	5.860(4.413) ± 0.023	29.82(22.83) ± 2.20	0.55(14.4)	±0.72	±0.35	±2.34
0.284	5.450(4.115) ± 0.022	29.04(22.41) ± 2.27	0.54(13.7)	±0.57	±0.36	±2.37
0.263	5.037(3.813) ± 0.021	28.60(22.23) ± 2.41	0.57(13.1)	±0.44	±0.43	±2.49
0.241	4.623(3.508) ± 0.020	28.11(21.89) ± 2.48	0.55(12.4)	±0.47	±0.42	±2.56
0.219	4.205(3.196) ± 0.016	27.55(21.51) ± 2.15	0.55(11.8)	±0.45	±0.38	±2.23
0.197	3.785(2.879) ± 0.015	27.20(21.34) ± 2.35	0.56(11.0)	±0.42	±0.41	±2.42
0.175	3.364(2.558) ± 0.012	26.76(21.15) ± 2.25	0.58(10.3)	±0.45	±0.40	±2.33
0.153	2.943(2.236) ± 0.011	26.24(20.74) ± 2.47	0.57(9.4)	±0.16	±0.40	±2.50
0.131	2.523(1.913) ± 0.009	25.81(20.49) ± 2.54	0.53(8.5)	±0.12	±0.42	±2.57
0.109	2.104(1.592) ± 0.008	25.12(19.94) ± 2.71	0.48(7.6)	±0.09	±0.52	±2.76
0.087	1.692(1.306) ± 0.006	23.73(18.71) ± 2.55	0.45(6.6)	±0.14	±0.38	±2.58
0.066	1.277(1.014) ± 0.004	21.69(16.94) ± 2.72	0.49(5.4)	±0.51	±0.45	±2.80

TABLE XXV: NBD fit results in centrality 50-55%.

$\delta\eta$	$\langle\mu_c\rangle(\langle\mu\rangle)$	$\langle k_c\rangle(\langle k\rangle)$	$\langle\chi^2/NDF\rangle(\langle NDF\rangle)$	$\delta\langle k_c\rangle(dead)$	$\delta\langle k_c\rangle(fake)$	$\delta\langle k_c\rangle(total)$
0.700	10.177(7.877) ± 0.046	27.08(20.96) ± 1.52	1.18(24.0)	±1.23	±0.17	±1.96
0.678	9.898(7.667) ± 0.045	26.98(20.90) ± 1.53	1.14(23.0)	±0.62	±0.26	±1.67
0.656	9.584(7.414) ± 0.044	26.02(20.12) ± 1.50	1.07(21.9)	±0.94	±0.23	±1.79
0.634	9.257(7.151) ± 0.044	25.65(19.81) ± 1.51	0.97(21.2)	±0.43	±0.21	±1.58
0.613	8.935(6.897) ± 0.043	25.16(19.42) ± 1.52	0.85(20.8)	±0.63	±0.16	±1.66
0.591	8.613(6.647) ± 0.042	24.75(19.10) ± 1.53	0.82(20.0)	±0.77	±0.21	±1.73
0.569	8.287(6.389) ± 0.041	24.69(19.03) ± 1.58	0.80(19.6)	±0.54	±0.10	±1.68
0.547	7.964(6.130) ± 0.040	24.46(18.82) ± 1.62	0.79(19.1)	±0.70	±0.22	±1.77
0.525	7.640(5.872) ± 0.039	24.42(18.76) ± 1.67	0.79(18.5)	±0.67	±0.28	±1.81
0.503	7.318(5.614) ± 0.038	24.25(18.59) ± 1.72	0.74(18.0)	±0.67	±0.25	±1.86
0.481	6.991(5.351) ± 0.037	24.35(18.62) ± 1.80	0.74(17.5)	±0.57	±0.26	±1.91
0.459	6.664(5.085) ± 0.036	24.37(18.58) ± 1.89	0.70(16.9)	±0.79	±0.24	±2.06
0.438	6.338(4.818) ± 0.035	24.32(18.48) ± 1.96	0.61(16.3)	±0.93	±0.26	±2.19
0.416	6.013(4.554) ± 0.034	24.34(18.42) ± 2.05	0.55(15.7)	±0.93	±0.39	±2.28
0.394	5.689(4.292) ± 0.033	24.43(18.41) ± 2.14	0.52(15.0)	±1.01	±0.22	±2.38
0.372	5.365(4.031) ± 0.032	24.59(18.43) ± 2.28	0.52(14.3)	±0.85	±0.35	±2.46
0.350	5.047(3.781) ± 0.022	24.82(18.54) ± 1.71	0.54(13.8)	±0.85	±0.37	±1.94
0.328	4.731(3.554) ± 0.021	24.90(18.65) ± 1.81	0.62(13.4)	±0.58	±0.26	±1.92
0.306	4.421(3.331) ± 0.020	24.53(18.49) ± 1.90	0.62(12.9)	±0.47	±0.35	±1.99
0.284	4.110(3.106) ± 0.019	24.09(18.29) ± 2.00	0.58(12.3)	±0.62	±0.20	±2.10
0.263	3.798(2.877) ± 0.018	23.76(18.20) ± 2.19	0.61(11.6)	±0.57	±0.11	±2.27
0.241	3.487(2.646) ± 0.018	23.58(18.20) ± 2.34	0.59(11.1)	±0.59	±0.23	±2.43
0.219	3.173(2.412) ± 0.013	23.10(17.98) ± 2.13	0.56(10.5)	±0.77	±0.24	±2.28
0.197	2.858(2.174) ± 0.013	22.73(17.85) ± 2.36	0.53(9.8)	±0.74	±0.25	±2.49
0.175	2.541(1.932) ± 0.010	22.47(17.74) ± 2.36	0.54(9.0)	±0.95	±0.27	±2.56
0.153	2.224(1.691) ± 0.010	22.22(17.61) ± 2.64	0.57(8.2)	±0.89	±0.29	±2.80
0.131	1.906(1.447) ± 0.008	21.76(17.39) ± 2.93	0.64(7.4)	±0.75	±0.36	±3.05
0.109	1.593(1.215) ± 0.006	20.48(16.47) ± 3.02	0.59(6.6)	±0.69	±0.35	±3.11
0.087	1.279(0.982) ± 0.005	19.00(15.26) ± 2.67	0.54(5.5)	±0.67	±0.47	±2.80
0.066	0.969(0.770) ± 0.004	16.64(13.48) ± 2.31	0.52(4.5)	±0.59	±0.54	±2.45

TABLE XXVI: NBD fit results in centrality 55-60%.

$\delta\eta$	$\langle\mu_c\rangle(\langle\mu\rangle)$	$\langle k_c\rangle(\langle k\rangle)$	$\langle\chi^2/NDF\rangle(\langle NDF\rangle)$	$\delta\langle k_c\rangle(dead)$	$\delta\langle k_c\rangle(fake)$	$\delta\langle k_c\rangle(total)$
0.700	7.465(5.778) ± 0.041	18.75(14.52) ± 1.12	0.71(16.0)	±0.59	±0.13	±1.27
0.678	7.258(5.622) ± 0.040	19.02(14.74) ± 1.14	0.76(16.0)	±0.60	±0.08	±1.29
0.656	7.021(5.431) ± 0.039	18.80(14.54) ± 1.14	0.73(15.8)	±0.61	±0.09	±1.29
0.634	6.781(5.238) ± 0.038	18.41(14.22) ± 1.14	0.57(15.4)	±0.57	±0.09	±1.28
0.613	6.547(5.054) ± 0.038	18.01(13.89) ± 1.13	0.51(14.7)	±0.70	±0.07	±1.33
0.591	6.307(4.867) ± 0.037	17.98(13.87) ± 1.15	0.56(14.4)	±0.70	±0.07	±1.34
0.569	6.070(4.680) ± 0.036	17.84(13.75) ± 1.15	0.51(14.1)	±0.69	±0.07	±1.35
0.547	5.833(4.490) ± 0.035	17.66(13.59) ± 1.17	0.47(13.7)	±0.63	±0.07	±1.33
0.525	5.596(4.301) ± 0.034	17.52(13.46) ± 1.19	0.44(13.4)	±0.60	±0.08	±1.34
0.503	5.360(4.112) ± 0.033	17.52(13.43) ± 1.22	0.43(13.2)	±0.67	±0.09	±1.40
0.481	5.122(3.920) ± 0.033	17.49(13.38) ± 1.26	0.47(13.1)	±0.66	±0.09	±1.43
0.459	4.885(3.728) ± 0.032	17.37(13.24) ± 1.30	0.49(12.6)	±0.69	±0.09	±1.47
0.438	4.648(3.534) ± 0.031	17.22(13.08) ± 1.33	0.51(12.1)	±0.74	±0.10	±1.53
0.416	4.411(3.340) ± 0.030	17.20(13.01) ± 1.39	0.58(11.5)	±0.62	±0.10	±1.52
0.394	4.173(3.148) ± 0.029	17.18(12.95) ± 1.44	0.62(10.9)	±0.78	±0.12	±1.64
0.372	3.935(2.955) ± 0.028	17.34(13.00) ± 1.54	0.63(10.4)	±0.84	±0.13	±1.76
0.350	3.701(2.772) ± 0.019	17.31(12.94) ± 1.15	0.65(9.9)	±0.67	±0.08	±1.33
0.328	3.472(2.607) ± 0.018	17.17(12.87) ± 1.19	0.66(9.5)	±0.71	±0.10	±1.39
0.306	3.244(2.444) ± 0.018	17.09(12.85) ± 1.25	0.68(9.2)	±0.64	±0.09	±1.41
0.284	3.016(2.279) ± 0.017	16.91(12.74) ± 1.32	0.67(8.6)	±0.53	±0.08	±1.42
0.263	2.787(2.111) ± 0.016	16.61(12.58) ± 1.40	0.62(8.1)	±0.56	±0.09	±1.51
0.241	2.558(1.942) ± 0.015	16.53(12.57) ± 1.50	0.61(7.6)	±0.52	±0.11	±1.59
0.219	2.326(1.769) ± 0.012	16.34(12.46) ± 1.35	0.66(7.1)	±0.49	±0.10	±1.44
0.197	2.095(1.595) ± 0.011	16.13(12.30) ± 1.44	0.62(6.7)	±0.48	±0.11	±1.52
0.175	1.861(1.417) ± 0.009	16.07(12.24) ± 1.45	0.72(6.3)	±0.34	±0.12	±1.49
0.153	1.630(1.240) ± 0.009	15.67(11.91) ± 1.54	0.59(5.7)	±0.17	±0.13	±1.56
0.131	1.399(1.062) ± 0.007	14.90(11.39) ± 1.50	0.47(5.1)	±0.35	±0.15	±1.54
0.109	1.166(0.882) ± 0.006	14.25(10.82) ± 1.56	0.42(4.5)	±0.37	±0.17	±1.61
0.087	0.935(0.714) ± 0.004	13.41(10.20) ± 1.63	0.46(4.0)	±0.30	±0.15	±1.66
0.066	0.703(0.548) ± 0.003	11.85(9.19) ± 1.63	0.53(3.3)	±0.35	±0.17	±1.67

TABLE XXVII: NBD fit results in centrality 60-65%.

$\delta\eta$	$\langle\mu_c\rangle(\langle\mu\rangle)$	$\langle k_c\rangle(\langle k\rangle)$	$\langle\chi^2/NDF\rangle(\langle NDF\rangle)$	$\delta\langle k_c\rangle(dead)$	$\delta\langle k_c\rangle(fake)$	$\delta\langle k_c\rangle(total)$
0.700	5.337(4.131) ± 0.033	14.40(11.14) ± 0.81	0.79(15.0)	±0.33	±0.04	±0.88
0.678	5.197(4.026) ± 0.033	14.25(11.04) ± 0.82	0.77(14.8)	±0.45	±0.04	±0.94
0.656	5.031(3.892) ± 0.032	14.37(11.12) ± 0.86	0.61(14.2)	±0.46	±0.03	±0.97
0.634	4.861(3.755) ± 0.032	14.35(11.09) ± 0.88	0.53(13.8)	±0.47	±0.04	±0.99
0.613	4.686(3.617) ± 0.031	14.41(11.13) ± 0.93	0.78(13.1)	±0.44	±0.04	±1.03
0.591	4.519(3.487) ± 0.030	13.99(10.80) ± 0.90	0.63(12.9)	±0.53	±0.04	±1.05
0.569	4.344(3.349) ± 0.029	14.01(10.80) ± 0.92	0.73(12.7)	±0.51	±0.05	±1.06
0.547	4.169(3.209) ± 0.029	14.23(10.96) ± 0.97	0.82(12.5)	±0.41	±0.04	±1.05
0.525	4.003(3.077) ± 0.028	13.97(10.74) ± 0.97	0.64(12.0)	±0.41	±0.04	±1.06
0.503	3.835(2.942) ± 0.027	13.88(10.65) ± 1.00	0.59(11.8)	±0.45	±0.04	±1.10
0.481	3.665(2.805) ± 0.027	13.89(10.63) ± 1.04	0.60(11.6)	±0.43	±0.04	±1.12
0.459	3.495(2.667) ± 0.026	13.85(10.57) ± 1.07	0.59(11.1)	±0.34	±0.05	±1.12
0.438	3.326(2.529) ± 0.025	13.78(10.48) ± 1.11	0.56(10.5)	±0.33	±0.06	±1.16
0.416	3.159(2.393) ± 0.025	13.65(10.35) ± 1.15	0.48(9.9)	±0.38	±0.06	±1.22
0.394	2.989(2.255) ± 0.024	13.71(10.35) ± 1.23	0.46(9.5)	±0.37	±0.05	±1.28
0.372	2.818(2.117) ± 0.023	13.95(10.48) ± 1.33	0.52(8.9)	±0.40	±0.05	±1.39
0.350	2.652(1.986) ± 0.016	14.10(10.57) ± 1.00	0.54(8.5)	±0.41	±0.06	±1.09
0.328	2.487(1.867) ± 0.015	14.06(10.58) ± 1.06	0.56(8.1)	±0.41	±0.06	±1.15
0.306	2.324(1.750) ± 0.015	14.16(10.71) ± 1.14	0.66(7.6)	±0.34	±0.06	±1.19
0.284	2.160(1.631) ± 0.014	14.12(10.76) ± 1.22	0.66(7.1)	±0.38	±0.06	±1.28
0.263	1.996(1.511) ± 0.013	14.01(10.76) ± 1.31	0.63(6.6)	±0.36	±0.06	±1.36
0.241	1.832(1.390) ± 0.013	13.79(10.64) ± 1.39	0.53(6.3)	±0.40	±0.06	±1.45
0.219	1.667(1.267) ± 0.010	13.49(10.50) ± 1.24	0.51(5.9)	±0.40	±0.07	±1.30
0.197	1.502(1.143) ± 0.009	13.23(10.37) ± 1.35	0.47(5.5)	±0.46	±0.07	±1.43
0.175	1.335(1.015) ± 0.007	13.17(10.38) ± 1.32	0.50(5.1)	±0.47	±0.08	±1.40
0.153	1.168(0.888) ± 0.007	12.96(10.25) ± 1.55	0.56(4.7)	±0.38	±0.10	±1.60
0.131	1.005(0.768) ± 0.006	12.13(9.56) ± 1.46	0.45(4.3)	±0.29	±0.10	±1.50
0.109	0.838(0.639) ± 0.005	11.68(9.21) ± 1.66	0.44(3.8)	±0.15	±0.12	±1.67
0.087	0.673(0.524) ± 0.004	10.96(8.64) ± 1.65	0.54(3.3)	±0.14	±0.14	±1.66
0.066	0.507(0.405) ± 0.003	9.15(7.32) ± 1.29	0.41(2.7)	±0.16	±0.09	±1.31

[1] M. A. Stephanov, Prog. Theor. Phys. Suppl. **153**, 139 (2004); Int. J. Mod. Phys. A **20**, 4387 (2005).
[2] M. Asakawa *et al.*, Nucl. Phys. A **504**, 668 (1989).
[3] A. Barducci *et al.*, Phys. Lett. B **231**, 463 (1989). Phys. Rev. D **41**, 1610 (1990).
[4] A. Barducci *et al.*, Phys. Rev. D **49**, 426 (1994).
[5] J. Berges *et al.*, Nucl. Phys. B **538**, 215 (1999).
[6] M. A. Halasz *et al.*, Phys. Rev. D **58**, 096007 (1998).
[7] O. Scavenius *et al.*, Phys. Rev. C **64**, 045202 (2001).
[8] N. G. Antoniou *et al.*, Phys. Lett. B **563**, 165 (2003).
[9] Y. Hatta *et al.*, Phys. Rev. D **67**, 014028 (2003).
[10] F. R. Brown *et al.*, Phys. Rev. Lett. **65**, 2491 (1990).
[11] M. Stephanov*et al.*, Phys. Rev. Lett. **81**, 4816-4819 (1998).
[12] K. Adcox *et al.*, PHENIX Collaboration, Nucl. Phys. A **757**, 184 (2005).
[13] S. S. Adler *et al.*, PHENIX Collaboration, Phys. Rev. Lett. **91**, 072301 (2003).
[14] S. S. Adler *et al.*, PHENIX Collaboration, Phys. Rev. C **69**, 034910 (2004).
[15] A. Adare *et al.*, PHENIX Collaboration, nucl-ex/0611018, Phys. Rev. Lett. (to be published).
[16] A. Adare *et al.*, PHENIX Collaboration, nucl-ex/0608033, Phys. Rev. Lett. (to be published).
[17] Y. Aoki *et al.*, Phys. Lett. B **643**, 46-54 (2006).
[18] L. S. Ornstein and F. Zernike, Proc. Sect. Sci. K. med. Akad. Wet. **17**, 793 (1914).
[19] V. L. Ginzburg and L. D. Landau, Zh. Eksp. Teor. Fiz. **20**, 1064 (1950).
[20] N. Sasaki *et al.*, Europhys. Lett. **54**, 38-44 (2001).
[21] J. D. Bjorken, Phys. Rev. D **27**, 140 (1983).
[22] S. S. Adler *et al.*, PHENIX Collaboration, Phys. Rev. C **71**, 034908 (2005).
[23] N. G. Antoniou *et al.*, Eur. Phys. J. C **4**, 513 (1998).
[24] N. G. Antoniou *et al.*, Phys. Rev. Lett. **97**, 032002 (2006).
[25] N. G. Antoniou *et al.*, Nucl. Phys. A **693**, 799 (2001).
[26] E. A. De Wolf, I. M. Dremin and W. Kittel, Phys. Repts. **270**, 1 (1996).
[27] A. Bialas and R. Peschanski, Nucl. Phys. B **273**, 703 (1986); Nucl. Phys. B **308**, 857 (1988).
[28] T. Abbott *et al.*, E-802 Collaboration, Phys. Rev. C **52**, 2663 (1995).
[29] H. Nakamura and R. Seki, Phys. Rev. C **66**, 024902 (2002).
[30] K. Adcox *et al.*, PHENIX Collaboration, Nucl. Instrum. Methods A **499**, 469 (2003).
[31] S. S. Adler *et al.*, PHENIX Collaboration, Phys. Rev. C **69**, 034909 (2004).
[32] Computer code GEANT 3.21 (CERN, Genva, 1993).
[33] F. James and M. Roos, Comput. Phys. Commun. **10**, 343 (1975).
[34] P. Carruthers and C. C. Shih, Phys. Lett. B **165**, 209 (1985).
[35] M. J. Tannenbaum, E802 Internal Report No. E-802-MEM-58 (1993).
[36] G. Baym *et al.*, Phys. Rev. C **52**, 1604 (1995).
[37] M. Rybczynski *et al.*, NA49 Collaboration, J.Phys.Conf.Ser. **5**, 74 (2005).
[38] V. P. Konchakovski *et al.*, Phys. Rev. C **73**, 034902 (2006).
[39] B. B. Back *et al.*, PHOBOS Collaboration, Phys. Rev. C **72**, 051901 (2005); E. B. Johnson, AIP Conf. Proc. **842**, 137 (2006).
[40] J. Adams *et al.*, STAR Collaboration, nucl-ex/0606014, Phys. Rev. Lett. (to be published); nucl-ex/0601042, Phys. Rev. C (to be published).
[41] Y. Akiba *et al.*, E-802 Collaboration, Phys. Rev. C **56**, 1544 (1997).
[42] S. S. Adler *et al.*, PHENIX Collaboration, Phys. Rev. Lett. **93**, 152302 (2004).
[43] A. Enokizono, Ph. D. thesis, Department of Physical Science, Hiroshima University (2004).
[44] D. J. Scalapino and R. L. Sugar, Phys. Rev. D **8**, 2284 (1973).